

AD-A128 763

ADA-128 763

NRL Memorandum Report 5073

# Application of Time-Resolved Spectroscopies to the Study of Energetic Materials — 1982

J. M. SCHNUR

*Optical Probes Branch  
Optical Sciences Division*

**TECHNICAL  
LIBRARY**

May 24, 1983

This research was supported in part by the Office of Naval Research and the Naval Research Laboratory.



**NAVAL RESEARCH LABORATORY  
Washington, D.C.**

Approved for public release; distribution unlimited.



## CONTENTS

- I. Executive Summary
- II. "Picosecond UV Photolysis and Laser-Induced Fluorescence Probing of Gas-Phase Nitromethane", P. E. Schoen, M. J. Marrone, J. M. Schnur and L. S. Goldberg, Chem. Phys. Lett. 90, 272 (1982).
- III. "Picosecond Photofragmentation Experiments with a Repetitively Pulsed Mode-Locked Nd:Phosphate Glass Laser System", L. S. Goldberg, M. J. Marrone and P. E. Schoen, Proc. of SPIE Vol. 322, 199 (1982).
- IV. "Fabry-Perot Photothermal Trace Detection", A. J. Campillo, S. J. Petuchowski, C. C. Davis, H-B. Lin, Appl. Phys. Lett. 41, 327 (1982).
- V. "UV Short-Pulse Fragmentation of Isotopically Labeled Acetylene: Studies of Emission with Subnanosecond Resolution", B. B. Craig, W. L. Faust, L. S. Goldberg and R. G. Weiss, J. Chem. Phys. 76, 5014 (1982).
- VI. "Repetitively Pulsed Mode-Locked Nd:Phosphate Glass Laser Oscillator-Amplifier System", L. S. Goldberg, P. E. Schoen and M. J. Marrone, Appl. Optics 21, 1474 (1982).
- VII. "Picosecond Continuum Broad-Band CARS Probe", L. S. Goldberg, Appl. Physics B, B28, 219 (1982).
- VIII. "Picosecond Streak Camera Fluorometry: A Review", A. J. Campillo and S. L. Shapiro, IEEE J. of Quantum Electron. (in Press).
- IX. "Delayed Formation of Emissive CN and C<sub>2</sub> Fragments Following Short-Pulse UV Excitation of Isotopically Labeled CH<sub>3</sub>CN", B. B. Craig, W. L. Faust and R. G. Weiss, Proceedings of the Lasers in Chemistry Conference, Howard University, May 1982 (in Press).
- X "Broadband CARS Probe Using the Picosecond Continuum", L. S. Goldberg, in "Picosecond Phenomena III, R. M. Hochstrasser, Ed (Springer-Verlag, Berlin - in press).
- XI. "Application of Time Resolved Laser Spectroscopies to the Study of Energetic Materials", B. Craig, P. Schoen, A. Campillo, W. Faust, L. Goldberg, M. Marrone, J. Schnur and R. Weiss, CPIA Publication 366, Vol. 1, p. 187, Oct. 82.

## APPLICATION OF TIME-RESOLVED SPECTROSCOPIES TO THE STUDY OF ENERGETIC MATERIALS — 1982

### I. Introduction

The research described in this report is a continuation of an experimental program to apply short pulse laser techniques to determine the critical reactions that lead to explosions and detonations in energetic materials. The objectives of the program are to identify, and where possible, control the important initial stages of energetic reactions. In order to accomplish this, laser techniques are being applied to initiate the reactions and to probe (with the requisite time resolution of ca.  $10^{-11}$  sec.) the subsequent chemistry. Previously, we have employed picosecond bursts of UV laser radiation to (nearly) instantaneously deposit significant amounts of energy in small relevant molecules and have applied ultrafast spectroscopy to follow the subsequent molecular fragmentation and photophysics. This work has been quite successful and we summarize results in Section B. Because shock plays such an important role in the detonation process, greater emphasis will be placed on initiating chemistry with laser driven shocks in FY83 and in future years. (See Section C. By repeatedly shocking small amounts of different materials as a function of peak pressure and by utilizing laser spectroscopy to identify the resulting products (e.g. free radicals, new species, etc.) it is hoped to better understand the role of shock in detonation.

The experiments were performed in the Short Pulse Section of the Optical Probes Branch (Code 6510) at NRL in collaboration when appropriate with other research groups at NRL currently participating in the SFP for controlled energy release. Collaboration with Georgetown University's Chemistry Department under this project has been very productive and will continue to be supported. A substantial part of the program is supported by the ONR Special Focus Program in Energetic Materials.

## II. Progress FY82

The fluid-mechanical phenomenon of detonation is reasonably well understood but the detailed chemical reactions and thermodynamics that cause a detonation are still largely a mystery. For many explosives even the final chemical composition after detonation is not accurately known and the reaction mechanisms are only guessed. The lack of relevant data is due in part to the difficulties of identifying short lived molecular species under the extremes of temperature and pressures generated in explosives. Recent advances in laser techniques tantalizingly suggest that it should be possible to chart the precise initial physical and chemical changes occurring in such reactions. Unfortunately, it presently appears to be too difficult to apply such laser spectroscopic techniques directly to actual explosions at this time and hope to unravel the molecular sequence of events. However, it should be possible to learn a great deal by applying existing probes to simplified pseudo-detonations, while at the same time developing the necessary probes and protocols to eventually allow realistic detonation studies. Consequently during the past year detonations have been mimicked by using picosecond duration UV light pulses to dissociate small relevant molecules in the gas phase. The picosecond timescale of these experiments is a good approximation to the rapid energy uptake of molecular species from a detonation wave. The immediately formed excited states and fragments and their rates of decay to other species should bear close resemblance to those occurring in explosive detonations. The goal of these studies was to identify species, measure their lifetimes and determine which spectroscopic techniques would be best for their detection. In those cases where detection has proven difficult with existing techniques, new diagnostic schemes are under development.

A variety of emissive fragments (CN, C<sub>2</sub>, NH, CH, NO<sub>2</sub>, etc.) have been generated by u.v. photolysis of several parent molecules. These fragments are species we expect to see in the initial steps of nitramine chemistry. Parent molecules studied include Nitromethane (Section i), Acetonitrile (Section ii), and cyanobearing species (Section iii). The studies described in i detail simple low intensity dissociation of the parent molecules via a one photon process. In section ii and iii, the light fluxes were considerably higher and the fragmentation caused by two and three photon processes as well as the creation of 'super excited' states. Section iv gives a short description of an extremely useful spectroscopic technique called picosecond continuum broadband CARS, which has been recently developed under this program.

(i) Nitromethane

An extensive series of experiments were performed on nitromethane gas and on several compounds related to nitromethane. The gas at pressures from 0.1 to 10.0 torr was photolyzed with pulses at 264 nm, the fourth harmonic of the Nd:glass laser. A second laser pulse at 527 nm, delayed with respect to the first photolyzing pulse, was sent into the gas to probe the species present by the laser induced fluorescence technique (LIF). Light emitted from the gas cell was detected with a phototube/ oscilloscope system, the spectrum of the light being determined by combinations of color filters.

In summary the findings were as follows:

- 1) Nitromethane is photolyzed by 264 nm light to yield the CH<sub>3</sub> (methyl) and NO<sub>2</sub> radicals. The NO<sub>2</sub> radical is identified by its

emission spectrum, emission lifetime, and considerations of energetics. The methyl radical is not observed directly, but its presence is inferred from the observation of  $\text{NO}_2$ .

2) The time required for the decomposition of  $\text{CH}_3\text{NO}_2$  upon absorption of a 264 nm photon is very short, less than the 5 ps resolution of our glass laser.

3) The photolysis is a single quantum effect - i.e. the yield of  $\text{NO}_2$  is linear in UV energy.

4) Two species of  $\text{NO}_2$  are produced in the decomposition of nitromethane: ground state  $\text{NO}_2$  and electronically excited  $\text{NO}_2^*$ .

The ground state fragments can be seen only when they are exposed to the LIF probe pulse which excites them to emit light. The  $\text{NO}_2^*$  fragment is created in an emitting state. The latter species is probably kinetically "hot" (i.e. fast moving) since its emission (collisional) lifetime is significantly shorter than the LIF-probed ground state  $\text{NO}_2$ .

5) The quantum yield of  $\text{NO}_2$  is high -  $70\% \pm 30\%$  - thus most UV photons absorbed by nitromethane result in molecular decomposition.

6) The analogs of nitromethane do not all respond in the same fashion. Deuterated nitromethane and nitroethane appear to photolyze in a manner indistinguishable from nitromethane.

2-methyl-2 nitromethane and chloropicrin (trichloro-nitromethane) yield  $\text{NO}_2^*$  fragments, but no ground state  $\text{NO}_2$ . LIF techniques produce no signal. The quantum yield of  $\text{NO}_2^*$  from chloropicrin is perhaps ten times as large as that for nitromethane.

Several follow-on experiments were performed on these materials, prompted by the observations 4) through 6) above on quantum yields. Noting from the UV absorption spectra of these compounds that they have at least two electronic transitions in the energy neighborhood of our photolyzing pulse. The photolyzing energy was shifted using a Raman-shifting cell. The two electronic transitions are labeled  $\pi-\pi^*$  for the higher energy and  $n-\pi^*$  for the lower, with the  $n-\pi^*$  absorption generally being regarded as responsible for the photolysis of nitromethane. The evidence from the Raman-shifted photolyzing experiments is that the  $\pi-\pi^*$  transition is responsible for decomposition to the  $\text{NO}_2^*$  fragment, while  $n-\pi^*$  excitation at lower energies causes photolysis to ground state  $\text{NO}_2$ . Results for chloropicrin were consistent with earlier observations -only  $\text{NO}_2^*$  was observed -LIF revealed no ground state  $\text{NO}_2$ , and when lower energy photolysis was attempted such that the  $\pi-\pi^*$  transition was not activated, no photolysis of any sort was observed.

One significant fact from the viewpoint of obtaining information about energetic materials that should be emphasized is that the kinetic energy of the fragments (i.e. their molecular velocity) appears to be a function not directly of the photon input but rather of the electronic state excited: the  $\pi-\pi^*$  transition results in fast moving photofragments. Thus maximizing energy output from a fuel or explosive may depend critically upon the predissociative states available in that material and upon our ability to access those states.

(ii) Acetonitrile

In contrast to the studies with acetylene (reported in last year's) all emissive fragments (CN, C<sub>2</sub>, NH, and CH) from acetonitrile appear with pressure-dependent rates. The dominant components of emission are the CN B<sup>2</sup>Σ<sup>+</sup>→X<sup>2</sup>Σ<sup>+</sup> violet system and the C<sub>2</sub>d<sup>3</sup>Π<sub>g</sub>→a<sup>3</sup>Π<sub>u</sub> Swan system. Over the pressure range 0.27-10 torr, the temporal properties of these emissive fragments have been studied.

The rise of the CN and C<sub>2</sub> populations have been characterized by pseudo first order rate constants  $k_1^V$  and  $k_1^S$ , which exhibit a linear pressure dependence. The formation rates of the fragments must correspond to the decay rates of some unobserved precursors; and the zero pressure intercepts reflect unimolecular processes depleting the precursor. The removal rate for the precursors in collisions with the parent CH<sub>3</sub>CN was determined. For CN B<sup>2</sup>Σ<sup>+</sup>, the bimolecular quenching constant,  $k_q$ , of  $13 \pm 2 \times 10^{-10} \text{ cm}^3 \text{ s}^{-1}$  and for C<sub>2</sub> d<sup>3</sup>Π<sub>g</sub>  $k_q$  is  $19 \pm 1 \times 10^{-10} \text{ cm}^3 \text{ s}^{-1}$ . The non-zero intercepts correspond to precursor lifetimes of 20 ns (CN B state) and 33 ns (C<sub>2</sub> d state). The large  $k_q$ 's suggest precursors of ionic or Rydberg character. The former has been ruled out; identical formation rates were obtained in the presence of an applied field of 475V/cm.

Results with isotopically labeled CH<sub>3</sub>CN, make it evident that, as for C<sub>2</sub>H<sub>2</sub>, a major portion of emissive CN and C<sub>2</sub> consist of atoms from a single parent molecule. It has been shown that the preferred channel of CN B state formation preserves the CN moiety of the parent (i.e., CN production involves C-C cleavage). However, the spectrum from <sup>12</sup>CH<sub>3</sub><sup>13</sup>CN confirms the existence of a CN channel involving methyl carbons (i.e., an isomerisation process is involved).

The isotope experiments establish that the formation rate constants,  $k_1^V$  and  $k_1^S$  are composite; they approximate multiple formation channels to a single exponential process. It is possible to compare the rise of emission at the  $^{12}\text{C}^{14}\text{N}(0,1)$  band head for the  $^{13}\text{CH}_3^{12}\text{C}^{14}\text{N}$  and  $^{12}\text{CH}_3^{13}\text{C}^{14}\text{N}$  parents. Such  $^{12}\text{C}^{14}\text{N}$  can not be generated through identical reaction pathways for the two labeled isotopes. Nevertheless, waveforms obtained at 5, 2, 1 and 0.5 torr display very similar pressure-dependent risetimes. This suggests a common precursor for the different source channels. Conceivably the intramolecular  $\text{C}_2$  channel also shares the same intermediate. We consider super excited states e.g.,  $\text{CH}_2\text{CN}^{**}$ ,  $\text{CHCN}^{**}$  may very be precursors.

(iii). Other Cyanobearing Parents

Preliminary fragmentation studies of  $\text{C}_2\text{N}_2$  and  $\text{ClCN}$  indicate that CN B is a dominant product. However, for these parents, we are able to discern a prompt B state population in addition to a pressure-dependent component (the risetime of this process is slower than that for  $\text{CH}_3\text{CN}$ ). The prompt CN emission from  $\text{CH}_3\text{NO}_2$  and the delayed emission from  $\text{CH}_3\text{CN}$  have been observed. This observation is remarkable when one considers the CN bond energy in each parent:  $59\text{kcal mol}^{-1}$  ( $\text{CH}_3\text{NO}_2$ ),  $213\text{kcal mol}^{-1}$  ( $\text{CH}_3\text{CN}$ ). It was determined that the single photon excitation of  $\text{CH}_3\text{NO}_2$  at 264 nm results in  $\text{NO}_2$  cleavage with an efficiency of 0.7 ( $\pm 0.3$ ). Evidently at higher flux levels we are able to compete with the dissociation channel and produce a prompt CN emissive fragment. Neither m-nitrotoluene nor o-nitrotoluene produced emissive CN.  $\text{C}_2$  emission was observed from o-nitrotoluene but not from the meta form.

(iv) Picosecond Continuum Broadband CARS

This method utilizes a picosecond white-light continuum generated in a nonlinear medium as Stokes light in a four photon coherent Raman process and enables an extensive, time resolved antistokes spectrum to be obtained in a single laser shot. Complete information on the position and population of Raman active modes is thus obtained. In normal CARS, three beams are used to generate a fourth intense coherent beam called the antistokes wave. Experimentally, one intense laser source, at  $\omega_L$ , is used to provide two of the beams. This is mixed with a Stokes beam at a frequency  $\omega_S$  such that the difference frequency condition,  $\omega_L - \omega_S = \omega_V$ , is satisfied where  $\omega_V$  is a Raman active vibrational mode. A fourth beam, called the antistokes, is generated at the frequency  $\omega_{AS} = 2\omega_L - \omega_S$ . Photons at  $\omega_S$  and  $\omega_{AS}$  are created at the expense of photons lost from the field at  $\omega_L$ . In the broadband CARS setup, the laser source is at 527 nm and a red continuum constitutes the Stokes source. Consequently a broad antistokes continuum is generated in the blue with resonances,  $\omega_{AS} = 2\omega_L - \omega_S$ , corresponding to the Raman-active vibrational resonances,  $\omega_L - \omega_S = \omega_V$ , of the system under study. The antistokes beam is monitored by a spectrograph coupled to a linear photoelectric recording system and the complete spectrum is conveniently displayed on an oscilloscope.

### III. Shock Wave Studies in Condensed Media

Some of the most energetic explosives would not detonate at all were it not for their nonuniform mechanical response to shock waves. However, the manner in which this mechanical form of energy initiates explosive reactions in condensed media is unfortunately not clearly understood. There are two principle trains of thought currently on the subject. In one interpretation, often called the "catastrophic" theory of shock,<sup>1,2</sup> non-thermal concentrations of energy in certain bonds or vibrational degrees of freedom are induced in molecules on very short time scales (<100ps) by the passage of a shock wave. These inequilibria in the internal excitation then cause bond breakage, free radical formation, polymerization, isomerization and other effects which are not observed in systems subjected to similar stresses from static temperature and pressure. The opposing interpretation, favoring a "benign" theory of shock holds that the above list of effects is due simply to the local rise of temperature and pressure caused by the shock, and that molecular systems relax and redistribute energy among their internal degrees of freedom much more rapidly than any processes occurring in or induced by a shock wave. In this view the shock plays an important role only insofar that it provided a convenient mechanism for quickly heating the explosive.

At present it has not been possible to determine which of the above views is correct because of a scarcity of appropriate data on shock induced transient species. It is extremely difficult to characterize chemical reactions under the extremes of temperature and pressure generated in explosives. Even in test systems under less stressful conditions, experimental difficulties arise in the shock generation process and in synchronizing diagnostic techniques to the subsequent chemistry as well as the single shot nature of the experiments. The laser diagnostic probes that are

being developed under this contract would of course be extremely valuable in obtaining such data. Recently, for example, pulsed spontaneous Raman spectroscopy has been utilized to estimate the temperature behind a detonation shock wave in nitromethane. However, the low repetition rate ( $\sim 1/\text{day}$ ) of this conventional type of experiment and the problems of synchronizing laser to blast wave make this a difficult approach. A program of laser driven shock wave studies coupled with spectroscopic identification of reaction products would avoid synchronization difficulties and could however be performed on a table top setup with respectable repetition rates ( $\sim 10/\text{hr}$ ).

For the last decade, laser fusion programs have been utilizing laser ablative techniques to generate extremely high pressures ( $>100$  Mbar) to compress hydrogen microballoons. We propose to utilize a scaled down (table top) version of this technology to generate shock pressures in the 10-300 kbar range. The physics of the formation and decay of laser-generated shock waves is well known and can be adequately described by a hydrodynamic model.<sup>6</sup> Several groups have generated stress shock waves of this magnitude in materials studies but have not to date applied these techniques to the study of energetic materials. In addition, no one has employed laser probes to examine the states of molecules behind such laser driven shocks. These extensions while obvious and straightforward, will represent a significant advance in the field. The high repetition rates available with this approach would allow extensive experimental surveys to be conducted. It should be possible to repeatedly shock small amounts of different materials as a function of peak pressure and to utilize laser spectroscopy to identify excited state species, molecular conformational changes, free radical formation and new species production.

Consequently, as part of NRL's Special Focus Program on Controlled Energy Release in Energetic Materials a Laser Driven Shock Wave Test facility based on this concept will be constructed. A laser is used to heat a thin opaque metal film contacted to the sample (or acting as a window in the case of a liquid). Rapid heating causes metal evaporation, partial target blowoff and generation of an intense shock wave in the film. The shock wave propagates from the remaining metal into the HE and the subsequent reactions followed using laser spectroscopy.

A high Laser beam is required to achieve intensities sufficient to generate 100 kbar<sup>+</sup> pressures over an area large enough ( $\sim 1\text{mm}^2$ ) to counteract additional rarefaction waves which propagate from the sides of the stressed region. A 1J laser, focused to  $1\text{mm}^2$  will yield pressures of approximately 100 kbar<sup>6</sup>. The laser test facility should therefore allow samples of greater than  $1\text{mm}^3$  to be shocked. A portion of the driver laser pulse can be temporally truncated and employed to generate additional probe frequencies.

On-line Schlieren interferometry or reflectivity measurements will be employed to characterize the shock front on a shot-to-shot basis. Reflectivity measurements are especially attractive as they also yield an on-line estimate of the shock pressure (via the induced change in index of refraction) and will allow the Hugoniot relationships to be determined for materials of interest. Laser probing of chemical changes as a function of time after shock front excitation can be performed. The spatial separation between the shock front and the region probed allows a well defined time interval to be accessed (time delay = distance/shock velocity). This should allow the chemical kinetics to be followed on a nanosecond time scale. It is also possible (and simpler) to remove the sample after shocking and search for end product species using sensitive c.w. Raman techniques. The goal of this

work, however is to employ fast laser spectroscopy to identify the initial steps in shock induced chemistry and compare them with other mechanisms resulting from other initiation techniques.

## PICOSECOND UV PHOTOLYSIS AND LASER-INDUCED FLUORESCENCE PROBING \* OF GAS-PHASE NITROMETHANE

P.E. SCHOEN, M.J. MARRONE, J.M. SCHNUR and L.S. GOLDBERG

*Naval Research Laboratory, Washington, D.C. 20375, USA*

Received 27 May 1982

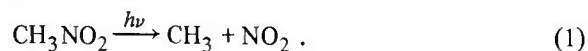
Ground-state NO<sub>2</sub> radicals are formed in <5 ps with a quantum yield of ≈70% in 264 nm photolysis of low pressure nitromethane, as revealed by laser-induced fluorescence probing. Raman shifted photolyzing pulses indicate the NO<sub>2</sub> yield varies little with wavelength, although a small yield of excited state NO<sub>2</sub>\* produced at 264 nm increases significantly at 238 nm.

### 1. Introduction

The UV photolysis of nitromethane has been studied extensively for many years [1–9]. A number of authors have inferred, generally on the basis of chemical analysis of final products, that the primary photodissociation process leads to formation of the free radicals CH<sub>3</sub> and NO<sub>2</sub>. However, identification of these fragments has been difficult because of their high reactivity. The first direct evidence for their presence among the photolysis products of nitromethane was provided by the electron paramagnetic resonance experiments of Bielski and Timmons [3]. Colles et al. [7] utilized optoacoustic detection to provide the first spectral identification of the NO<sub>2</sub> fragment from continuous photolysis of nitromethane. Recently, laser techniques using UV [8,9] and multiphoton IR [10,11] excitation have led to the generation and detection of the NO<sub>2</sub> fragment. In the case of UV laser photolysis in the gas phase, Spears and Brugge observed vibrationally excited NO<sub>2</sub> fragments by means of laser-induced fluorescence (LIF) on a microsecond time scale [8]. However, experiments by Kwok et al. [12] employing nanosecond 266 nm excitation of nitromethane in a supersonic molecular beam and mass spectroscopic fragment detection techniques, observed no photodecomposition under collision-free conditions. More recent work by this

group, using 248 nm photolysis, has resulted in observation of NO<sub>2</sub> photofragments [13].

In this letter, we report the first direct observation on a picosecond time scale of fragment formation in the UV photolysis of gas-phase nitromethane. Using a dual-beam experiment with LIF probing, we have determined that NO<sub>2</sub> fragments, identified from their fluorescence spectrum and kinetics, are generated promptly and with high quantum yield by the 264 nm excitation, within the 5 ps pulse resolution of the experiment. This supports assignment of the primary reaction as:



### 2. Experiment

The nitromethane samples were obtained from Baker reagent grade material, which we distilled under nitrogen, collecting the middle fraction, b.p. 101–102°C. Individual samples were degassed by several freeze–thaw vacuum pumping cycles. Samples of 0.1–10 Torr pressure were loaded into a 15 cm diameter stainless-steel cell whose interior walls had been coated with black Teflon to reduce scattered light. The entrance and exit cell windows were of lithium fluoride, and internal baffling was provided to prevent window fluorescence induced by the laser pulses from reaching the photodetector. Light emitted at 90°

\* A preliminary account of this work was presented at the Xth International Conference on Photochemistry [25].

from the laser path was collected by a lens and focused through long-wavelength-pass color filters onto a slit in front of an EMI 9658 phototube. The tube had an S-20 photocathode (red sensitive to 900 nm) and a pulse response (fwhm) of 20 ns. The signal was processed by a Tektronix 7912AD digitizing oscilloscope coupled to a Tektronix 4052 computer for time integration of waveforms and for data manipulation and storage.

The laser was a passively mode-locked Nd : phosphate glass oscillator/amplifier system [14] which generated 1054 nm single pulses typically of 5 ps duration and 25 mJ energy at a repetition rate of 0.2 Hz. The IR pulse was frequency-doubled twice to give a photolyzing UV pulse energy of up to 3 mJ at 264 nm. The residual IR pulse energy was separated from the direct laser path by a beam splitter and was frequency-doubled independently, to give a probe pulse of up to 5 mJ at 527 nm. The probe pulse was directed along an optical delay line, and subsequently recombined co-axially with the photolyzing pulse. Both pulses were then sent into the sample cell without focusing, giving a photolyzing beam diameter of  $\approx 4$  mm. Pulse energies were monitored independently with joulemeters on each shot, and were used to normalize the observed sample fluorescence data. The temporal and spectral quality of the pulses were monitored as the experiment progressed by a two-photon fluorescence cell/vidicon and by a 0.8 m spectrograph/Reticon array.

The zero time delay between the UV and probe pulses was determined by a photobleaching measurement in which the two pulses were focused into a thin cell filled with rhodamine 6G dye solution. The UV pulse depopulated the dye ground state sufficiently that a weak probe pulse arriving after the UV pulse was transmitted.

### 3. Results

Fig. 1 shows two representative traces of fluorescence intensity versus time, averaged over eight laser shots, for a nitromethane pressure of 2.2 Torr. The lower trace shows the fluorescence signal for the UV photolyzing pulse alone. The upper trace was generated by a UV pulse plus a 527 nm probe pulse delayed by  $\approx 200$  ps. A probe pulse alone produced virtually no

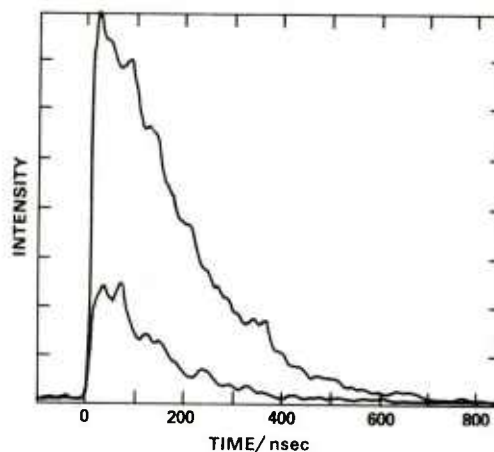


Fig. 1. Fluorescence from photolyzed nitromethane at a pressure of 2.2 Torr, averaged for eight laser shots. Lower trace shows emission resulting from excitation with 264 nm (UV) pulses; upper trace shows emission produced by UV irradiation followed after a 200 ps delay by a 527 nm probe pulse. Emission is filtered in both cases with a Corning 2-73 filter which transmits wavelengths  $>560$  nm.

signal either initially or after hundreds of UV shots into the cell. The emission in fig. 1 was filtered by a Corning 2-73 filter, which transmits wavelengths longer than  $\approx 560$  nm. While the UV pulse itself obviously produces a fluorescing fragment, input of the 527 nm pulse has increased the fluorescence intensity roughly three-fold.

The observed fluorescence has a risetime that is phototube limited; its decay can be fitted satisfactorily, within constraints of the noise, by a single-exponential fall time which is dependent on gas pressure. The decay time for the signal in the UV-only case is  $\approx 0.7$  times that for the LIF signal, suggesting that the initially excited fragments may have a greater collisional cross section or may be produced with a higher velocity distribution than the ground-state product. The integrated fluorescence intensity reaches a maximum at  $\approx 10$  Torr of nitromethane, but the quenching rate at this pressure is too fast to be resolved with our phototube. At our lowest usable nitromethane pressure of 100 mTorr we observe a decay time of  $\approx 1.6$   $\mu$ s. A Stern-Volmer plot of decay rate versus pressure is linear over the pressure range of our experiment, and when extrapolated to zero pressure, indicates a natural lifetime that is quite long. This is consistent with emission from the  $\text{NO}_2$  species whose collision-

free ( $<1$  mTorr) lifetime is approximately  $100 \mu\text{s}$  [15].

The spectral character of the fluorescence emission in both single beam and LIF experiments was also consistent with  $\text{NO}_2$ . Since the signal level was too weak to yield a spectrum with a monochromator or intensified vidicon system, a sequence of long-wavelength-pass filters was used to study the region from probe wavelength to beyond  $750 \text{ nm}$ . The observed emission was spectrally broad, extending throughout the sensitivity region of the phototube, and without any apparent strong narrow-line emission features. Band-pass

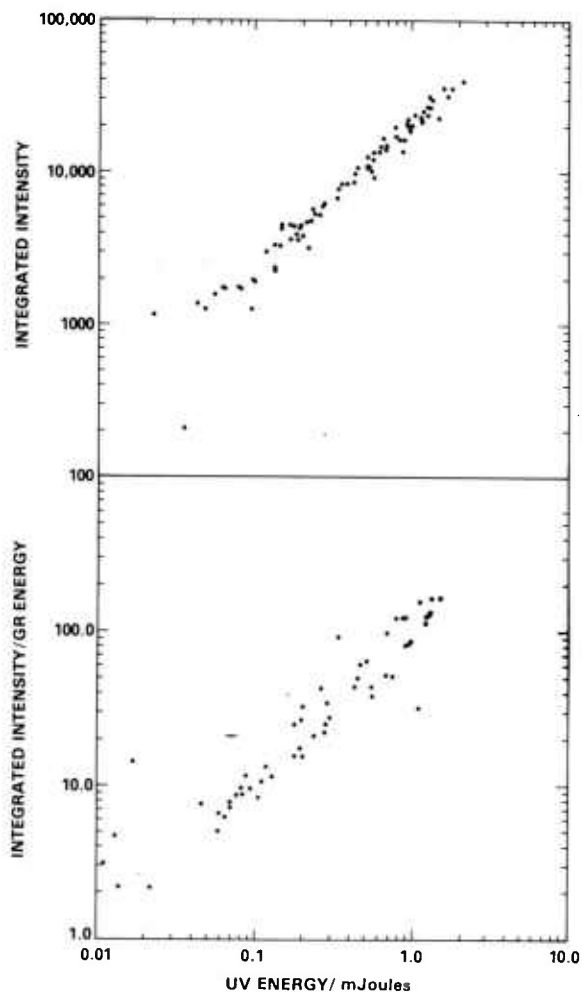


Fig. 2. Fluorescence power-law dependence in nitromethane photolysis at 0.2 Torr: time-integrated fluorescence signal versus UV excitation pulse energy. Upper trace: Fluorescence caused by UV-only excitation. Lower trace: Fluorescence caused by UV + probe excitation, normalized to probe pulse energy. Probe time delay was 1 ns.

filters isolating regions of possible CN and HNO emission showed no discernable signal. Similarly, the anti-Stokes side of the probe wavelength was studied and gave no signal to within our detection limit.

We performed a series of experiments to determine the power-law dependence of the fluorescence. Fig. 2 shows a log-log plot of the time-integrated fluorescence intensity as a function of UV pulse energy, for individual laser shots. The lower curve shows the UV + probe induced fluorescence, normalized by probe pulse energy. The upper curve shows UV-only induced fluorescence. Both curves exhibit a unit slope extending over almost two decades in UV energy, indicating an effect linear in excitation pulse energy. Since the energy of the photolyzing photon is  $\approx 4.7 \text{ eV}$  and C-N bond cleavage requires  $\approx 2.6 \text{ eV}$  [16], the excess energy for single UV photon induced photolysis should yield excited fragments fluorescence only at wavelengths longer than  $\approx 590 \text{ nm}$ . This is supported by our observations, further substantiating that only a single-quantum excitation is involved. The evidence, thus, clearly points to identification of the photofragment as  $\text{NO}_2$ : absorption of the  $527 \text{ nm}$  probe, broad emission spectrum, long lifetime, and the relationship of fluorescence onset wavelength to C-N bond energy.

A variable time delay was introduced between the UV and probe pulses to determine whether there was a measurable induction period between excitation of the nitromethane molecules and the appearance of  $\text{NO}_2$  fragments. The results shown in fig. 3 indicate that the population of ground state  $\text{NO}_2$  probed by the  $527 \text{ nm}$  pulse appears and rises to a plateau within the  $\approx 5 \text{ ps}$  pulse resolution of the experiment. For delay times as long as  $20 \text{ ns}$  the height of the plateau remains approximately constant. Formation time remains unaffected by changes in nitromethane pressure. Each point in fig. 3 represents the time-integrated fluorescence intensity averaged over ten laser shots and normalized to the UV and probe pulse energies. The non-zero fluorescence signal for negative delay times represents the effect of the UV pulse alone.

We have measured the quantum yield for formation of  $\text{NO}_2$  by comparing the signal intensity for LIF in photolyzed nitromethane with that obtained in neat  $\text{NO}_2$  gas. Taking into account the relative quenching rates observed in these two experiments, and using an absorption cross section of  $3 \times 10^{-20} \text{ cm}^2$  at  $264 \text{ nm}$  [17], we calculate the yield of ground electronic state

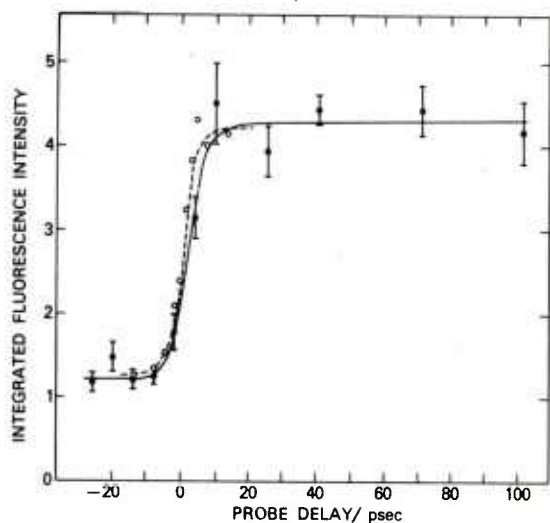


Fig. 3. Solid line: LIF signal as a function of probe time delay for nitromethane at 0.8 Torr. Intensity is normalized to UV and probe pulse energies. Each data point represents an average of ten laser shots. Dashed line: System temporal response function (see text) determined by photobleaching experiment in rhodamine dye solution.

$\text{NO}_2$  to be  $70 \pm 30\%$ . In a representative experiment (0.63 Torr nitromethane,  $185 \mu\text{J}$  UV energy),  $2.2 \times 10^{11}$  ground state  $\text{NO}_2$  photofragments are produced in an observable volume element of  $0.25 \text{ cm}^3$ . A small fraction of these are excited by the LIF probe pulse: for a probe energy of  $940 \mu\text{J}$ , and an  $\text{NO}_2$  absorption cross section extrapolated to  $527 \text{ nm}$  of  $1.4 \times 10^{-19} \text{ cm}^2$  [18], we obtain  $6.2 \times 10^8 \text{ NO}_2$  molecules (0.3%) excited by the probe. Only  $\approx 4.6 \times 10^8$  molecules (0.2%) are produced initially as electronically excited  $\text{NO}_2^*$  in the UV-only experiment.

The dependence of quantum yield on photolyzing wavelength was examined using stimulated Raman scattering in  $\text{H}_2$  gas (5–20 bar) to produce wavelength-shifted excitation pulses at 296 and 337 nm (first and second Stokes) and at 238 nm (first anti-Stokes). The Raman lines were isolated with a dispersing prism before entering the sample cell. Fig. 4 (upper half) shows the wavelength dependence of the quantum yield obtained for excited state  $\text{NO}_2^*$  (UV only) and ground state  $\text{NO}_2$  (UV + probe). The yield for ground state  $\text{NO}_2$  does not vary appreciably over these photolyzing wavelengths. However, the yield for  $\text{NO}_2^*$  increases sharply for 237 nm excitation and becomes essentially zero at 296 nm. These results

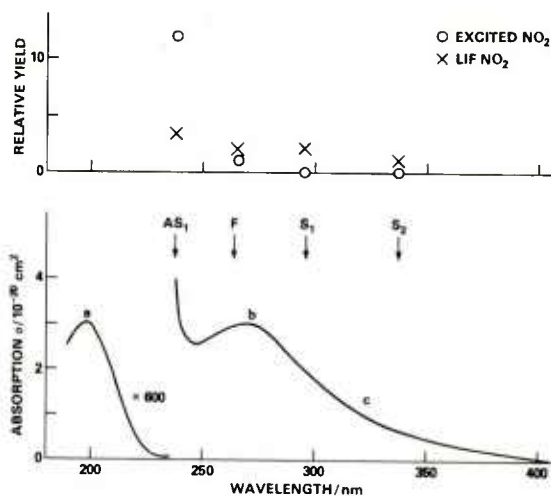
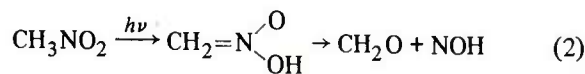


Fig. 4. Upper half: Relative yield of  $\text{NO}_2^*$  (○) and  $\text{NO}_2$  (×) versus wavelength. The yields are not shown to the same scale. Lower half: UV absorption spectrum of nitromethane gas showing the  $\pi \rightarrow \pi^*$  singlet-singlet transition (a), the  $n \rightarrow \pi^*$  singlet-singlet transition (b), and the  $n \rightarrow \pi^*$  singlet-triplet transition (c). The arrows indicate the UV photolyzing wavelengths obtained from stimulated Raman scattering in  $\text{H}_2$ : first anti-Stokes ( $\text{AS}_1$ ), UV fundamental (F), and first and second Stokes ( $\text{S}_1$ ) and ( $\text{S}_2$ ).

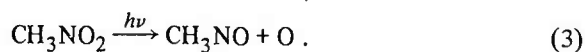
were obtained with the same Corning 2-73 filter before the phototube and are uncorrected for changes in the onset wavelength of  $\text{NO}_2^*$  fluorescence emission for each  $4155 \text{ cm}^{-1}$  Raman shift. Such correction would make the actual increase in  $\text{NO}_2^*$  yield at 237 nm even more dramatic.

#### 4. Discussion

In most early photolysis experiments on nitromethane the final products were determined by chemical analysis, in which case a large number of secondary products were found, including  $\text{CH}_3\text{ONO}$ ,  $\text{CH}_2\text{O}$ ,  $\text{CH}_3\text{NO}$ ,  $\text{NO}$ , and  $\text{N}_2\text{O}$  [4,6,12]. This, and the dependence of the relative quantum yield of methyl nitrite [2] upon the exciting UV wavelength led to the suggestion that there are other primary photolysis processes besides (1), specifically [6]:



and



Rebbert and Slagg [2] suggested that more than one excited state of nitromethane was involved in its decomposition, and Honda et al. [6] and Flicker et al. [19] have supported this idea. Two states are observed in its optical absorption spectrum (fig. 4, lower half) [17,19,20]: a strong feature at  $\approx 198$  nm assigned to a  $\pi \rightarrow \pi^*$  singlet-singlet transition, and a weak satellite at  $\approx 270$  nm suggested to be an  $n \rightarrow \pi^*$  singlet-singlet transition. A third, still lower energy state has been found by electron energy-loss spectroscopy at  $\approx 326$  nm [19], which the authors suggest has  $n \rightarrow \pi^*$  singlet-triplet character, but which may be a composite of overlapping transitions of different character. Theoretical calculations indicate that other transitions may exist in this energy region [21-24], but they have not been identified experimentally. Most investigators have supported process (1) as the main primary photolysis channel for nitromethane [1-5]. Honda et al. [6] and Flicker et al. [19] suggest that the lower energy transition to the triplet state at  $\approx 326$  nm addresses process (1) particularly while the singlet-singlet excitation near 270 nm induces reaction (2).

Our observations that ground-state  $\text{NO}_2$  fragments are formed promptly and with high quantum yield from 264 nm photolysis of low-pressure nitromethane support the conclusion that excitation of the  $n \rightarrow \pi^*$  transition near 270 nm results in dissociation predominantly via reaction (1). The time scale of  $< 5$  ps for  $\text{NO}_2$  production is clearly short compared to any possible mediating collisions. The single-quantum nature of the excitation process has been verified experimentally. Our Raman shifting experiments indicate that the yield of the primary product ground state  $\text{NO}_2$ , as distinct from final products, does not vary appreciably over the excitation range studied. The lower energy transition near 326 nm does not appear to have a significant effect upon this reaction. These experiments do show, however, that the higher energy  $\pi \rightarrow \pi^*$  transition near 198 nm is probably responsible for  $\text{NO}_2^*$  production.

#### Acknowledgement

The authors wish to thank Professor R.G. Weiss for his very useful advice and discussions. We also grate-

fully acknowledge the Office of Naval Research Power Program for partial support of this research.

#### References

- [1] E. Hirschlaff and R.G.W. Norrish, *J. Chem. Soc.* (1936) 1580.
- [2] R.E. Rebbert and N. Slagg, *Bull. Soc. Chim. Belges* 71 (1962) 709.
- [3] B.H.J. Bielski and R.B. Timmons, *J. Phys. Chem.* 68 (1964) 347.
- [4] I.M. Napier and R.G.W. Norrish, *Proc. Roy. Soc. A* 299 (1967) 317.
- [5] R.B. Cundall, A.W. Locke and G.C. Street, in: *The chemistry of ionization and excitation*, eds. G.R.A. Johnson and G. Scholes (Taylor and Francis, London, 1967) pp. 131-140.
- [6] K. Honda, H. Mikuni and M. Takahashi, *Bull. Chem. Soc. Japan* 45 (1972) 3534.
- [7] M.J. Colles, A.M. Angus and E.E. Marinaro, *Nature* 262 (1976) 681.
- [8] K.G. Spears and S.P. Brugge, *Chem. Phys. Letters* 54 (1978) 373.
- [9] W.L. Faust, L.S. Goldberg, T.R. Royt, J.N. Bradford, J.M. Schnur, P.G. Stone and R.G. Weiss, in: *Picosecond phenomena*, eds. C.V. Shank, E.P. Ippen and S.L. Shapiro (Springer, Berlin, 1978) p. 43.
- [10] Ph. Avouris, I.Y. Chan and M.M.T. Loy, *J. Photochem.* 13 (1980) 13.
- [11] B.H. Rockney and E.R. Grant, *Chem. Phys. Letters* 79 (1981) 15.
- [12] H.S. Kwok, G.Z. He, R.K. Sparks and Y.T. Lee, *Intern. J. Chem. Kinet.* 13 (1981) 1125.
- [13] Y.T. Lee, private communication.
- [14] L.S. Goldberg, P.E. Schoen and M.J. Marrone, *Appl. Optics* 21 (1982) 1474.
- [15] L.F. Keyser, S.Z. Levine and F. Kaufman, *J. Chem. Phys.* 54 (1971) 355.
- [16] R. Kandel, *J. Chem. Phys.* 23 (1955) 84.
- [17] W.D. Taylor, R.D. Allston, M.J. Moscato, G.B. Fazekas, R. Kozlowski and G.A. Takacs, *Intern. J. Chem. Kinet.* 12 (1980) 231.
- [18] T.C. Hall Jr. and F.E. Blacet, *J. Chem. Phys.* 20 (1962) 1745.
- [19] W.M. Flicker, O.A. Mosher and A. Kuppermann, *Chem. Phys. Letters* 60 (1979) 518.
- [20] S. Nagakura, *Mol. Phys.* 3 (1960) 152.
- [21] J.W. Rabelais, *J. Chem. Phys.* 57 (1972) 960.
- [22] L.E. Harris, *J. Chem. Phys.* 58 (1973) 5615.
- [23] J.N. Murrell, B. Vidal and M.F. Guest, *J. Chem. Soc. Faraday Trans. 11* 71 (1975) 1577.
- [24] K.L. McEwen, *J. Chem. Phys.* 32 (1960) 1801.
- [25] M.J. Marrone, P.E. Schoen, L.S. Goldberg, R.G. Weiss, J.M. Schuur and W.L. Faust, *Xth International Conference on Photochemistry*, The University of Iraklion, Crete, Greece, 6-12 Sept., 1981.

## Picosecond photofragmentation experiments with a repetitively pulsed mode-locked Nd:Phosphate glass laser system

L. S. Goldberg, M. J. Marrone, P. E. Schoen  
Naval Research Laboratory, Washington, D.C. 20375

### Abstract

We describe direct observations on a picosecond time scale of  $\text{NO}_2$  fragment formation from 264 nm photolysis of low-pressure nitromethane. Using laser induced fluorescence probing, we find that the population of ground-state  $\text{NO}_2$  products rises and saturates within  $<5$  ps, with a measured yield of near unity. The experiments were conducted with a newly developed mode-locked Nd:phosphate glass oscillator/amplifier system which can generate energetic short pulses of high beam quality at repetition rates of 1/5 Hz.

### Introduction

Picosecond laser photolysis experiments have enabled study of the primary events in photofragment formation from gaseous and condensed-phase molecular systems. The high time definition for laser initiation and interrogation has afforded a deeper insight into the possible dissociative pathways available to the molecule. We have recently been studying the dynamics of emissive fragment populations produced by multiquantum UV excitation of simple gaseous molecules, among them carbon monoxide<sup>1</sup> and acetylene<sup>2</sup>. In order to study ground-state product formation, we have devised two-beam experiments utilizing laser induced fluorescence (LIF) as the probe technique. This method, in which a probe pulse excites ground-state molecules to a fluorescing state, is particularly well adapted to detecting gas-phase species at low concentrations, substantially below that required for absorption measurements. The present paper will describe experiments in which we use LIF probing to establish, on a picosecond time scale, the formation of  $\text{NO}_2$  radical fragments from UV photolysis of low-pressure nitromethane ( $\text{CH}_3\text{NO}_2$ ).<sup>3</sup> Although this molecule has been subject to extensive study over many years, little direct evidence as to its initial dissociation products exists.<sup>4-8</sup>

We will also describe the mode-locked Nd:phosphate glass laser system used for these measurements, which employs athermal phosphate glass in both oscillator and amplifier stages.<sup>9</sup> The repetitive pulsing capability of this glass laser, and its shorter pulse duration compared with Nd:YAG (5 ps vs. 30 ps), provide significant advantages for its application in picosecond spectroscopy experiments.

### Laser system

Figure 1 shows a schematic of the laser system. The laser rods in both oscillator and amplifier stages were Owens-Illinois EV-4 phosphate glass, which is thermally compensated to minimize optical-path-length changes with temperature. Eastman A9740 saturable dye in 1,2 dichloroethane, flowing through a contact dye cell, was used to passively mode-lock and Q-switch the flashlamp-pumped oscillator. The oscillator was capable of a pulse repetition rate in excess of 1 Hz.<sup>10</sup>

Use of an uncoated 100- $\mu\text{m}$ -thick solid etalon inside the oscillator cavity significantly improved its passive mode-locking performance, while still enabling generation of short pulses. Figure 2 shows the regular bell-shaped pulse trains generated with the tilted etalon in place, evidencing no distortion in the train envelope. The statistical success rate for generating well-formed trains was  $\sim 80\%$ . A  $\text{TEM}_{00}$  spatial mode structure was obtained throughout the pulse train without requiring use of an intracavity aperture. This was rarely achieved without an etalon unless a forcing aperture was used, and then only at markedly higher pumping energy. By maintaining a relatively low value of pulse-train energy, typically 5 mJ, transform-limited pulses could be extracted fairly high in the train envelope ( $\sim 1/3$  of peak, 25  $\mu\text{J}$  energy) before significant spectral broadening and distortion of the pulse due to self-phase modulation occurred.

Figure 3b shows the concurrent spectrum (Reticon recorded) and two-photon fluorescence (TPF) autocorrelation time profile (vidicon recorded) of the pulse selected from the train in Fig. 2, with the 100  $\mu\text{m}$  intracavity etalon. The TPF trace has a contrast ratio close to 3:1. Assuming a Gaussian shape, the deconvolved pulse duration (FWHM) is 4.7 ps; the pulse spectral width (FWHM) is 4.2  $\text{cm}^{-1}$ . This corresponds to a time-bandwidth product  $\Delta\nu\Delta\tau \approx 0.6$ , very near to the transform limit of 0.44 for Gaussian pulses. In Figs. 3a and 3b, use of

50  $\mu\text{m}$  and 150  $\mu\text{m}$  etalons results in pulses that are clearly longer (7.1, 8.5 ps), with corresponding narrower spectra (3.6, 2.4  $\text{cm}^{-1}$ ). Fig. 3d shows a well-formed pulse (3.3 ps, 6  $\text{cm}^{-1}$ ) obtained with no etalon in the cavity. This pulse necessarily was selected early in the train, at  $\sim 1/10$  peak envelope intensity.

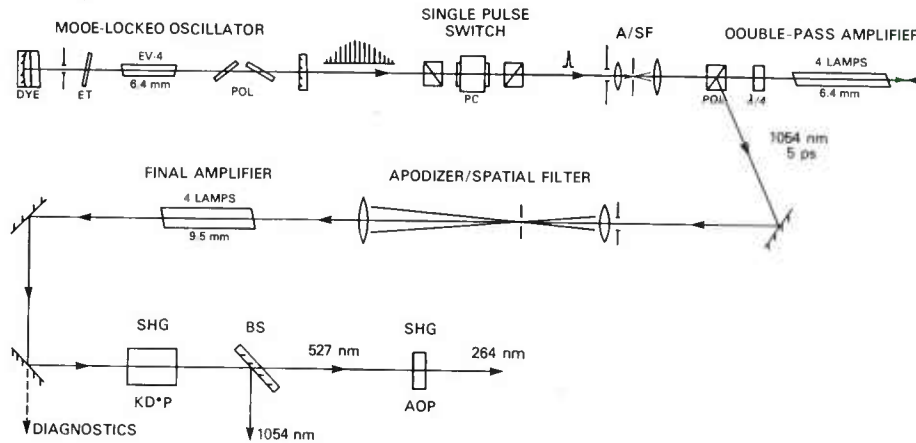


Fig. 1. Schematic of laser system.

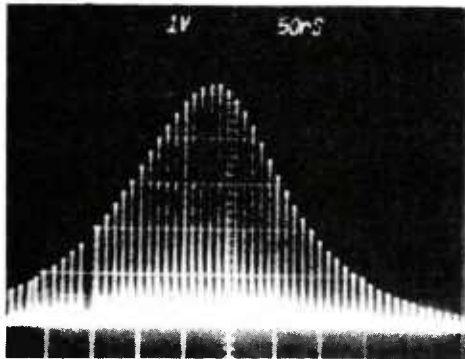


Fig. 2. Mode-locked pulse train with switched out single pulse, 100  $\mu\text{m}$  intracavity etalon.

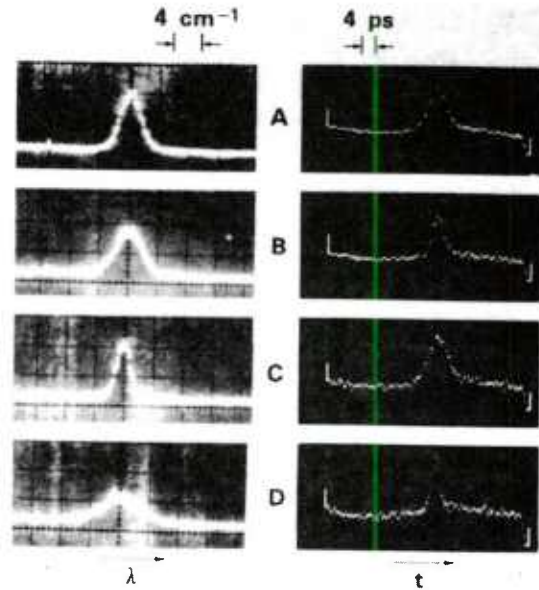


Fig. 3. Spectrum (left) and TPF duration (right) of single laser pulse. (a) 50  $\mu\text{m}$  etalon; (b) 100  $\mu\text{m}$ ; (c) 150  $\mu\text{m}$ ; (d) no etalon.

The single pulse extracted from the oscillator was amplified in two stages, first in a double-pass arrangement (6.4 mm dia. rod) to an energy of  $\sim 3$  mJ, and then in a single pass (9.5 mm dia. rod) to an energy of  $\sim 25$  mJ. For the respective amplifier rod diameters, pulse energies much beyond these values resulted in excessive nonlinear pulse distortion. Each amplifier rod was pumped over a length of 192 mm by a quad-configuration of linear Xenon flashlamps in a close-coupled diffusing pumping chamber (J-K Lasers). A gain of  $\sim 300$  was readily achieved for the double-pass at a total flashlamp energy of 400 J. The good thermal

dissipation in the small diameter rod allowed this amplifier to operate at  $\sim 1/2$  Hz repetition rate without significant thermal lensing. This proved a major convenience for rapid set-up of experiments. The final amplifier provided a gain of  $\sim 15$  at an input energy of 575 J. With the repetition rate set conservatively at  $\sim 1/5$  Hz, a moderate degree of thermal lensing occurred which stabilized within several laser pulses. Burn patterns of the output beam were smooth, showing no noticeable diffraction structure, and were also fairly circular, as a result of the symmetric four-lamp pumping geometry.

Prior to entering each amplifier stage, the laser beam was shaped by apodization to remove the wings of the Gaussian intensity distribution and was spatially filtered. This procedure produced a beam which could better fill the amplifier aperture and propagate without developing edge-generated diffraction ring structure. The spatial filtering removed the high-spatial-frequency intensity fluctuations from the beam, which at high input energies can lead to small-scale self-focusing and consequent optical component damage. Such spatial beam structure also results in a severely modulated intensity profile after successive stages of nonlinear harmonic generation.

The laser second harmonic was generated in a 2-cm-length Type I KDP crystal. Optimum conversion efficiency in this angle-tuned crystal required a highly-collimated beam, since the phase-matching acceptance angle was 0.8 mrad. We obtained a doubling efficiency of approximately 50%, giving a pulse energy of  $\sim 12$  mJ at 527 nm. The fourth harmonic was produced by a second doubling step in a temperature-tuned,  $90^\circ$ -oriented ADP crystal. Because of increased dispersion in refractive indices in the UV, a short 5-mm-length crystal was used. The phase-matching frequency bandwidth then was  $8.8 \text{ cm}^{-1}$ , which adequately encompassed the near-transform-limited spectrum of the 527 nm input pulse. However, the group-velocity mismatch estimated between fundamental and harmonic frequencies was 8 ps, which implies a temporal walk-off in the crystal that should reduce the conversion efficiency and stretch the harmonic pulse.<sup>11</sup> In our experiments, we obtained a pulse energy of  $\sim 3$  mJ at 264 nm, corresponding to a doubling efficiency of approximately 25%. The overall conversion efficiency of pulse energy from 1054 nm to the fourth harmonic was  $\sim 12\%$ .

#### Experimental arrangement

Figure 4 shows the optical arrangement for the two-beam experiment. The probe pulse, at 527 nm, after independent frequency doubling, was directed along an optical delay line and subsequently recombined coaxially with the photolysing beam, at 264 nm. The pulses were sent unfocused into a 15-cm-dia. stainless steel cell. The cell had internal baffling and interior walls coated with black Teflon to minimize stray fluorescence from cell windows from reaching the photodetector. The side collected light was focussed through long-wavelength-pass color filters onto a slit in front of an EMI 9658 Photomultiplier (extended red S-20). The signal was processed by a Tektronix 7912AD digitizing oscilloscope, which was coupled to a Tektronix 4052 computer for time integration of waveforms.

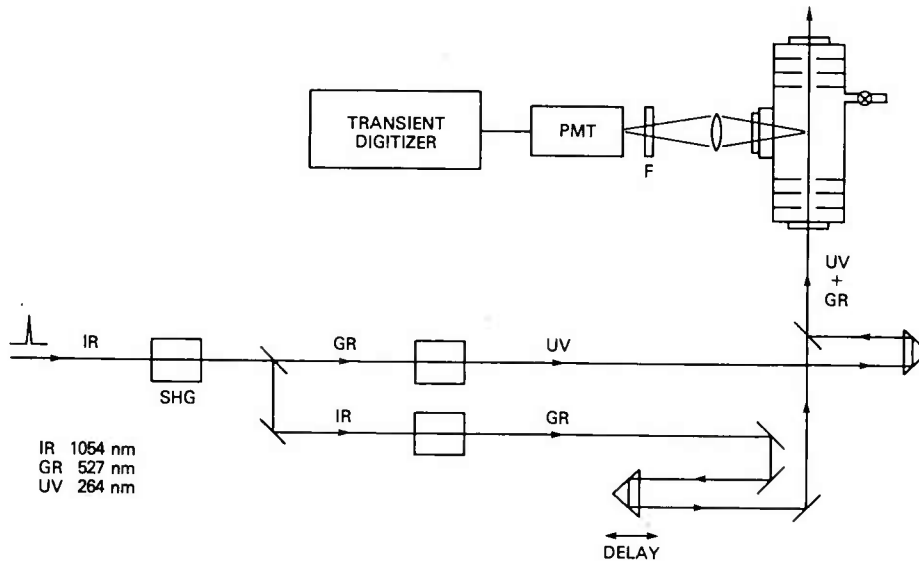


Fig. 4. Schematic of experimental arrangement.

The zero time delay between the UV and probe pulses was determined by a photobleaching experiment in which the two pulses were focused into a thin cell filled with rhodamine 6G dye solution. The UV pulse depopulated the dye ground state sufficiently that a weak probe pulse arriving after the UV pulse would experience reduced absorption and be transmitted.

The nitromethane samples were prepared by distilling Baker reagent grade material under nitrogen, collecting the middle fraction, b.p. 101-102 C. Individual samples were degassed by freeze/thaw pumping cycles, and loaded into the cell at pressures from 0.1 to ~3 Torr.

#### Nitromethane photolysis and LIF probing

Figure 5 shows representative traces of fluorescence intensity ( $\lambda > 560$  nm) versus time, averaged over 8 laser shots, for 2.2 Torr nitromethane. The lower trace shows the fluorescence signal for the UV photolyzing pulse alone. The upper trace was generated by a UV pulse plus a 527 nm probe pulse delayed by 200 ps. A probe pulse alone produced virtually no signal either initially or after hundreds of UV shots into the cell. While the UV pulse itself obviously produces a fluorescing fragment, input of the 527 nm pulse increased the fluorescence intensity roughly 3-fold.

The observed fluorescence showed a single exponential decay time which was strongly dependent on gas pressure. The decay time was roughly the same for the UV-only case as for UV + probe. The collision-free ( $\sim 1$  mTorr) lifetime reported for  $\text{NO}_2$  fluorescence is approximately 100  $\mu\text{s}$ .<sup>12</sup> At our lowest nitromethane pressure of 0.1 Torr we observed a decay time of  $\sim 1.6$   $\mu\text{s}$ . The emission was more rapidly quenched at still higher pressure; at 2.8 Torr the decay time was  $\sim 70$  ns. A Stern-Volmer plot of decay rate versus pressure is linear over the limited pressure range of our experiment and, when extrapolated to zero pressure, indicates a long natural lifetime for the emitting species. Although the fluorescence signal intensity was too weak to yield a spectrum, use of a sequence of long-wavelength-pass filters indicated that in the region from the probe wavelength to  $\sim 750$  nm the probe-induced emission was broad and without any apparent strong spectral line features. Similar emission characteristics were observed for the fluorescence induced by the UV pulse alone. Emission on the antistokes side of the probe wavelength was too weak to be detected. Thus the broad spectral character and long lifetime of the emitting species are clearly consistent with  $\text{NO}_2$ .

Figure 6 shows a log-log plot of the time-integrated fluorescence intensity as a function of UV pulse energy, for individual laser shots. The lower curve shows the UV + probe induced fluorescence, at 1 ns delay, normalized by probe pulse energy. The upper curve shows UV-only induced fluorescence. Both curves exhibit a unity slope extending over almost 2 decades in UV energy, indicating an effect linear in excitation pulse energy. The energy of a single UV photon is 4.7 eV, and C-N bond scission requires approximately 2.6 eV. An  $\text{NO}_2$  fragment produced initially in an excited state by absorption of a single UV photon would have sufficient excess energy to fluoresce at wavelengths only beyond  $\sim 590$  nm, which is consistent with our observations.

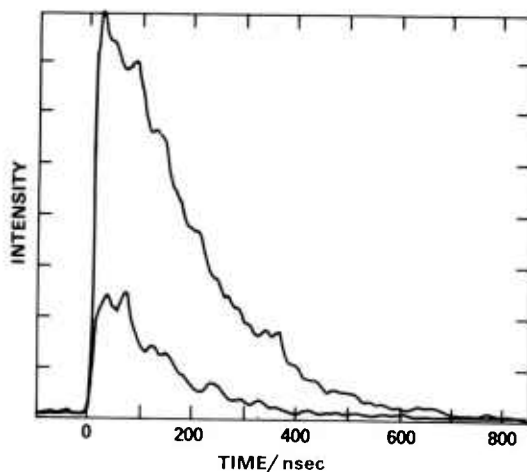


Fig. 5. Waveforms of fluorescence ( $>560$  nm) from photolyzed nitromethane at 2.2 Torr. Lower trace: 264 nm excitation alone; upper trace: UV + 527 nm probe delayed by 200 ps.

A variable time delay was introduced between the UV and probe pulses to determine whether there was a measurable induction period between excitation of the nitromethane molecules and the appearance of  $\text{NO}_2$  fragments. The results shown in Fig. 7, for 0.8 Torr nitromethane, indicate that the population of ground-state  $\text{NO}_2$  fragments probed by the 527 nm pulse appears and rises to a plateau within the  $\sim 5$  ps pulse resolution of the experiment. For delay times as long as 20 ns the induced fluorescence signal remained approximately constant. The observed formation time was unaffected by changes in nitromethane pressure. Each point in Fig. 7 represents the time-integrated fluorescence intensity averaged over ten laser shots and normalized to the UV and probe pulse energies. The non-zero fluorescence signal for negative delay times represents the effect of the UV pulse alone. The dashed line represents the system temporal response function determined by the rhodamine dye photobleaching measurements.

We have measured the quantum yield for formation of  $\text{NO}_2$  in our experiment to be near unity. This is the equivalent of 100  $\mu\text{Torr}$  of  $\text{NO}_2$  produced in the photolysis beam. A prepared sample of 100 ppm of  $\text{NO}_2$  in  $\text{N}_2$  gas was flowed through the cell at 1 Torr pressure. The  $\text{NO}_2$  LIF signal obtained from this trace gas sample was measured and compared directly with the LIF signal from  $\text{NO}_2$  produced by nitromethane photolysis. The data were normalized to probe pulse energies and account was taken of the different fluorescence quenching rates. The UV energy deposited in the nitromethane sample was determined using the absorption cross section of  $3 \times 10^{-20} \text{ cm}^2$ .

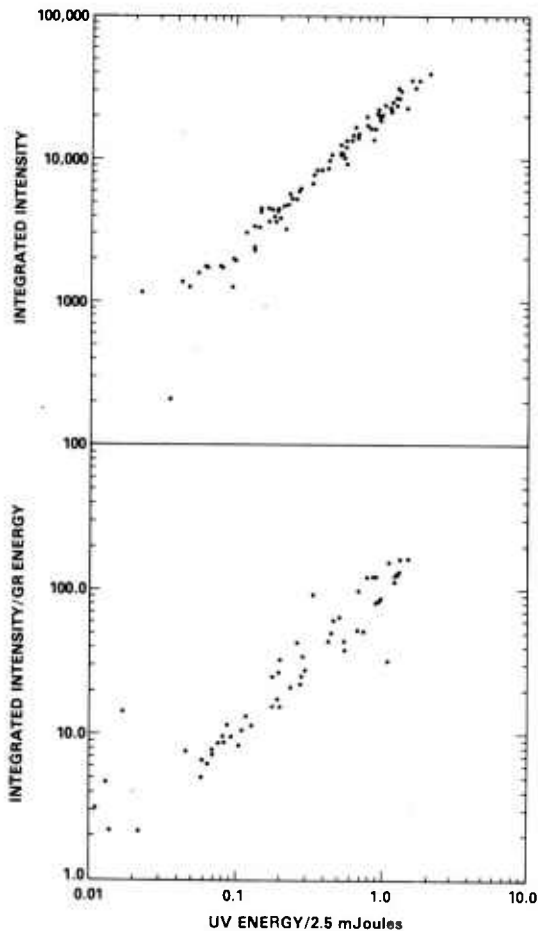


Fig. 6. Power-law dependence of fluorescence intensity versus UV pulse energy, for 0.2 Torr nitromethane. Upper: UV only; lower: UV + probe delayed by 1 ns.

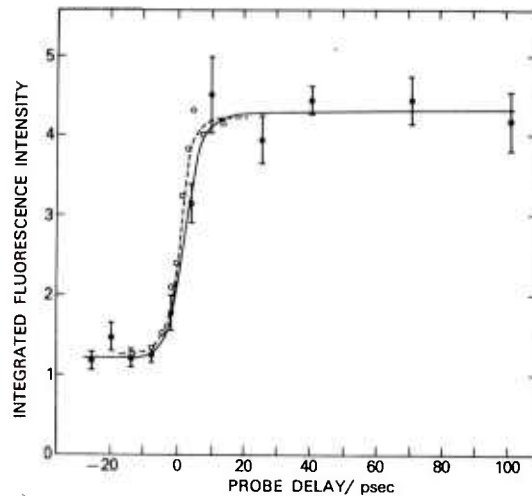


Fig. 7. Induced fluorescence signal as a function of probe time delay, normalized to UV and probe pulse energies, for 0.8 Torr nitromethane. Dashed line: system temporal response determined by photobleaching experiment in rhodamine dye solution.

### Discussion

The observation that ground-state NO<sub>2</sub> fragments are formed promptly from 264 nm photolysis of low-pressure nitromethane supports assignment of the reaction as:



The time scale of <5 ps for their production is clearly short compared to any possible mediating collisions. The single-quantum nature of the excitation process has been verified experimentally. The quantum yield measured at this photolyzing wavelength is near unity, implying that this is the principle decay channel.

Spears and Brugge<sup>6</sup>, in microsecond photolysis experiments at 253 nm, observed vibrationally-excited NO<sub>2</sub> products by means of LIF probing. They interpreted their results as an indirect predissociation of the nitromethane molecule, requiring vibrational redistribution of the excitation energy before C-N bond cleavage. However, recently, Kwok, He, Sparks and Lee<sup>8</sup> photolyzed nitromethane at 266 nm in a molecular beam under collision-free conditions and, using mass spectroscopy detection techniques, observed no dissociation products from the isolated nitromethane molecule. They concluded that CH<sub>3</sub>NO<sub>2</sub> excited at 266 nm does not dissociate directly, but likely requires a collisionally-assisted process. Their estimated detection sensitivity placed an upper bound on yield at ~3%.

Rebbert and Slagg<sup>13</sup> have suggested that more than one excited state of nitromethane is involved in its decomposition. Honda et al.<sup>14</sup> and Flicker et al.<sup>15</sup> have supported this view. Two states are observed in its optical absorption spectrum: 15-17 a strong feature at ~198 nm assigned to a  $\pi \rightarrow \pi^*$  transition, and a weak satellite at ~270 nm suggested to be an  $n \rightarrow \pi^*$  singlet-singlet transition. A third, still-lower energy state has been found by electron energy-loss spectroscopy at ~326 nm,<sup>15</sup> which the authors suggest has  $n \rightarrow \pi^*$  singlet-triplet character, but which may be a composite of overlapping transitions of different character. Theoretical calculations indicate that other transitions may exist in this energy region, but they have not been identified experimentally. Most investigators previously have supported reaction (1) as the primary photolysis channel for nitromethane. Flicker et al. and Honda et al. suggest, however, that it is the lower energy transition to the triplet state at ~326 nm that addresses reaction (1) particularly, while the singlet-singlet excitation at ~270 nm induces a molecular elimination reaction yielding CH<sub>2</sub>O and HNO.

Our picosecond photolysis experiments have enabled study of nitromethane photo-dissociation under collision-free conditions and support the conclusion that excitation of the  $n \rightarrow \pi^*$  singlet-singlet transition near 270 nm results in dissociation of CH<sub>3</sub>NO<sub>2</sub> dominantly via reaction (1).

### Acknowledgements

The authors wish to thank R. G. Weiss and J. M. Schnur for many useful discussions. We also thank H-B. Lin of the Brookhaven National Laboratory for providing the calibrated NO<sub>2</sub> trace gas sample. This research was supported in part by the Office of Naval Research.

### References

1. Craig, B. B., Faust, W. L., Goldberg, L. S., and Weiss, R. G., Chem. Phys. Lett., Vol. 83, pp.265-269. 1981.
2. Craig, B. B., Faust, W. L., Goldberg, L. S., and Weiss, R. G., J. Chem. Phys., in press. 1982.
3. Schoen, P. E., Marrone, M. J., Schnur, J. M., and Goldberg, L. S., Chem. Phys. Lett., to be published. 1982.
4. Bielski, B. H. G., and Timmons, R. B., J. Phys. Chem., Vol. 68, pp. 347-352. 1964.
5. Colles, M. J., Angus, A. M., and Marinero, E. E., Nature, Vol. 262, pp.681-683. 1976.
6. Spears, K. G., and Brugge, S. P., Chem. Phys. Lett., Vol. 54, pp. 373-377. 1978.
7. Faust, W. L., Goldberg, L. S., Royt, T. R., Bradford, J. N., Williams, R. T., Schnur, J. M., Stone, P. E., and Weiss, R. G., in Chemical Physics, Vol. 4, Picosecond Phenomena, Springer-Verlag, New York 1978.
8. Kwok, H. S., He, G. Z., Sparks, R. K., and Lee, Y. T., Internat. J. Chem. Kinetics, Vol. 13, pp. 1125-1131. 1981.
9. Goldberg, L. S., Schoen, P. E., and Marrone, M. J., Applied Optics, in press. 1982.
10. Royt, T. R., Optics Comm., Vol. 35, pp. 271-276. 1980.
11. Glenn, W. H., IEEE J. Quantum Electr., Vol. QE-5, pp. 284-290. 1969.
12. Donnelly, V. M., and Kaufman, F., J. Chem. Phys., Vol. 69, pp. 1456-1460. 1978.
13. Rebbert., R. E., and Slagg, N., Bull. Soc. Chim. Belges, Vol. 71, p. 709. 1962.

14. Honda, K., Mikuni, H., and Takahasi, M., Bull. Chem. Soc. Japan, Vol. 45, pp. 3534-3541. 1972.
15. Flicker, W. M., Mosher, O. A., and Kupperman, A., Chem. Phys. Lett., Vol. 60, pp. 518-522. 1979.
16. Taylor, W. D., Allston, T. D., Moscato, M. J., Fazekos, G. B., Kozlowski, R., and Takacs, G. A., Int. J. Chem. Kinetics, Vol. 12, pp. 231-239. 1980.
17. Nagakura, S., Mol. Phys., Vol. 3, pp. 152-162. 1960.

## FABRY-PEROT PHOTOTHERMAL TRACE DETECTION

A. J. Campillo  
U. S. Naval Research Laboratory  
Washington, D. C. 20375

S. J. Petuchowski  
Phoenix Corporation  
McLean, Virginia 22102

Christopher C. Davis  
Department of Electrical Engineering  
University of Maryland  
College, Park, Maryland 20742

H. B. Lin  
Department of Energy and the Environment  
Brookhaven National Laboratory  
Upton, New York 11973

### Abstract

A novel trace gas detection scheme based upon the photo-thermal effect following light absorption is described. The resulting index change, which is proportional to the trace species absorption and concentration, is measured interferometrically in a stabilized Fabry-Perot cavity. An experimental noise limit corresponding to an absorption coefficient of  $4 \times 10^{-8} \text{ cm}^{-1}/\sqrt{\text{Hz}}$  was observed. We discuss possible improvements and estimate the ultimate sensitivities achievable with this technique.

Local interrogation of the index of refraction modulation produced in a medium by photo-induced heating constitutes the basis of several photothermal schemes for measuring small absorptions. Examples include phase fluctuation optical heterodyne (PFLOH) detection<sup>1</sup>, thermal lensing<sup>2</sup>, and laser beam deflection techniques<sup>3</sup>. The first of these has been proven useful in sensitive trace-gas detection schemes<sup>4,5</sup>, the study of aerosol absorption<sup>6</sup> and of microwave absorption in liquids<sup>7</sup>, and has been shown to be competitive with photoacoustic (PA) detection<sup>8</sup>. PFLOH detection monitors the refractive index change by placing the heated sample in a Mach-Zehnder interferometer employing a stable single frequency helium neon laser.

We report a new technique in which the refractive index change is also monitored interferometrically but in a Fabry-Perot cavity incorporating the sample medium, thereby enhancing the detection sensitivity over that obtained in PFLOH detection by a factor which depends on the finesse of the cavity. The finesse expresses the ratio of peak spacing to peak full-width at half-maximum for the transmitted probe power as a function of optical phase delay per pass. We have demonstrated the feasibility of this scheme in a preliminary experiment in which a calibrated mixture of NO<sub>2</sub> in nitrogen flowed through a Fabry-Perot cavity and its absorption at 514.5 nm was detected.

An experimental noise limit corresponding to an absorption coefficient of  $4 \times 10^{-8} \text{ cm}^{-1}/\sqrt{\text{Hz}}$  was observed. In this letter we discuss possible improvements and estimate the ultimate sensitivities achievable with this technique. It appears that measurement of absorption coefficients less than  $10^{-10} \text{ cm}^{-1}$  is possible.

As in kindred photothermal detection techniques, energy is deposited and excites the medium by resonant absorption of electromagnetic radiation.

Collisional relaxation of the excited mode results in local heating of the background medium and, consequently, to induced local variation in the density of the medium. Detection by transduction of the pressure change is the basis of PA which necessarily involves the integration of signal over the volume from which acoustic or barometric waves impinge on the transducer. The density variation is also manifested in the concomitant change of index of refraction given, in a gas, by the Clausius-Mossotti relation:

$$dn = - (n-1)dT/T_{\text{abs}}, \quad (1)$$

where  $n$  is the refractive index,  $T_{\text{abs}}$  is the absolute temperature, and  $dT$  is the increment of induced local temperature elevation. Over a pathlength  $L$ , this change is tantamount to a variation in optical path or phase delay of:

$$d\phi = (\pi L/\lambda) dn \quad (2)$$

where  $\lambda$  is the wavelength of the probe beam whose heating effect, can be neglected.

Our technique is based upon the multipass interferometric measurement of optical path variations in a Fabry-Perot etalon containing the excited medium. Since only the path traversed by the probe beam is interrogated, this technique affords spatial resolution and the application to tomographic flame analysis is suggested.

The fractional transmission of an ideally monochromatic probe beam through the etalon is a periodic function of the optical phase delay per traversal,  $\phi$ :

$$\begin{aligned} T &= T_{\text{max}} f(\phi) \\ f(\phi) &= (1 + \delta \sin^2 \phi)^{-1} \\ \delta &= (F/\pi)^2 \end{aligned} \quad (3)$$

where  $F$  is the cavity finesse. Maximum sensitivity of transmission to variations in phase delay occur at a phase delay of  $\phi_0$  for which:

$$\cos 2\phi_0 = 1/2 \sqrt{9 + 4/\delta + 4/\delta^2} - 1/\delta - 1/2 \quad (4)$$

$$\approx 1 - 2/(3\delta)$$

$$\delta \gg 1$$

The trace detection technique entails maintaining the static phase delay at  $\phi_0$  by means of servo-control of the etalon spacing and inducing a periodic phase perturbation,  $\phi_m \cos \omega_m t$ . In the case of  $\delta \gg 1$ ,

$$f(t) \approx \left\{ 1 + 1/3 \cos 2\phi_m \cos \omega_m t + \delta/3 \sin 2\phi_m \cos \omega_m t \right\}^{-1} \quad (5)$$

From the small argument limit of the Bessel function expansion, one obtains the Fourier component of the transmitted intensity at the fundamental excitation frequency:

$$T^{\omega_m} = T_{\max} \frac{\sqrt{3\delta}}{2} \phi_m = T_{\max} \frac{\sqrt{3}}{\pi} F \phi_m \quad (6)$$

It is thus evident that the induced signal, in the linear limit, is directly proportional to the finesse. The attraction of this technique is the smaller sample path required for comparable sensitivity to that afforded by the Mach-Zehnder PFLOH configuration.

This advantage is translated into increased detection sensitivity only to the extent that the source of limiting noise is not similarly enhanced. Of the contributions to system noise, phase noise of the probe source laser (deviation from monochromaticity), mechanical noise inducing either a cavity  $\langle \Delta L \rangle$  or beam misalignment, and window effects due to periodic heating of the etalon plates scale with finesse, as does the signal. Amplitude noise on

the source beam can, in principle, be compensated, and detector shot noise depends solely on net power incident on the detector and scales with  $T_{\max}^{1/2}$ .

The experiment was implemented as depicted schematically in Fig. 1. A single-frequency He-Ne laser (Tropel 200) was used as the interferometer source. The Fabry-Perot cavity was a Burleigh RC-110 with an etalon spacing of 12 cm. The mirrors, one flat and one concave ( $R = 6m$ ), were dielectric-coated for high reflectivity at 633 nm, and a finesse of 50 could be achieved. Optical isolation of the reflected beam and phase-matching of the beam into the etalon were accomplished by the polarizer/retarder combination and lens L, respectively. Aperture A was inserted in the cavity to inhibit higher order transverse cavity modes.

Absorption was detected in a flowing calibrated mixture of 99 ppm  $\text{NO}_2$  in nitrogen. The excitation source was the continuous wave beam of an argon ion laser chopped with a mechanical chopping wheel. This 514.5 nm beam was coupled into the Fabry-Perot cavity at a slight angle from the normal so as to minimize dependence of the intracavity excitation density on etalon spacing. Filter F blocked the green beam from detection by the photomultiplier, PM, and no signal was present in the absence of the He-Ne probe beam.

The sample flowed, at a rate of 0.2 l/min, through a windowless cell consisting of a 10-cm long by 3-mm diameter bore glass tube with a central gas inlet mounted centrally in the Fabry-Perot cavity. Both beams were approximately  $\text{TEM}_{00}$  and nearly coaxial with the cell, and focused to beam waists (radius at half field strength) at  $M_1$  of 0.38 mm and 0.2 mm for the excitation and probe beams respectively. In order to maintain the etalon at a spacing corresponding to the optical phase delay of maximum sensitivity in the face of slow thermal drift due to cumulative heating, the difference between the

photomultiplier load voltage and a fixed reference voltage was amplified, integrated, and fed back to a piezoelectric element to translate one of the etalon plates. Noise spectra were measured using a Tektronix 7L5 Spectrum Analyzer.

The heating of a cylindrical gas sample by a Gaussian beam has been studied by Davis and Petuchowski<sup>5</sup>. In the current experiment, the condition of  $b \gg w_e$ , where  $b$  is the container radius and  $w_e$  is the beam parameter of the excitation beam, was not rigorously satisfied. Thus the heating along the axis in the region interrogated by the probe is probably somewhat less efficient at low frequencies than would otherwise be the case. However, at a chopping frequency of 400Hz, the modulation period is short compared to the thermal diffusion time across the sample in air at 1 atm, and:

$$T(r \ll w_e, t) \approx I_0 \alpha / (2C_p \omega_m) \sin \omega_m t, \quad (7)$$

where  $I_0$  is the peak excitation power density,  $\alpha$  is the absorption coefficient of the sample, and  $C_p$  is the specific heat at constant pressure.

Inserting Eq. 7 into earlier expressions for index and optical phase and evaluating, for atmospheric pressure nitrogen,  $n-1=2.92 \times 10^{-4}$ ,  $C_p = 1.17 \times 10^{-3} \text{ cal/cm}^3$ ,  $T_{\text{abs}} = 300^\circ\text{K}$ ,  $\omega_m = 2\pi \times 400 \text{ sec}^{-1}$ ,  $L = 10 \text{ cm}$ ,  $\lambda = 633 \text{ nm}$ , one calculates  $\Delta\phi_m / (I_0 \alpha) = .17 \text{ rad -cm}^3/\text{W}$ .

For 99 ppm  $\text{NO}_2$  ( $\alpha = 6 \times 10^{-4} \text{ cm}^{-1}$ )<sup>9</sup> in 1 atm  $\text{N}_2$ , the phase modulation amplitude due to excitation at 400 Hz with 30 mW average power ( $I_0 = 26 \text{ W/cm}^2$ ) is calculated to be 2.7 mrad. The observed signal is shown against the background noise spectrum in Fig. 3. The ordinate is normalized to the DC voltage corresponding to maximum transmission indicating a signal of -40 dB or 1.0% modulation. At a finesse of 50, Eq. 6 implies an expected signal of 7.3% or -22.7 dB.

The lower sensitivity actually observed is attributed to operation at other than the optimal phase point and possible finesse degradation during the course of the experiment.

The noise floor at 400 Hz shown in Fig. 3 corresponds to a minimum detectable absorption (1 Hz detection bandwidth) of  $1.3 \times 10^{-7} \text{ cm}^{-1} \text{ -W}$  (or 7 ppb  $\text{NO}_2$  with 3 watts excitation). Actual sensitivity was limited by a residual signal of -55.7 dB present even when the cell was continuously flushed with pure  $\text{N}_2$ . This limitation is attributed to synchronous heating of the optics and the adjacent air layers by the excitation beam, and could be overcome by coupling the excitation beams into the cavity transversely to the probe.

In order to estimate ultimate sensitivity limitations of the technique, we note that the noise floor ( $\Delta f = 1\text{Hz}$ ) of -83 dBV observed at 400 Hz is due to mechanical noise,  $\langle \Delta L \rangle / L$ , to which the cavity is as sensitive as to signal. Careful design of a stable etalon, deliberate choice of operating frequency at an acoustic null, and electronic subtraction of source amplitude noise should allow operation limited by shot noise, for our source, at -132 dBV. Density fluctuations in the sample will not limit sensitivity for samples at atmospheric pressure even of dimensions on the order of the He-Ne beam waist.

Shot noise limited detection with a cavity finesse of 50 corresponds to a phase sensitivity of  $9 \times 10^{-9} \text{ rad}/\sqrt{\text{Hz}}$ . Considering the extreme stability required, this might be achievable only in sealed environments or condensed phase samples. A more reasonable phase sensitivity of  $10^{-7} \text{ rad}/\sqrt{\text{Hz}}$  in our system with  $L = 1 \text{ cm}$  corresponds to an absorption sensitivity of  $1.9 \times 10^{-10} \text{ cm}^{-1} \text{ -W}$ .

We have demonstrated a simple interferometric technique for performing photothermal spectroscopy of transparent media with extreme sensitivity and spatial resolution.

## References

1. C. C. Davis, Appl. Phys. Lett. 36, 515 (1980).
2. J. P. Gordon, R. C. C. Leite, R. S. Moore, S. P. S. Porto and J. R. Whinnery, J. Appl. Phys. 36, 3 (1965).
3. J. C. Murphy and L. C. Aamodt, J. Appl. Phys. 51, 4580, 1980.
4. A. J. Campillo, H-B. Lin, C. J. Dodge, and C. C. Davis, Opt. Lett. 5, 424 (1980).
5. C. C. Davis, S. J. Petuchowski, Appl. Opt. 20, 2539 (1981).
6. A. J. Campillo and H-B. Lin, SPIE Proceedings 286, 24 (1981).
7. M. L. Swicord and C. C. Davis, Radio Science, in press.
8. Y. H. Pao, ed. Optoacoustic Spectroscopy and Detection (Academic Press, New York 1977).
9. R. W. Terhune and J. E. Anderson, Opt. Lett. 1, 70 (1977).

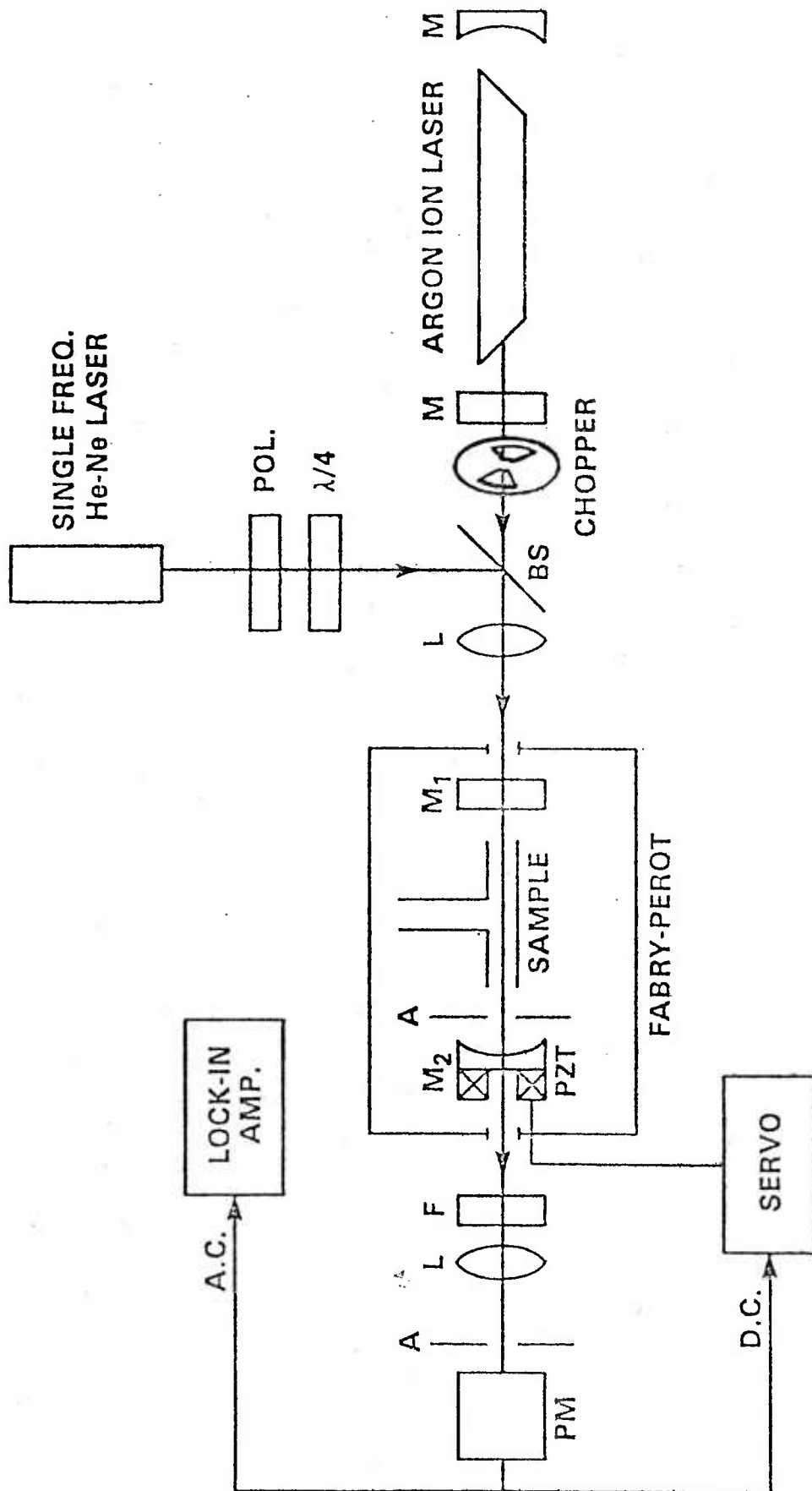


Figure 1: Experimental configuration. BS-beam splitter; L - lens;

M<sub>1</sub>, M<sub>2</sub> - Fabry-Perot mirrors; F - 633 nm bandpass filter;

PM - photomultiplier tube.

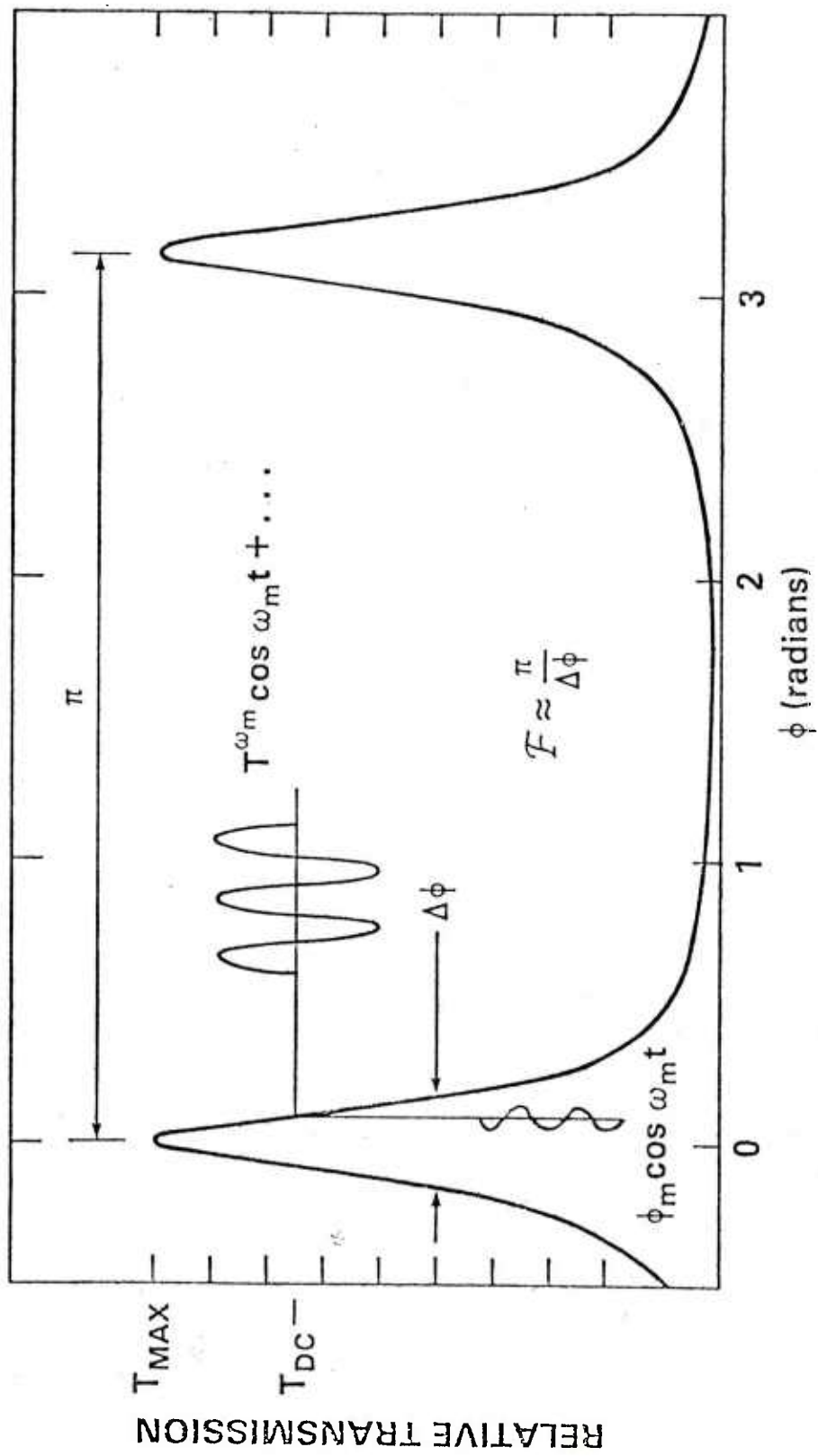


Figure 2: Calculated Fabry-Perot transmission function for a finesse  $F=15$ .

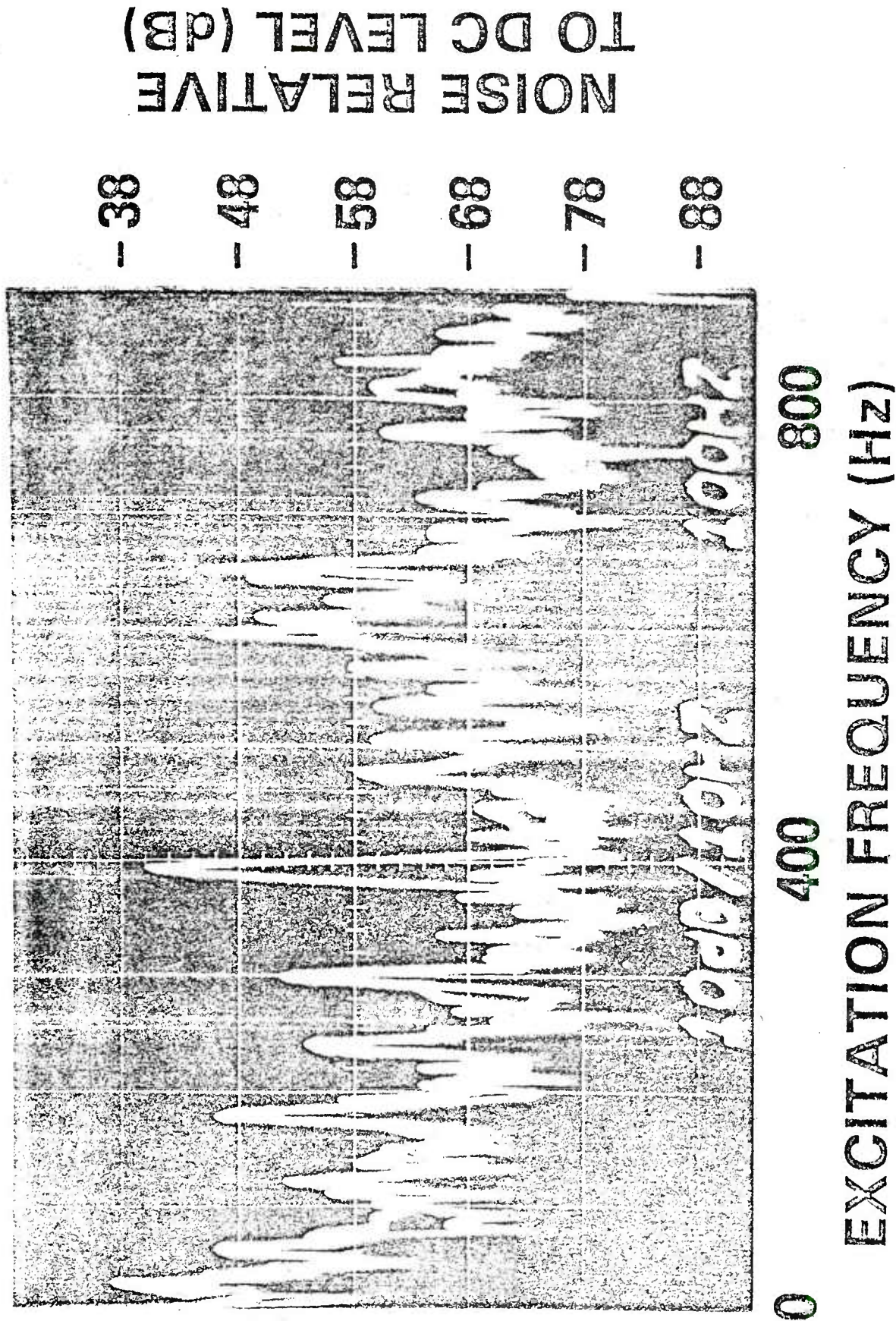


Figure 3: Interferometer noise level, showing signal at 400 Hz due to 99 ppm NO<sub>2</sub> in nitrogen with 30 mW excitation at 514.5 nm.

# UV short-pulse fragmentation of isotopically labeled acetylene: Studies of emission with subnanosecond resolution

B. B. Craig, W. L. Faust, and L. S. Goldberg

Naval Research Laboratory, Washington, D. C. 20375

R. G. Weiss

Department of Chemistry, Georgetown University, Washington, D.C. 20057

(Received 14 December 1981; accepted 8 February 1982)

We have studied fragment emission in the spectral range 200 to 900 nm, following photolysis of acetylene (1–10 Torr) by short ultraviolet pulses (25 ps, 266 nm, 2.5–12 mJ). The dominant component of emission is the  $C_2 d^3\Pi_g \rightarrow a^3\Pi_u$  Swan system. Weak singlet  $C_2$  emission is observed. CH is also observed, in the  $A^2\Delta \rightarrow X^2\Pi$  and  $C^2\Sigma^+ \rightarrow X^2\Pi$  systems. With isotopic labeling and with streak camera recording, we have demonstrated distinct unimolecular and intermolecular processes yielding  $C_2 d^3\Pi_g$ . The unimolecular channel proceeds with risetime  $\tau_1 = 215 \pm 15$  ps, while the pressure-dependent intermolecular component develops over a period of nanoseconds. We discuss the underlying kinetics and the mechanistic implications of the 25 ps excitation.

## I. INTRODUCTION

The primary dissociative channels in vacuum-UV photolysis of acetylene have been inferred by analysis of the final products.  $C_2H$  and an unspecified metastable state, denoted as  $C_2H_2^{**}$ , have been advocated as important intermediates.<sup>1–4</sup> In the present investigation, we have studied the temporal development of emissive fragments produced by short-pulse UV excitation of low pressure (1–10 Torr) acetylene. The high flux of the UV laser source allows nonresonant two-photon absorption by the parent, producing excited states similar to those addressed in VUV excitation. Employing isotopically labeled parents and benefiting from subnanosecond detection risetimes, we have demonstrated both unimolecular and collisional formation of  $C_2 d^3\Pi_g$ . Parallel processes for  $CH A^2\Delta$  and  $C^2\Sigma^+$  are also considered. Dissociative routes for excited  $C_2H_2$ , consistent with  $C_2H$  and  $C_2H_2^{**}$  as intermediates, are discussed.

## II. EXPERIMENTAL

Much of the apparatus has been described previously.<sup>5,6</sup> UV pulses (266 nm, 25 ps) of up to 12 mJ energy were obtained by twice-doubling the amplified single-pulse output from an active/passive mode-locked Nd:YAG laser system. The photolyzing pulse was focused into a static gas sample cell by a quartz lens. A study of the focal region with a Reticon diode array yielded a representative beam diameter of 0.15 mm. Emission was collected through a side window and dispersed in a 1 m Czerny–Turner spectrometer. A Varian VPM-154M crossed-field photomultiplier (sapphire window, GaAs photocathode) provided a spectral range 200–900 nm, and a risetime 0.15 ns. Waveforms were acquired and averaged, typically for 64 laser pulses, with a Tektronix 7912AD digitizing oscilloscope. The net risetime of the detection system was 0.6 ns. Data were processed with a Tektronix 4052 computer system. An OMA II ISIT vidicon also was available for acquisition of time-averaged spectra.

For measurements of emission lifetimes under higher time resolution, we employed an Electrophotonics model 512 streak camera equipped with an S-20 Photochron II streak tube. The Krytron trigger circuitry was modified to reduce sweep jitter. Traces were recorded by a Nuclear Data vidicon system interfaced to a Nicolet minicomputer. To obtain adequate signal levels, color glass filters were used to isolate certain molecular bands. For temporal reference, second-harmonic pulse pairs were provided via a second path to a distinct portion of the streak camera entrance slit. With the sample cell at atmospheric pressure, the first 532 nm pulse was brought into synchronism with the near-instantaneous rise of breakdown emission produced by the 266 nm pulse. The second 532 nm pulse was delivered with a delay set to 500 ps. The streak data were computer-averaged to improve the signal-to-noise of the weak emission. Because of trigger jitter, each streak trace and its corresponding reference were stored individually. The traces were normalized to the response function of the streak camera and vidicon recording system. They were then shifted to a common timing mark and averaged.

Acetylene  $^{12}C_2H_2$  was Matheson high-purity grade, further purified by repeated vacuum distillation from liquid nitrogen/*n*-propanol slush (~148 K) to liquid nitrogen.  $^{13}C_2H_2$  was used as supplied by Merck, Inc. The isotopic content of the heavy acetylene was ascertained to be 83.17%  $^{13}C_2H_2$  and 16.9%  $H^{13}C^{12}CH$ ; this is based upon an analysis by the supplier of isotopic acetaldehyde prepared from acetylene of the same batch.

## III. RESULTS

Acetylene at pressures 1–10 Torr was irradiated under the conditions described above. The triplet  $C_2$  Swan system (430–670 nm) was by far the strongest component of emission. Very weak singlet  $C_2$  emission was observed in the Mulliken system  $D^1\Sigma_u^+ \rightarrow X^1\Sigma_g^+$  (230–240 nm) and in the Deslandres–D’Azambuja system  $C^1\Pi_u \rightarrow A^1\Pi_u$  (340–410 nm).<sup>7</sup> The CH systems

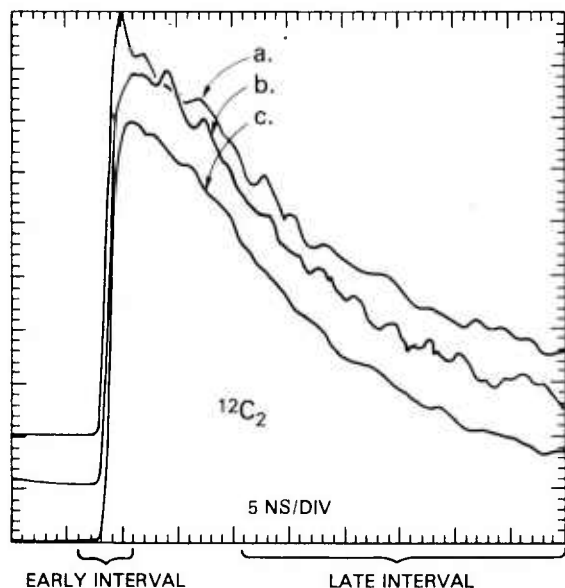


FIG. 1. Comparison of temporal profiles for  $C_2$  Swan emission at bandheads and amid rotation; averages of 64 pulses. The curves have been scaled to equal peak heights. 5 Torr of  $^{12}C_2H_2$ ; the same total pressure pertains for each figure. UV pulse energy  $\sim 12$  mJ. The early and late time intervals identified pertain to integrals employed in subsequent construction of Figs. 3, 4, and 6. (a) (1, 0) bandhead at 473.9 nm. (b) Rotation associated with the (1, 0) head, at 472.7 nm. (c) (2, 1) head at 471.7 nm.

$A^2\Delta - X^2\Pi$  (430–490 nm) and  $C^2\Sigma^+ - X^2\Pi$  (314.5 nm) were also quite evident. There was no emission from molecular species other than these two diatomics. Molecular continua have been observed in other studies of acetylene photolysis,<sup>2,8,9</sup> and continua have been found in our own work with other parents.<sup>5,6</sup> Nevertheless, continuum emission was absent or minimal in the present work with acetylene. Monatomic emission was limited to a few lines; e.g., C (247.6 nm), H (656.3 nm), and C\* (283.7 nm). The integrated intensity for each case was much less than for the diatomics.

#### A. Detailed studies of $C_2$ Swan band emission

Figure 1 displays typical oscilloscope waveforms of the  $\Delta v = +1$  Swan emission obtained from 5 Torr of  $^{12}C_2H_2$ , illustrating similar shapes at two vibrational heads and amid rotation. The risetimes are instrumentally limited. These curves were obtained at relatively high excitation energy ( $\sim 12$  mJ). For decay beyond 80% of the maximum, they accept exponential fits with a time constant  $\tau_2 = 45$  ns. A plot of  $1/\tau_2$  versus acetylene pressure accommodates a straight line through the zero pressure intercept ( $\tau_2 = 119$  ns<sup>3</sup>). The time histories in Fig. 1 therefore represent the residence time of individual  $C_2 d^3\Pi_g$  molecules rather than the destruction of some longer-lived precursor (cf. in contrast Ref. 10). The slope yields an estimate of the quenching constant of  $C_2 d^3\Pi_g$  by  $C_2H_2$ ,  $k_Q = 0.92 \pm 0.1 \times 10^{10}$  cm<sup>3</sup> s<sup>-1</sup>.

Streak camera recording allowed a study of the rise of Swan emission with greatly extended time resolution. Since there was essentially no interfering emission, Schott GG 455 and Corning 5-56 filters (in tandem) served to isolate the  $\Delta v = +1$  and  $\Delta v = 0$  Swan bands near 474 and 516 nm. Figure 2 presents the resolved rise of  $C_2^+$  emission, from 5 Torr of acetylene. The figure includes also the reference pulses and a fit of the rise of Swan emission by a model curve of the form  $1 - \exp(-t/\tau_1)$ , with  $\tau_1 = 215$  ps. Clearly, collisionless  $C_2 d^3\Pi_g$  formation, e.g., unimolecular dissociation, is implied.

To confirm this, we undertook a study of Swan emission from isotopically labeled  $C_2H_2$  parents. On the basis of spectra from the literature,<sup>11</sup> the  $\Delta v = +1$  series was selected for our detailed studies, the signal-to-noise and magnitudes of isotopic splitting being most favorable. Waveforms were acquired representing emission at increments of 0.2 nm over the range 471.1–476.1 nm, encompassing the (1, 0) and (2, 1) bandheads for each of the three isotopic forms. The  $^{13}C_2(3, 2)$  bandhead is also present, but it is not effectively resolved from the  $^{12}C_2(2, 1)$  head. A total pressure of 5 Torr was employed uniformly for the single-isotope materials and for a 1:1  $^{12}C_2H_2$ : $^{13}C_2H_2$  mixture.

For the mixed-parent gas fills it was immediately apparent that the temporal emission profiles at the band heads of  $^{12}C^{13}C$  were not identical in shape to those of the corresponding  $^{12}C_2$  and  $^{13}C_2$  heads. Qualitatively, the  $^{12}C^{13}C$  heads exhibited an excess of emission during an intermediate interval of time,  $\sim 5$ –25 ns after the laser pulse; the asymptotic decays, however, are alike. For a systematic display of this, spectra were constructed as follows: at each wavelength an integral of the emission waveform was taken over an "early" or a "late" interval of time (see Fig. 1; as measured from the laser pulse, early ca.  $-2$  to  $+3$  ns and late  $\sim 13$ –42 ns). Such spectra were obtained for laser amplifier settings yielding two values of average UV pulse energy,  $\sim 2.5$  and 12 mJ. In Fig. 3, two of the curves display low-energy early-integral spectra for the distinct parent gases. The third is a similar spectrum for the mixed parents. At this low level of excitation, the early signal associated with the crossed isotope  $^{12}C^{13}C$  is relatively small; i.e., the prompt product  $C_2$  largely corresponds to the isotopic parents.

Figure 4 displays, for the equal mixture of parents, the four cases of energy and time interval. The progression of curves from low-energy/early to high-energy/late confirms the prompt (unimolecular) process asserted above and illustrates also a delayed (collisional) process in which the isotopes are scrambled.

In Fig. 5 this point is developed in greater detail, by further manipulation of waveforms (data obtained at 5 Torr, with  $\sim 12$  mJ energy). The primary waveform at the wavelength of the  $^{12}C^{13}C$  bandhead, 474.5 nm (curve a of Fig. 5), is *not* a direct history of the scrambling process: rotation attached to the  $^{13}C_2$  bandhead at 475.3 nm underlies the  $^{12}C^{13}C$  bandhead, and the heavy acetylene is not altogether pure. However, we have de-

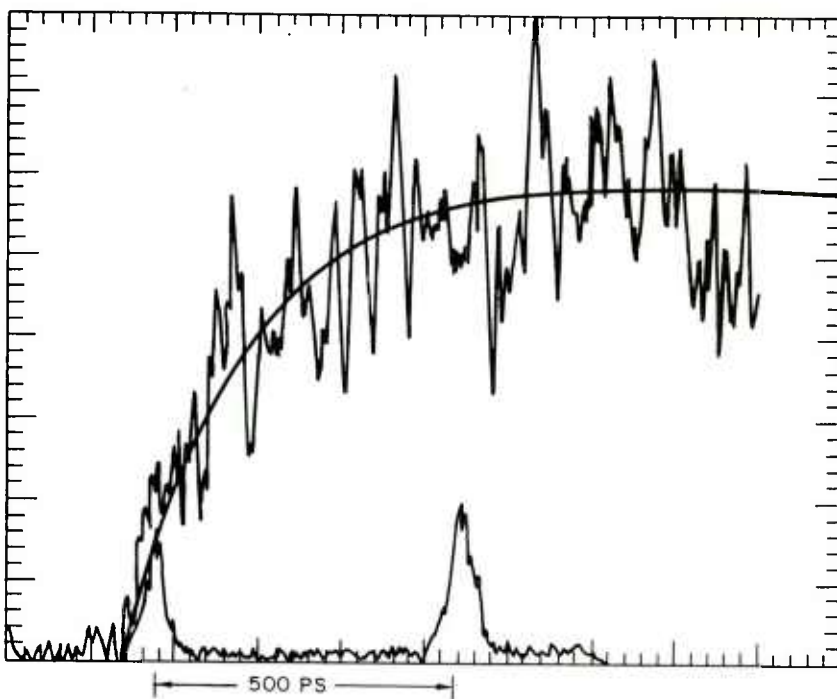


FIG. 2. Streak camera record of the rise of Swan emission in the  $\Delta v = +1$  and  $\Delta v = 0$  bands; the average of 10 pulses. Also shown are a model curve with time constant 215 ps, and second-harmonic reference pulses at a pair separation of 500 ps.

veloped a procedure effectively to strip out the latter components of signal, employing waveforms at 474.5 and 475.3 nm from the heavy-isotope material to establish the relative signal at 474.5 nm due to these

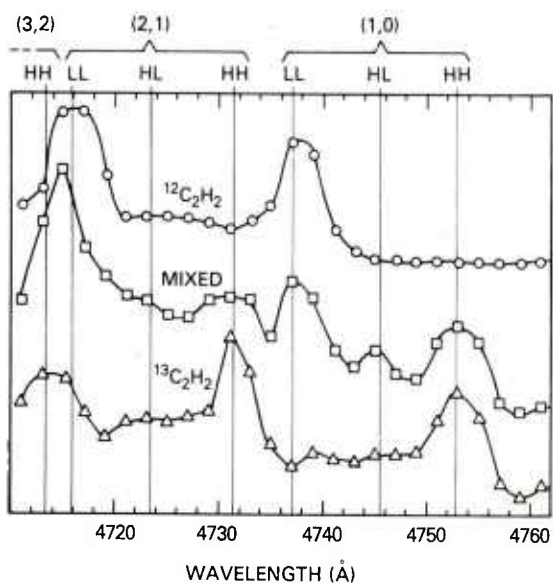


FIG. 3. Spectra of early emission (first 5 ns; see Fig. 1) in the  $C_2$   $\Delta v = +1$  Swan series; UV pulse energy  $\sim 2.5$  mJ. Curves for isotopically distinct parent acetylenes, and for a 1:1 mixture of  $^{12}C_2H_2$  and  $^{13}C_2H_2$ . In Figs. 3, 4, and 6 the notations HH, HL, and LL attached to bandheads refer to light or to heavy carbon masses, respectively as  $^{13}C^{13}C$ ,  $^{13}C^{12}C$ , and  $^{12}C^{12}C$ .

components. Curve *c* in the figure should then represent the collisional production of  $^{12}C^{13}C$  due to the joint presence of both parent acetylene isotopes. Waveforms such as *c* were consistently reproducible. Such data also were gathered and analyzed for 8 and 2.5 Torr of acetylene. The growing-in time was found to decrease with increasing pressure but was uniformly insensitive to the pulse energy; it is clearly indicated that this risetime is controlled by collisions of a precursor with the parent.

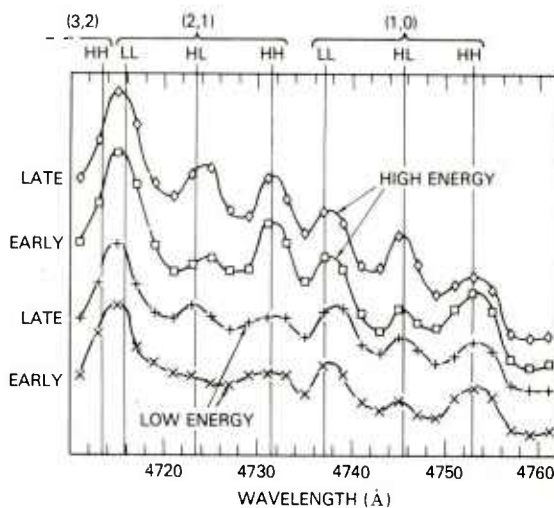


FIG. 4. Spectra of Swan emission ( $\Delta v = +1$ ) within early and within late intervals of time (see Fig. 1); curves for UV pulse energies  $\sim 2.5$  mJ and  $\sim 12$  mJ. 1:1  $^{12}C_2H_2$ : $^{13}C_2H_2$  mixture.

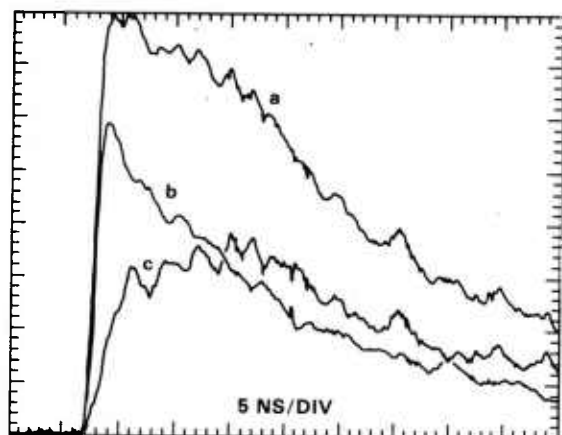


FIG. 5. Construction of the time history of Swan  $^{13}\text{C}^{12}\text{C}$  arising in the collisional process; UV pulse energy  $\sim 12$  mJ. 1:1  $^{13}\text{C}_2\text{H}_2$ : $^{12}\text{C}_2\text{H}_2$  mixture. (a) Primary record of emission at the  $^{13}\text{C}^{12}\text{C}$  (1,0) head, 474.5 nm. (b) Reference waveform obtained by appropriate scaling of the emission record at the  $^{13}\text{C}_2$  (1,0) head, 475.3 nm. (c) Subtraction of curve *b* from curve *a*, representing collisionally formed  $^{13}\text{C}^{12}\text{C}$ .

We have noted that the collisional process is accentuated for higher UV pulse energies (Fig. 4); it is possible to pursue this more quantitatively. For isotopically pure parent gases at equal partial pressures, complete scrambling should yield  $^{12}\text{C}_2$ ,  $^{12}\text{C}^{13}\text{C}$ , and  $^{13}\text{C}_2$  in abundance ratios 1:2:1. At 12 mJ, where the collisional  $\text{C}_2$  formation is most prominent, all-time integrals were constructed of the excess  $^{12}\text{C}^{13}\text{C}$  signal (Fig. 5, curve *c*) and of the  $^{13}\text{C}_2$  signal. The ratio (potentially 2:1) was found to be 1.1:1, corresponding to 70% of total  $\text{C}_2$  produced in the collisional process at this rela-

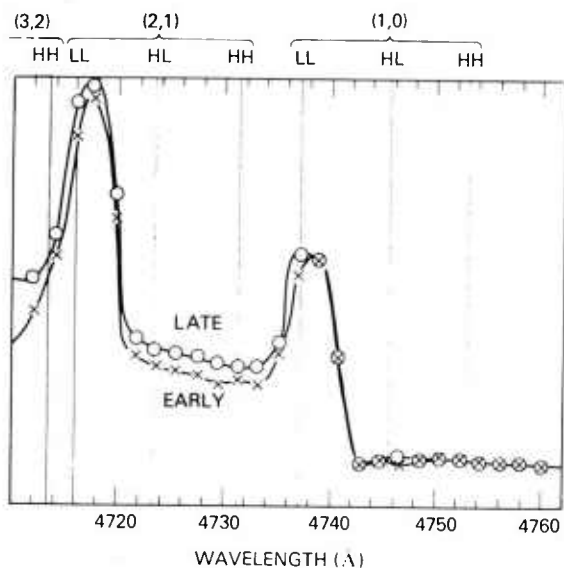


FIG. 6. Comparison of vibrational/rotational distributions for early and late  $\text{C}_2$   $d^3\Pi_g$  populations,  $\Delta v = +1$  series; UV pulse energy  $\sim 12$  mJ.

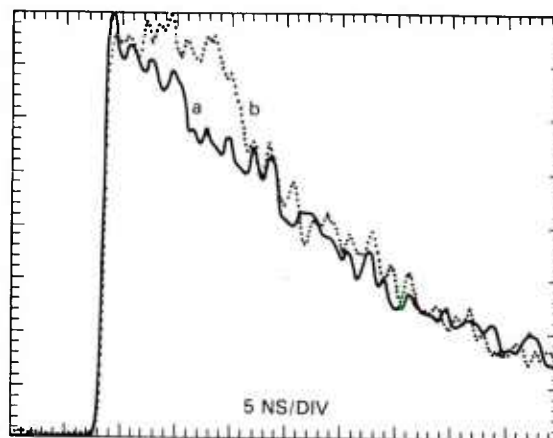


FIG. 7. Comparison of temporal profiles for  $\text{C}_2$  Swan emission amid states of high rotation and at a bandhead. The curves have been scaled to a common late-term signal level. (a) 473.9 nm, the (1,0) bandhead. (b) 462.8 nm, hot rotation.

tively high pulse-energy level.

The participation of two processes generating  $\text{C}_2$   $d^3\Pi_g$ , prompt (unimolecular) and delayed (intermolecular), is regarded as established. It has long been recognized that under many conditions Swan emission exhibits high levels of rotational excitation.<sup>6,9,10,12</sup> Thus it is interesting to consider the possibility of distinct degrees of rotational or of vibrational excitation for the prompt and delayed processes generating  $\text{C}_2^*$ . This question is addressed in Fig. 6, where the data benefit from enhancement of the signal-to-noise ratio inherent in integral spectra. There is no indication of distinct levels of vibrational excitation; but the data points below 473.9 nm, associated with rotational excitation, are uniformly higher for the late-term integrals. Quantitatively, the signal-amid-rotation relative to that at the band head is 20% greater for the late time interval. This modest enhancement of rotational excitation for the intermolecular process proved to be quite reproducible. The vidicon is incapable of gating at a speed appropriate for investigation of this issue by temporal separation. However, a spectrum at 25 Torr shows more rotation than one at 5 Torr; this is consistent with relative enhancement of the collisional process at the higher pressure, and with a higher level of associated rotation for the late collisional process. In a related study of ethylene with 10.6  $\mu$  pulses of 250 ns duration,<sup>13</sup> a pressure dependence was observed for vibrational as well as for rotational excitation of  $\text{C}_2^*$  fragments.

Emission associated with high levels of rotation can be observed well to the blue of each bandhead series<sup>5,6</sup> (e.g.,  $\Delta v = +1$ ). In Fig. 7, we compare waveforms obtained at 473.9 nm, the (1,0) bandhead, and at 462.8 nm, amid rotation associated with the entire  $\Delta v = +1$  series. The apparent protracted formation of rotationally hot  $\text{C}_2^*$  reflects a larger fractional contribution of the collisional process, corroborating the inference from Fig. 6 (cf. also Fig. 5, curve *c*).

## B. C<sub>2</sub> singlet emission

C<sub>2</sub> possesses a complex structure of electronic states, including singlets and quintets as well as triplets.<sup>14</sup> Several systems of emission are known,<sup>7</sup> among triplet states and among singlets. The systems C<sup>1</sup>Π<sub>g</sub> → A<sup>1</sup>Π<sub>u</sub> (0,0 at 385.2 nm) and D<sup>1</sup>Σ<sub>u</sub><sup>+</sup> → X<sup>1</sup>Σ<sub>g</sub><sup>+</sup> (0,0 at 231.3 nm) were observed, but the integrated intensity for each was <10<sup>-2</sup> of that in the Swan system. The C<sup>1</sup>Π<sub>g</sub> signal appears within a time less than the instrumental limit of 0.6 ns. There is a delay for the maximum of D<sup>1</sup>Σ<sub>u</sub><sup>+</sup> signal, which suggests a collisional formation mechanism. Each signal decays to 30% of maximum within 25 ns.

It is particularly interesting that McDonald *et al.*,<sup>9</sup> photolyzing C<sub>2</sub>H<sub>2</sub> (30 mTorr) with an ArF laser at 193 nm, reported the Phillips system (A<sup>1</sup>Π<sub>u</sub> → X<sup>1</sup>Σ<sub>g</sub><sup>+</sup>, with 3,0 at 771.5 nm and 2,0 at 875.1 nm) to be ~10<sup>2</sup> stronger than the Swan system. We did not detect the Phillips system; a careful test led only to an upper bound on the intensity of such emission. A thorough treatment involves several considerations: the A<sup>1</sup>Π<sub>u</sub> emission rate (small), the spectral sensitivity of detection (relatively flat), and the detectivity-threshold (pertaining in our work to instantaneous rather than to time-averaged signal). The finding is that the initial A<sup>1</sup>Π<sub>u</sub> population is no more than 5 × 10<sup>-2</sup> of the d<sup>3</sup>Π<sub>g</sub> population; i. e., the relative Phillips population is ≤ 5 × 10<sup>-4</sup> of the found in the ArF work.

## C. CH emission

In less extensive studies, the rise of emission in the CH A band (0,0 at 431.3 nm) was found to contain two components. At 1 Torr there is a prompt rise to 60% of the peak signal; a further increase occurs within approximately 10 ns. The secondary formation process shows a definite pressure dependence. Unimolecular and intermolecular processes are implied in CH A<sup>2</sup>Δ formation, although we do not have supportive information from labeled isotopes. The curves accept exponential decay with characteristic times of 20 ns at 5 Torr and 70 ns at 1 Torr, corresponding to k<sub>0</sub> = 2.8 ± 0.5 × 10<sup>-10</sup> cm<sup>3</sup> s<sup>-1</sup>.

The integrated intensity of the CH C band (0,0 at 314.4 nm) is similar to that of the A band. However, only a prompt component of formation is observed. At 5 Torr the emission decays to 30% of the peak within ~15 ns. In contrast with the observation of Jackson *et al.*,<sup>15</sup> no emission was observed in the B band (0,0 at 388.9 nm); the integrated intensity was not greater than 5% of that for the A band.

## IV. DISCUSSION

### A. Unimolecular dissociation processes

The primary observations here directly establish the existence of a unimolecular dissociation process of acetylene yielding C<sub>2</sub>d<sup>3</sup>Π<sub>g</sub>. Such channels also are implied for C<sub>2</sub>C<sup>1</sup>Π<sub>g</sub> and for CHA<sup>2</sup>Δ and C<sup>2</sup>Σ<sup>+</sup>. The character and identity of the intermediates remain unresolved and present some challenging questions: e. g., does the process leading to the emissive species (cf. the 215 ps

Swan risetime) represent dissociation from a sufficiently energetic state of the parent manifold, or is there additional excitation (necessarily within the pulse duration) of an intermediate fragment? Also, we must consider the quantum order of the dissociative routes and the role of resonant and nonresonant excitations.

Excitation at 266 nm (4.66 eV, 107 kcal mol<sup>-1</sup>) is less energetic than the recognized onset of single-quantum absorption in acetylene at 237.7 nm.<sup>16</sup> There is evidence of a triplet state as low as 2.6 to 4.7 eV,<sup>17</sup> so that single-quantum excitation cannot be excluded absolutely; but such a transition is both Franck-Condon and spin-forbidden. The VUV absorption spectrum of acetylene<sup>18,19</sup> displays the following features in near-coincidence with our 2hν = 214 kcal mol<sup>-1</sup>: a Rydberg state 3R' (212.8 kcal mol<sup>-1</sup>), and two valence states C (213.6 kcal mol<sup>-1</sup>) and B (213.2 kcal mol<sup>-1</sup>).

We now consider the competing channels for a Franck-Condon C<sub>2</sub>H<sub>2</sub><sup>\*</sup> state at 214 kcal mol<sup>-1</sup>. Employing high resolution in a search for rotational structure near this energy, Wilkinson found none.<sup>18</sup> This demands prompt (<1.6 ps) coupling to other states, whether bound (internal conversion to a vibrationally excited ground state or to some other isoenergetic state) or dissociative. The pertinent thermodynamic thresholds for decomposition are<sup>2</sup>: C<sub>2</sub>H + H, 124 kcal mol<sup>-1</sup> and C<sub>2</sub> + H<sub>2</sub>, 144 kcal mol<sup>-1</sup>. Potential curve calculations<sup>20</sup> and spectroscopic studies<sup>18</sup> have failed to identify a *cis* state of C<sub>2</sub>H<sub>2</sub>, which might have lent support in affording an acceptable transition state for H<sub>2</sub> elimination. Final product analyses in conventional photolysis experiments<sup>1,4,21</sup> yield no clear indication of unimolecular H<sub>2</sub> elimination (quantum yield < 0.1<sup>1</sup>). Rather, H atom elimination proceeds with a quantum efficiency 0.3, in competition with significant conversion to a postulated metastable of the parent, C<sub>2</sub>H<sub>2</sub><sup>\*\*</sup>.<sup>1</sup> The first step in either channel must occur within 1.6 ps, to be competitive. The H atom elimination is not concerted; this is evidenced by the limited quantum yield<sup>1</sup> and by the vibrational structure observed by Wilkinson.<sup>18</sup> Nevertheless, internal conversion is probably fast,<sup>22,23</sup> and H elimination from the energetic ground state should be fast.<sup>24,25</sup> Thus it seems very probable that C<sub>2</sub>H formation occurs within ~2 ps, whether from an electronic state at 2hν or from a vibrationally hot ground state.

### 1. Further excitation of C<sub>2</sub>H<sub>2</sub><sup>\*</sup>, C<sub>2</sub>H<sub>2</sub><sup>\*\*</sup>

With absorption of a third quantum (321 kcal mol<sup>-1</sup>) in the parent manifold, H atom elimination is expected to proceed at an enhanced rate; the fate of the resultant C<sub>2</sub>H is discussed in the following section. A competing process, which is thermodynamically allowed, is formation of CH A<sup>2</sup>Δ (C<sub>2</sub>H<sub>2</sub> → CH A<sup>2</sup>Δ + CH X<sup>2</sup>Π, 294 kcal mol<sup>-1,2</sup>). McDonald<sup>9</sup> has demonstrated such a channel at 296 kcal mol<sup>-1</sup>, and it is likely that this is the mechanism of our unimolecular CH A<sup>2</sup>Δ emission. Production of CH C<sup>2</sup>Σ<sup>+</sup> is also allowed for 3hν (C<sub>2</sub>H<sub>2</sub> → CH C<sup>2</sup>Σ<sup>+</sup> + CH X<sup>2</sup>Π, 320 kcal mol<sup>-1</sup>). Simultaneous elimination of two hydrogen atoms in a concerted three-center fission is rejected. Although 321 kcal mol<sup>-1</sup>

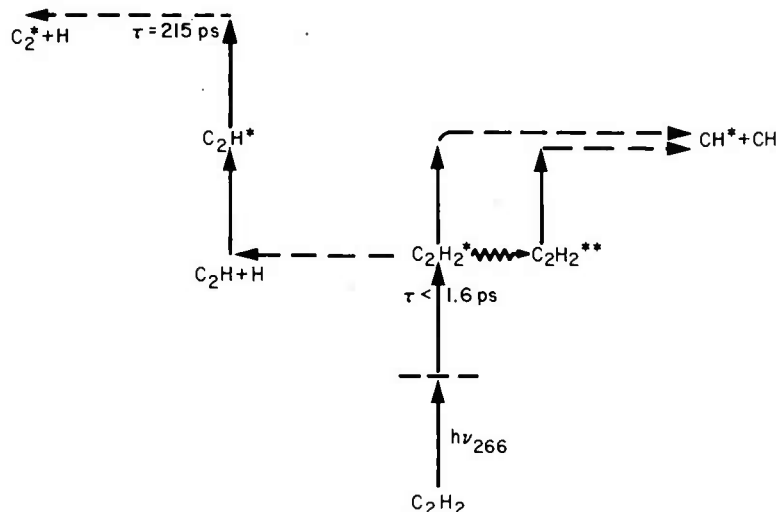


FIG. 8. Schematic of preferred channels of  $\pi \rightarrow \pi^*$  excitation (vertical arrows), intramolecular relaxation (wavy arrow), and unimolecular fragmentation (dashed arrows) for photolysis of  $C_2H_2$  by 266 nm 25 ps pulses.

exceeds the ionization limit of 263 kcal mol<sup>-1</sup>,<sup>26</sup> there is evidence that the other processes are dominant.<sup>27</sup> At the  $4h\nu$  level, the above elimination and ionization processes may proceed at higher rates. However, our data convey a general deficiency of ionic emission, which suggests that other processes intercede. For instance, visible  $CH^+$  emission, seen in helium/acetylene discharges,<sup>28</sup> was not observed, nor were there unidentified components which might have been assigned to ions. It appears then that our dominant unimolecular dissociative channels do not demand recognition of essential ionic intermediates (see, however, the discussion of collisional processes in Sec. IV B).

## 2. Further excitation of $C_2H$

The primary two-quantum H elimination from  $C_2H_2$  is 90 kcal mol<sup>-1</sup> above threshold. There is an ambiguity in the distribution of the excess energy between H atom recoil and the internal energy of the  $C_2H$  state addressed in subsequent excitation. Regardless of the energy content within the range 0–90 kcal mol<sup>-1</sup>, absorption of two additional quanta is required to produce  $C_2d^3\Pi_g, v' = 6$  ( $C_2H - C_2d^3\Pi_g, v' = 6 + H$ , 206 kcal mol<sup>-1</sup>).  $C_2C^1\Pi_g$  requires three additional quanta ( $C_2H - C_2C^1\Pi_g + H$ , 221 kcal mol<sup>-1</sup>).  $C_2H$  has been established as a gas-phase photolysis product of  $C_2H_2$  through observation of ESR signals in a rare gas matrix at 4 K.<sup>29</sup> In a theoretical analysis, Shih *et al.*<sup>30,31</sup> advocated  $\pi \rightarrow \pi^*$  excitation to a specific acetylene precursor state  $^1\Sigma_u^+$  leading to  $C_2H 3^2A'$  and  $2^2A''$ . The expected (0,0) excitation energy is 9.7 eV or somewhat less, very close to the valence states postulated by Wilkinson (who also suggested a  $\pi$  excitation). Absorption<sup>30</sup> and emission<sup>31</sup> of  $C_2H$  were treated in extensive *ab initio* calculations. Excitation of  $C_2H$  at 266 nm is supported through  $\pi \rightarrow \pi^*$  transitions, although the assignment is not complete in detail. Additional resonant absorption leading to further fragmentation (i. e., to  $C_2^*$ ) is then probable. In successive H eliminations, if dissociation occurs through singlet  $C_2H_2$ , then doublet  $C_2H$  has the appropriate spin

to account for the triplet Swan emission; but triplet  $C_2H_2$  would allow either doublet or quartet  $C_2H$ .

In other studies of acetylene photolysis<sup>2,8,9</sup> broad structureless continua, tentatively ascribed to  $C_2H^*$  (or to  $C_2H_2^*$ ), have been observed both in absorption and in emission. The bent geometry of the upper  $C_2H$  state identified in the analysis of Shih is entirely consistent with such a continuous spectrum and with the long lifetime (6.2  $\mu$ s) reported by Becker.<sup>8</sup> These emission characteristics are adverse to our conditions of detection. Our failure to observe continuum emission does not exclude  $C_2H$  as an intermediate.

We suggest a parallel to the process for  $C_2H_2$ : that  $\pi \rightarrow \pi^*$  excitation of  $C_2H$  leads to H elimination, with direct production of Swan emission ( $C_2H 2^2\Sigma^+ C_2^* + H$ ). Production of  $CHA^2\Delta$  or  $C^2\Sigma^+$  via  $C_2H$  would require a net absorption of  $5h\nu$ ;  $CH^*$  formation in direct dissociation of the parent at  $3h\nu$  is suggested. The above channels leading to the observed emissive fragments are represented in Fig. 8.

In the photolysis of  $C_2H_2$  by an ArF laser McDonald *et al.* favored a similar channel of successive H atom eliminations, but there  $C_2A^1\Pi_u$  was the dominant  $C_2$  fragment. In the present work, the appearance of  $C_2^*$  predominantly in the Swan system suggests a distinct channel of formation; it is not firmly excluded that excitation of the parent may occur entirely within the triplet manifold.

## 3. Considerations of flux and fluence in the excitation process

The conditions of excitation associated with our short pulses clearly are singular. These considerations can be expressed objectively in terms of flux and fluence, and resonant versus nonresonant transitions. The fluence estimated for the current work at low pulse energy is  $\sim 10^{19}$  cm<sup>-2</sup>; this is similar to levels employed with resonant excitation by pulses of  $\sim 20$  ns duration, in which fragments were detected either by lumines-

cence<sup>9</sup> or by mass spectrometry.<sup>32,33</sup> The larger ( $10^3$ – $10^4$ ) flux values here,  $\sim 10^{30}$  cm<sup>-2</sup> s<sup>-1</sup>, favor nonlinear excitation (through virtual states), but we shall show that the relative measure of nonlinear rates nevertheless is small.

Honig *et al.*<sup>34</sup> give a rough estimate of the ratio of rates for nonresonant two-photon and resonant single-photon transitions:  $\xi = 10^{-32} F_\lambda$ , where  $F_\lambda$  is the photon flux in units cm<sup>-2</sup> s<sup>-1</sup>. We estimate  $\xi = 10^{-2}$  for the present study. Together with the linear absorption at 133 nm ( $1.3$  cm<sup>-1</sup> Torr<sup>-1</sup>) this corresponds to an effective two-quantum absorption of  $\sim 10^{-2}$  cm<sup>-1</sup> Torr<sup>-1</sup>.

In acetylene, the initial excitation from the ground state must proceed with very low efficiency, whether to a resonant triplet or via two quanta to a singlet. Furthermore, our laser beam couples to a very small fraction of the sample cell volume (single transverse mode, longitudinal focusing). There was no indication of cumulative chemistry, other than a minor consumption of parent evidenced by a decrease ( $\sim 5\%$ ) in emission levels after some hundreds of shots. No new spectral components appeared in the course of such exposure, nor did the waveforms of individual shots exhibit changes in decay kinetics.

The small  $\xi$  value has a further implication. Given that transitions beyond the initial two-quantum event proceed through identified resonances, off-resonant terms should be relatively negligible. It follows that the extent of subsequent excitation should be determined by the fluence alone. Thus, for the minor fraction of irradiated molecules which participate at all, the severity of excitation should not be greater than in work with much longer pulses of similar fluence.

On the other hand, for subsequent allowed resonant excitations the rate is quite high. We consider as an instance continued vertical excitation from the  $2h\nu$  state of acetylene, with the lifetime  $\leq 1.6$  ps inferred above. The photon fluence within this time is  $\sim 10^{18}$  cm<sup>-2</sup>. Thus an allowed cross section as small as  $10^{-18}$  cm<sup>2</sup> would give a significant rate, and such channels cannot be dismissed on the basis of inadequate residence time. It is possible that such processes may compete with relaxation to  $C_2H_2^*$  or with  $C_2H$  production.

For further excitation through resonant states of lifetime greater than the pulse duration (whether from  $C_2H_2^*$ ,  $C_2H_2^{**}$ , or  $C_2H$ ), the entire fluence will be operative. Thus we suggest that sequential resonant excitations proceed to saturation,<sup>35</sup> until some effective spectral bottleneck is encountered.<sup>36</sup>

## B. Collisional processes

Collisional  $C_2 d^3\Pi_g$  formation has been established. Similar processes seem likely for  $C_2 D^1\Sigma_g^+$  and  $CH A^2\Delta$ . The risetimes of such emission (e. g., Fig. 5 curve *c*) must reflect depletion of precursor species. This depletion is not necessarily dominated by the process generative of the emissive fragments. In fact, large values of the precursor quenching constant  $k_Q$  are demanded even for partners at the full density of the parent (5 Torr  $C_2H_2$ ): for  $C_2 d^3\Pi_g$ ,  $\sim 12 \times 10^{10}$  cm<sup>3</sup> s<sup>-1</sup>; and for

$CH A^2\Delta$ ,  $\sim 30 \times 10^{10}$  cm<sup>3</sup> s<sup>-1</sup>. These values are substantially larger than a typical diffusion-controlled rate constant of  $10^{10}$  cm<sup>3</sup> s<sup>-1</sup><sup>37</sup> and seem relatively large even for reactive radical or excited state species.<sup>38–45</sup> Rydberg states or ionic species, affording long-range Coulomb forces, could account for the large cross sections implied in the observed quenching constants. Alternatively, suprathermal fragment velocities may be involved.

The intermolecular Swan component accepts poorly a fit to exponential formation. Thus, on an exploratory basis, an hypothesized formation rate proportional to  $[CH^*]^2$  was used to construct model  $C_2^*$  emission profiles. Faster processes are difficult to advance; nevertheless, the model curves still do not treat adequately the observed rapid rise.

## V. CONCLUSION

Short-pulse UV excitation of isotopically labeled  $C_2H_2$  has allowed us to identify prompt (unimolecular) and delayed (intermolecular) channels of  $C_2 d^3\Pi_g$  and  $CH A^2\Delta$  production. The unimolecular production of rotationally hot  $C_2 d^3\Pi_g$  is clearly an essential feature of one or of both of the H atom elimination processes. It indicates dissociation of  $C_2H_2$  or of  $C_2H$  through a bent transition state. The collisional process leads to a still higher degree of rotational excitation in the emissive fragments. Unimolecular formation of  $CH A^2\Delta$  and  $C^2\Sigma^+$  are tentatively attributed to successive excitation in the parent manifold, beyond the initial  $2h\nu$  state. In the collisional processes generating both  $C_2^*$  and  $CH^*$ , precursors experience pressure-dependent depletion rates which are indicative of ion–molecule reactions or of suprathermal velocities.

Considerations of flux and of fluence indicate that the measure of severity of excitation associated with short pulses (and consequent high peak flux) is not greater than in work with longer pulses. Indeed, long pulses may allow *relaxation* within the duration of the excitation pulse to yield parent-states or product fragments subject to further excitation. Thus a diversity of dissociative channels may be opened, which are not characteristic of the directly-excited parent (cf. excitation of  $C_2H$  even in the current work). Hering *et al.*<sup>46</sup> have given a very clear demonstration of such effects in fragmentation of benzene. It is possible that the high quantum yield of Phillips emission observed in ArF laser studies of acetylene<sup>9</sup> may be a consequence of the much longer excitation pulse.

The preferred unimolecular route to  $C_2^*$  is entirely consistent with the scheme outlined by Shih *et al.*<sup>30,31</sup>; successive excitations occur in the pi electron system of  $C_2H_2$  and of the intermediate  $C_2H$ . Following two-quantum nonresonant  $\pi \rightarrow \pi^*$  absorption by  $C_2H_2$ , the first H atom is lost within 2 ps. This elimination is not direct, however. It may occur indirectly at the initial electronic energy  $2h\nu$  (in branching other than to  $C_2H_2^*$ , which is taken to be stable) or it may proceed from a vibrationally excited ground state formed via rapid internal conversion. Subsequent excitation is taken to occur through successive resonant  $\pi \rightarrow \pi^*$  absorptions in  $C_2H$ , yielding

$C_2^*$ . Although our techniques detect only emissive fragments, the assignment by Okabe<sup>1</sup> of a quantum yield of 0.3 to the process  $C_2H_2 \rightarrow C_2H + H$  suggests that such  $C_2^*$  production may initiate via a major dissociative route of  $C_2H_2$ . The 215 ps risetime observed for  $C_2$  Swan emission may then reflect predissociation of  $C_2H^*$ , or or alternatively it may reflect a relaxation process from a higher triplet of  $C_2$ .

#### ACKNOWLEDGMENTS

We thank Dr. E. J. Friebele for valuable cooperative effort in achieving the necessary interface between the Nuclear Data vidicon system which serviced the streak camera and the Nicolet minicomputer system employed for processing the data. This work has been supported in part by the Office of Naval Research.

<sup>1</sup>H. Okabe, *J. Chem. Phys.* **75**, 2772 (1981).

<sup>2</sup>H. Okabe, *J. Chem. Phys.* **62**, 2782 (1975).

<sup>3</sup>A. H. Laufer, *J. Chem. Phys.* **73**, 49 (1980).

<sup>4</sup>L. J. Stief, V. J. Decarlo, and R. J. Mataloni, *J. Chem. Phys.* **42**, 3113 (1965).

<sup>5</sup>B. B. Craig, W. L. Faust, L. S. Goldberg, P. E. Schoen, and R. G. Weiss, *Proceedings of the Second International Conference on Picosecond Phenomena*, Cape Cod, Mass. June 18-20, 1980, edited by R. M. Hochstrasser, W. Kaiser, and C. V. Shank (Springer, Berlin, 1980), Vol. 2, p. 253; see also references therein.

<sup>6</sup>B. B. Craig, W. L. Faust, L. S. Goldberg, J. M. Schnur, P. E. Schoen, and R. G. Weiss, *Proceedings of the NATO Advanced Study Institute*, Preveza, Greece, July 6-19, 1980, edited by C. Capellos and R. F. Walker (Reidel, Dordrecht, The Netherlands, 1981), p. 419.

<sup>7</sup>R. W. B. Pearse and A. G. Gaydon, *Identification of Molecular Spectra* (Chapman and Hall, London, 1965).

<sup>8</sup>K. H. Becker, D. Haaks, and M. Schurgers, *Z. Naturforsch.* **A 26**, 1770 (1971).

<sup>9</sup>J. R. McDonald, A. P. Baronavski, and V. M. Donnelly, *Chem. Phys.* **33**, 161 (1978).

<sup>10</sup>B. B. Craig, W. L. Faust, L. S. Goldberg, and R. G. Weiss, *Chem. Phys. Lett.* **83**, 265 (1981).

<sup>11</sup>R. K. Dhumwad and N. A. Narasimham, *Can. J. Phys.* **46**, 1254 (1968).

<sup>12</sup>W. Lochte-Holtgreven, *Z. Phys.* **64**, 443 (1930).

<sup>13</sup>J. H. Hall, Jr., M. L. Lesiecki, and W. A. Guillory, *J. Chem. Phys.* **68**, 2247 (1978).

<sup>14</sup>K. Kirby and B. Liu, *J. Chem. Phys.* **70**, 893 (1979).

<sup>15</sup>W. M. Jackson, J. B. Halpern, and C. S. Lin, *Chem. Phys. Lett.* **55**, 254 (1978).

<sup>16</sup>G. B. Kistiakowsky, *Phys. Rev.* **37**, 276 (1931).

<sup>17</sup>C. S. Burton and H. E. Hunziker, *J. Chem. Phys.* **57**, 339 (1972).

<sup>18</sup>P. G. Wilkinson, *J. Mol. Spectrosc.* **2**, 387 (1958).

<sup>19</sup>T. Nakayama and K. Watanabe, *J. Chem. Phys.* **40**, 558 (1964).

<sup>20</sup>D. Demoulin, *Chem. Phys.* **11**, 329 (1975).

<sup>21</sup>A. H. Laufer and A. M. Bass, *J. Phys. Chem.* **83**, 310 (1978).

<sup>22</sup>Note that fluorescence is not ordinarily observed from acetylene. There is such a report for acetylene in an inert gas matrix: L. E. Brus, *J. Mol. Spectrosc.* **75**, 245 (1979).

<sup>23</sup>K. Evans, R. Scheps, S. A. Rice, and D. Heller, *Chem. Soc. Faraday Tran.* **2 69**, 856 (1973).

<sup>24</sup>W. L. Hase and D.-F. Feng, *J. Chem. Phys.* **61**, 4690 (1974).

<sup>25</sup>C. S. Sloane and W. L. Hase, *J. Chem. Phys.* **66**, 1523 (1977).

<sup>26</sup>V. H. Dibeler, J. A. Walker, and K. E. McCulloh, *J. Chem. Phys.* **59**, 2264 (1973).

<sup>27</sup>J. Kreile, A. Schweig, and W. Thiel, *Chem. Phys. Lett.* **79**, 547 (1981).

<sup>28</sup>A. E. Douglas and J. R. Morton, *Astrophys. J.* **131**, 1 (1960).

<sup>29</sup>W. R. M. Graham, K. I. Dismuke, and W. Weltner, Jr., *J. Chem. Phys.* **60**, 3817 (1974).

<sup>30</sup>S. Shih, S. D. Peyerimhoff, and R. J. Buenker, *J. Mol. Spectrosc.* **64**, 167 (1977).

<sup>31</sup>S. Shih, S. D. Peyerimhoff, and R. J. Buenker, *J. Mol. Spectrosc.* **74**, 124 (1979).

<sup>32</sup>L. Zandee and R. B. Bernstein, *J. Chem. Phys.* **71**, 1359 (1979).

<sup>33</sup>U. Boesl, H. J. Neusser, and E. W. Schlag, *J. Chem. Phys.* **72**, 4327 (1980).

<sup>34</sup>B. Honig, J. Jortner, and A. Szoke, *J. Chem. Phys.* **46**, 2714 (1967).

<sup>35</sup>Some support is afforded by measurements of emission intensity vs laser pulse energy, executed in the current work; the largest power-law observed was 1.4.

<sup>36</sup>A very attractive indication of bottleneck effects may be found in the observations of Boesl *et al.* (Ref. 33), upon photolysis of benzene. After an initial (ionizing) excitation, the primary UV pulse was ineffective toward subsequent fragmentation. But a parallel or following visible pulse was quite effective.

<sup>37</sup>V. N. Kondrat'ev, *Chemical Kinetics of Gas Reactions* (Pergamon, New York, 1964), pp. 146, 229.

<sup>38</sup>J. E. Butler, L. P. Gross, M. C. Lin, and J. W. Hudgens, *Chem. Phys. Lett.* **63**, 104 (1979).

<sup>39</sup>M. W. Bosnali and D. Perner, *Z. Naturforsch.* **A 26**, 1768 (1971).

<sup>40</sup>A. P. Baronavski and J. R. McDonald, *Chem. Phys. Lett.* **56**, 369 (1978).

<sup>41</sup>L. Pasternack and J. R. McDonald, *Chem. Phys.* **43**, 173 (1979).

<sup>42</sup>V. M. Donnelly and L. Pasternack, *Chem. Phys.* **39**, 427 (1979).

<sup>43</sup>M. N. R. Ashfold, M. A. Fullstone, G. Hancock, and G. W. Ketley, *Chem. Phys.* **55**, 245 (1981).

<sup>44</sup>C. K. Luk and R. Bersohn, *J. Chem. Phys.* **58**, 2153 (1972).

<sup>45</sup>W. M. Jackson, *J. Chem. Phys.* **61**, 4177 (1974).

<sup>46</sup>P. Ifering, A. G. M. Maaswinkel, and K. L. Kompa, *Chem. Phys. Lett.* **83**, 222 (1981).

# Repetitively pulsed mode-locked Nd:phosphate glass laser oscillator–amplifier system

L. S. Goldberg, P. E. Schoen, and M. J. Marrone

Performance of a repetitively pulsed mode-locked Nd:glass laser system employing athermal phosphate glass in the oscillator and amplifier stages is described. Improved passive mode-locking characteristics of the oscillator are achieved through use of a 100- $\mu\text{m}$  thick intracavity etalon, enabling reliable generation of transform-limited pulses typically of 5-psec duration. The system produces 1054-nm pulses of high beam quality and  $\sim 25\text{-mJ}$  energy at a pulse repetition rate of  $\sim 0.2$  Hz. Subsequent frequency-doubling steps give conversion efficiencies of  $\sim 50\%$  and  $25\%$ , respectively.

## I. Introduction

Nd-doped phosphate laser glass is becoming increasingly used as a replacement for silicate glass in mode-locked laser systems because of its higher gain, lower nonlinear refractive index, and better thermal properties. The development of thermally compensated formulations of phosphate glass, which minimizes the optical path length change with temperature, has enabled operation of the mode-locked glass oscillator at relatively high pulse repetition rates.<sup>1</sup> In recent picosecond photolysis experiments, we employed a mode-locked Nd:phosphate glass oscillator–amplifier system capable of generating energetic 5-psec duration pulses at 1054 nm and harmonics in repetitively pulsed operation.<sup>2</sup> The repetitive pulsing capability of this glass laser system now allows more rapid set up of experiments and substantially improved data acquisition rates. This paper will describe the laser system and its operating characteristics. In addition, we will present new data on improved performance of the passively mode-locked oscillator through use of an intracavity etalon.

## II. Oscillator

Figure 1 shows the optical arrangement of the laser system. The laser rods used in these experiments were Owens-Illinois EV-4 athermal phosphate glass. The oscillator rod had dimensions of  $6.4 \times 89$  mm and  $1^\circ$

wedged Ar-coated faces. It was housed in a single-ellipse pump cavity and excited by a simmered linear xenon flashlamp of 4-mm bore diam. Flashlamp energy was typically 18 J in a discharge of 300  $\mu\text{sec}$ . The oscillator was capable of a pulse repetition rate in excess of 1 Hz. The saturable absorbing dye was Eastman A9740 dissolved in 1,2-dichloroethane. The dye solution flowed through a cell with spacer thickness of 0.6 mm in optical contact with the 6-m curvature rear mirror. The flat output mirror at a cavity separation of 1.3 m had a reflectivity of 70%. Two Brewster angle plates served as polarizing elements. The cavity also contained an uncoated fused-silica etalon of 100- $\mu\text{m}$  thickness ( $35\text{-cm}^{-1}$  free spectral range and 0.15 finesse).

Use of a thin etalon inside the oscillator cavity was found to have a beneficial stabilizing influence on the passive mode locking, while still preserving generation of short pulses.<sup>3</sup> During the buildup of a short pulse from statistical noise fluctuations<sup>4</sup> restriction of the large gain bandwidth ( $\sim 180\text{ cm}^{-1}$ ) of the lasing medium by an etalon reduces the spectral width and limits the duration of the pulse developed at the end of the linear amplification stage before nonlinear pulse shaping and  $Q$ -switching by the saturable dye takes effect. A special case has been treated in the literature, however, in which an intracavity etalon is chosen of a thickness appropriate to match the gain width and is tuned critically for minimum transmission at line center.<sup>5–8</sup> The effect is to flatten the curvature at the peak of the gain curve, thereby enabling pulses of substantially wider bandwidth and correspondingly shorter duration to be generated.

We have observed several noteworthy characteristics in oscillator performance with use of a 100- $\mu\text{m}$  etalon. Very regular bell-shaped pulse trains were generated

The authors are with U.S. Naval Research Laboratory, Washington, D.C. 20375.

Received 5 December 1981.

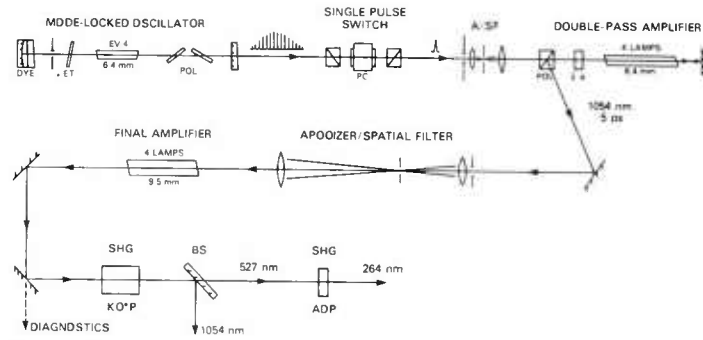


Fig. 1. Schematic of the passively mode-locked Nd:phosphate glass laser system.

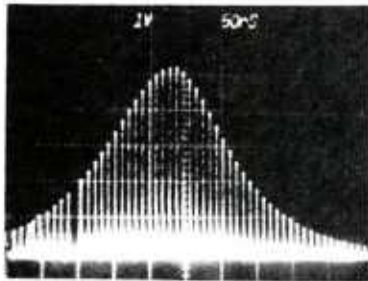


Fig. 2. Pulse train with switched-out pulse from mode-locked oscillator using a 100- $\mu\text{m}$  thick etalon inside the cavity.

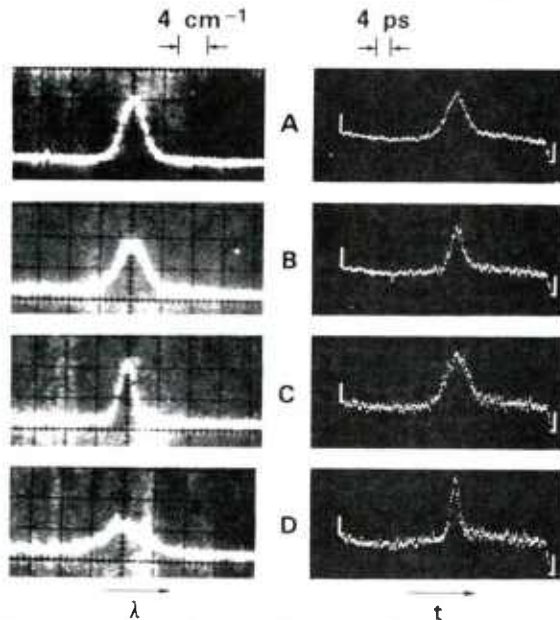


Fig. 3. Spectrum (left) and TPF time profile (right) of a single pulse from the mode-locked oscillator: (A) 50- $\mu\text{m}$  intracavity etalon; (B) 100- $\mu\text{m}$  etalon; (C) 150- $\mu\text{m}$  etalon; (D) no etalon.

(Fig. 2) with no noticeable distortion in the train envelope. The threshold pumping energy for mode locking was  $\sim 10\%$  lower. The statistical success rate for obtaining well-formed pulse trains was  $\sim 80\%$ , the remainder either containing satellite pulses or not lasing.

A  $\text{TEM}_{00}$  spatial mode structure was obtained over the entire duration of the pulse train without requiring use of an intracavity aperture. This was rarely achieved in the no-etalon case unless a forcing aperture was used and then only at markedly higher pumping energy. Pulse train output energy was maintained at a relatively low value, typically 5 mJ, to minimize self-phase modulation distortion of the pulse through the intensity-dependent nonlinear refractive index  $n_2$ .<sup>9</sup> This was accomplished at a low saturable dye concentration ( $\sim 85\%$  small-signal transmission) consistent with obtaining stable mode locking. In such an operation transform-limited pulses could be extracted from higher in the train envelope ( $\sim 1/3$  of peak), with accordingly greater energy content ( $\sim 25 \mu\text{J}$ ), before significant spectral broadening and distortion in the pulse occurred.

The spectral width of individual pulses was recorded with an 0.8-m spectrograph coupled to a Reticon diode array. Concurrently, the pulse duration was determined by the two-photon fluorescence (TPF) method in a colliding beam geometry, with the track imaged by an intensified vidicon system. Since only a small portion of the main beam was sampled (Fig. 1) for these measurements, the pulses were amplified by a factor of  $\sim 50$ . Figure 3(B) shows the spectrum and TPF autocorrelation time profile of the pulse selected from the train in Fig. 2 for use of a 100- $\mu\text{m}$  etalon in the oscillator cavity. The contrast ratio of the TPF trace is close to 3:1. Assuming a Gaussian pulse shape for deconvolution, the pulse duration (FWHM) is 4.7 psec; the pulse spectral width (FWHM) is  $4.2 \text{ cm}^{-1}$ . This corresponds to a time-bandwidth product  $\Delta\tau\Delta\nu \cong 0.6$ , very near to the transform limit of 0.44 for Gaussian pulses. The etalon was tilted to adjust the lasing spectrum to the peak of the gain curve, although no significant change in spectral width or pulse duration could be found when tuning throughout the etalon's free spectral range. Figures 3(A) and (C) show representative data for use of 50- and 150- $\mu\text{m}$  uncoated etalons, respectively. In these cases the pulses are clearly longer (7.1, 8.5 psec) than for use of the 100- $\mu\text{m}$  etalon, and their spectra are correspondingly narrower ( $3.6, 2.4 \text{ cm}^{-1}$ ). Figure 3(D) shows data for a well-formed pulse obtained with no etalon in the cavity. The pulse necessarily was selected

early in the train at  $\sim 1/10$  peak envelope intensity. The pulse duration is 3.3 psec, and the spectral width is  $6 \text{ cm}^{-1}$ .

### III. Amplifier Stages

A conventional Pockels cell switch with a photo-diode-triggered Krytron pulse circuit was used to extract a single pulse from the train. The contrast ratio for the switched-out pulse was  $2 \times 10^4$ . Two amplifier stages were used in the laser system, the first with a 6.4-mm diam laser rod in a double-pass configuration, and the second with a 9.5-mm diam rod. Both rods were pumped over a length of 192 mm. Each had parallel,  $0.5^\circ$  canted AR-coated faces. The pumping chambers, manufactured by J-K Lasers, contained a quad arrangement of linear xenon flashlamps (7-mm bore diam) in a close-coupled diffusely reflecting water-filled cavity. Each of the four lamps was wired independently in a series-triggered discharge circuit ( $C = 125 \mu\text{F}$ ,  $L = 128 \mu\text{H}$ ), charged through isolating diodes from the same high-voltage supply. The discharges were critically damped and of  $\sim 300$ - $\mu\text{sec}$  duration.

The input beam to the first amplifier stage was expanded by a factor of 2 and was shaped by apodization to remove the wings of the Gaussian intensity distribution. This was accomplished using an aperture of diameter  $d = 1.3 \text{ mm}$  to truncate the beam at approximately the  $e^{-1}$  intensity points. The far-field diffraction pattern formed in the focal plane of the adjacent lens was then spatially filtered by a  $200\text{-}\mu\text{m}$  pinhole. The pinhole size was chosen to clip the diffraction pattern at the first intensity null, of diameter  $2.44 \lambda f/d$ , thereby passing only the central Airy disk. This shaping procedure produced a beam which could better fill the amplifier aperture and propagate without developing an edge-generated diffraction ring structure.

The double-pass arrangement enabled the relatively weak single pulse from the oscillator to be amplified in a single stage to an energy of  $\sim 3 \text{ mJ}$ . At this energy the degree of intensity-dependent  $n_2$  distortion in the pulse remained within reasonable bounds. In this regard the  $\lambda/4$  plate provided a benefit in addition to its essential service as a double-pass polarization rotator, since propagation of circularly polarized radiation through the amplifying medium yields an effective  $n_2$  that is reduced by a factor of 1.35–1.5.<sup>10</sup> A gain of  $\sim 300$  was readily achieved for the double pass at a total flashlamp energy of 400 J. Because of good thermal dissipation in the small diameter rod, this amplifier could be operated at 0.5-Hz repetition rate without significant thermal lensing effects. Use of this amplifier alone proved a major convenience for rapid set up of experiments. The average power loading is well below burst levels for the rod (estimated at  $\sim 800 \text{ W}$ ). At about half of this level thermally induced stress birefringence would become a serious problem.

Before the beam entered the final amplifier it was again apodized and expanded to fill the 9.5-mm diam rod. The input aperture was set at 4.0 mm, and the pinhole spatial filter at  $400 \mu\text{m}$ . The spatial filter

served the important function at the higher input pulse energies of removing high spatial frequency intensity fluctuations from the beam. Such spatial beam structure can lead to small-scale self-focusing in the amplifier medium and consequent optical component damage.<sup>11</sup> It also results in a severely modulated intensity profile for a frequency-upconverted beam after successive stages of nonlinear harmonic generation.

Output pulses of  $\sim 25\text{-mJ}$  energy were obtained from the final amplifier at a gain setting of  $\sim 15$ . For the current rod diameter pulses amplified much above this energy experienced excessive nonlinear distortion. The flashlamp pumping energy required was 575 J. The pulse repetition rate was set conservatively at  $\sim 0.2 \text{ Hz}$ , although lower gain settings allowed still higher repetition rates. The resulting thermal loading of the amplifier rod produced a moderate degree of thermal lensing as the beam, observed several meters distant, diminished in size and then stabilized within several pulses after the laser began operating. Burn patterns of the output beam taken on developed Polaroid film were smooth, showing no noticeable diffraction structure; they were also fairly circular as a result of the symmetric four-lamp pumping geometry.

The thermal lensing could largely be corrected by adjusting the recollimating lens in the beam-expanding lens pair. This was important since optimum frequency doubling in an angle-tuned KD\*P crystal requires a highly collimated beam. For 1054-nm input the phase matching acceptance angle of the 2-cm length type I crystal used was 0.8 mrad. We obtained a doubling efficiency of  $\sim 50\%$ , giving a pulse energy of  $\sim 12 \text{ mJ}$  at 527 nm.

The fourth harmonic was produced by a second step of frequency doubling in a temperature-tuned  $90^\circ$  oriented ADP crystal. Because of increased dispersion in the refractive indices of the crystal in the UV, the spectral content of the pulse and group velocity dispersion become critical parameters in effective doubling of a 527-nm pulse.<sup>12</sup> As a consequence, a short 5-mm length ADP crystal (at  $32^\circ\text{C}$ ) was used. The phase matching frequency bandwidth then is  $8.8 \text{ cm}^{-1}$ , which adequately encompasses the near-transform-limited spectrum of the 527-nm input pulse. However, the group velocity mismatch between fundamental and harmonic frequencies is 8 psec, which implies a temporal walkoff in the crystal that will reduce the conversion efficiency and stretch the harmonic pulse. In our experiments we obtained a pulse energy of  $\sim 3 \text{ mJ}$  at 263.5 nm corresponding to a doubling efficiency of  $\sim 25\%$ . The overall conversion efficiency of pulse energy from 1054 nm to the fourth harmonic was  $\sim 12\%$ .

### IV. Conclusion

We have described a mode-locked Nd:phosphate glass laser system capable of producing energetic short pulses of high beam quality at fundamental and harmonic frequencies at repetition rates of 0.2 Hz or better. The higher data acquisition rates afforded by this glass laser system make it well-suited for use in picosecond laser spectroscopy experiments.

## References

1. T. R. Royt, *Opt. Commun.* **35**, 271 (1980).
  2. P. E. Schoen, M. J. Marrone, J. M. Schnur, and L. S. Goldberg, *Chem. Phys. Lett.* (1982), to be published.
  3. T. R. Royt, NRL; unpublished.
  4. G. H. C. New, *Proc. IEEE* **67**, 380 (1979).
  5. M. W. McGeoch, *Opt. Commun.* **7**, 116 (1973).
  6. D. von der Linde and K. F. Rodgers, *Opt. Commun.* **8**, 91 (1973).
  7. E. M. Gordeev *et al.*, *Sov. J. Quantum Electron.* **5**, 129 (1975).
  8. H. Graener and A. Laubereau, *Opt. Commun.* **37**, 138 (1981).
  9. D. H. Austin, in *Ultrashort Light Pulses*, S. L. Shapiro, Ed. (Springer, Berlin, 1977), p. 123.
  10. A. Feldman, D. Horowitz, and R. M. Waxler, *IEEE J. Quantum Electron.* **QE-9**, 1054 (1973); D. Auric and A. Labadens, *Opt. Commun.* **21**, 241 (1977).
  11. A. J. Campillo, S. L. Shapiro, and B. R. Suydam, *Appl. Phys. Lett.* **23**, 628 (1973); **24**, 178 (1974).
  12. W. H. Glenn, *IEEE J. Quantum Electron.* **QE-5**, 284 (1969).
-

Picosecond Continuum Broad-Band CARS Probe

Lawrence S. Goldberg

Naval Research Laboratory  
Washington, D.C. 20375, USA  
(202) 767-2499

Abstract

A picosecond broad-band CARS probe technique has been demonstrated which utilizes a white-light continuum pulse as Stokes light. The method is being applied to photolysis studies of transient molecular photofragment formation.

# Picosecond Continuum Broad-Band CARS Probe

Lawrence S. Goldberg

Naval Research Laboratory  
Washington, D.C. 20375, USA

## Summary

Coherent anti-Stokes Raman scattering (CARS) provides a powerful diagnostic approach to the identification and study of transient molecular fragment species produced as the primary events in UV laser photolysis of molecules. Gross *et al.*<sup>1</sup> applied nanosecond dye laser techniques to obtain scanned as well as broad-band single-shot CARS spectra of transient species from UV photolysis of gas-phase benzene and derivatives. Recently, Hetherington *et al.*<sup>2</sup> extended this work to the picosecond time scale using optical parametric generation to provide tunable frequency Stokes pulses for a point-by-point spectrum. This paper reports the first demonstration of a picosecond broad-band CARS probe technique. The method utilizes the picosecond white-light continuum<sup>3</sup> as Stokes light and enables an extensive, time-resolved anti-Stokes spectrum to be obtained in a single laser shot.

The experiments are being conducted with a recently developed repetitively-pulsed modelocked Nd:phosphate glass laser system.<sup>4</sup> The laser produces energetic 5 ps pulses of high beam quality at 1054 nm and harmonics, at a repetition rate of  $\sim 1/5$  Hz. The laser second harmonic at 527 nm serves as the pump frequency,  $\omega_1$ , for the four-wave nonlinear CARS interaction. The 1054 nm fundamental is focused into a 5-cm liquid D<sub>2</sub>O cell to produce a picosecond pulse continuum, extending throughout the visible and near IR spectrum. The continuum beam is filtered to pass wavelengths  $> 530$  nm, which provides a broad band of light at Stokes frequencies,  $\omega_2$ . The two pulses are combined spatially and

temporally, and focused into a gas sample cell. Relatively strong coherent antistokes signals are generated over the spectrum of frequencies,  $\omega_3 = 2\omega_1 - \omega_2$ , corresponding to Raman-active vibrational resonances,  $\omega_1 - \omega_2$ , of the system under study. The  $\omega_3$  beam is spectrally filtered and focused into a 0.3-m grating spectrograph. The dispersed CARS spectrum is then recorded by an intensified vidicon system.

Figure 1 presents an initial CARS spectrum, at low resolution, obtained with a single 5 ps pulse from ground-state benzene vapor at 40 Torr. The prominent narrow spectral feature is identified as the  $3070 \text{ cm}^{-1}$  symmetric C-H stretch mode of benzene. The vibrational frequency range encompassed in this spectrum extends from approximately  $1500 \text{ cm}^{-1}$  to beyond  $4000 \text{ cm}^{-1}$ . This corresponds to white-light emission from 570 nm to 670 nm: over this region the intensity does not vary greatly. There is, however, an exceptionally intense emission near 720 nm, which gives rise to a nonresonant CARS signal seen as the broad feature at the left edge of the spectrum in Fig. 1.

Experiments are continuing on gaseous and condensed-phase organic molecules to apply this probe technique to studies of transient photofragment formation and ultrafast reactions following 264 nm photolysis.

---

1. K.P. Gross, D.M. Guthals, and J.W. Nibler, J. Chem. Phys. 70, 4673 (1979).

2. W.M. Hetherington III, G.M. Korenowski, and K.B. Eisenthal, Chem. Phys. Lett. 77, 275 (1981).

3. The continuum has previously been applied to inverse Raman scattering; R.R. Alfano and S.L. Shapiro, Chem. Phys. Rev. 8, 631, (1971).

4. L.S. Goldberg, P.E. Schoen, and M.J. Marrone, Applied Optics, to be published.

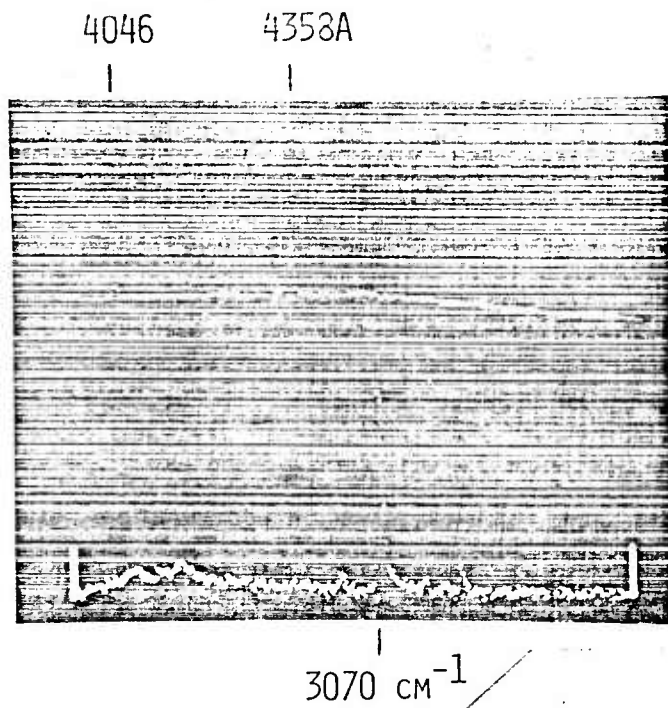


Figure 1. Lower trace: Single-shot picosecond CARS spectrum in benzene vapor, at low resolution. The prominent antistokes emission feature corresponds to the 3070 cm<sup>-1</sup> symmetric C-H stretch mode. Upper trace: Hg calibration spectrum.

REVISED

PICOSECOND STREAK CAMERA FLUOROMETRY: A REVIEW

INVITED PAPER

A. J. Campillo  
Optical Sciences Division  
U.S. Naval Research Laboratory  
Washington, D. C. 20375

S. L. Shapiro  
Molecular Spectroscopy Division  
National Bureau of Standards  
Washington, D. C. 20234

ABSTRACT

A general tutorial survey is presented describing the use of ultrafast streak cameras in picosecond fluorometry. Current instruments exhibit time resolutions of 1 to 10 ps with detection sensitivities of a few photoelectrons. When linear photoelectric recording is employed, a real-time direct display of optical transients is provided. Representative examples from the literature in physics, chemistry and biology are given as well as an extensive bibliography.

## INTRODUCTION

The ultrafast streak camera is one of the most versatile instruments used today in picosecond spectroscopy. Its usefulness arises from its excellent time resolution, its ability to determine optical temporal profiles directly and in a single shot, if need be, and its straightforward integration into remarkably simple experimental configurations. Although the device itself is electronically sophisticated, it resembles a photomultiplier/oscilloscope combination in convenience and operation. This is not coincidental since the streak camera is a photoelectric image converter camera possessing a time-base deflection system similar in principle to those used in cathode-ray oscilloscopes. However, the streak camera possesses two significant advantages over the oscilloscope. First, it yields the temporal history of one spatial dimension. Second, demonstrated bandwidths far exceed that of any present or projected oscilloscope.

The streak camera historically was first used as a diagnostic tool to characterize the output of mode-locked lasers and for monitoring laser fusion implosion experiments, principally at government laboratories. However, the exceptional sensitivity of these devices make them especially attractive for monitoring fluorescence. Recently, an explosive growth has occurred in streak camera fluorometry and this instrument is already regarded by many as a required laboratory device in this application. That this is true, considering the significant expense associated with such systems, is fair testimony to the power and reliability of the technique.

It seemed appropriate to include in this special issue devoted to Picosecond Phenomena a general tutorial and review paper describing the use of streak cameras in picosecond fluorometry. Several excellent reviews <sup>1-4</sup> have

appeared describing the operation and history of the streak camera. This present paper goes beyond the instrumental aspects and reviews the application of laser fluorescence spectroscopy in some detail. We hope this paper satisfies what appears to be a deficiency in this regard in the open literature. We have attempted to present a reasonably self-contained primer in streak camera operation, including examples from the literature in physics, chemistry and biology. We include an extensive bibliography representative of the field as a whole. Due to the continued growth of this subject we are not able to include a complete list of references here.

The key principles of electron optical streak camera operation were established during the period from the late 1940's through the early 1960's. In 1949, Courtney-Pratt employed a deflectable image converter <sup>5,6</sup> to measure temporal/spatial characteristics of light given off during explosive burning in lead azide. This early device resembled currently used systems in most essential details and exhibited a subnanosecond resolution. In the mid 1950's, Zavoiskii and Fanchenko <sup>7,8</sup> calculated the conditions under which picosecond or subpicosecond resolutions might be obtained from these devices and enumerated the fundamental limitations. They pointed out that picosecond resolution required the use of high electric fields (tens of kV/cm) to extract photoelectrons with sufficiently uniform velocity from the cathode. These authors also coined the term "electron-optical chronography", <sup>9</sup> for the new science that would employ these devices to study rapidly varying luminous phenomena. However, experimental progress was stalled because of the lack of suitable optical transients to test practical designs. The situation changed dramatically in 1966 with the invention of the mode-locked Nd:Glass laser

which provided the necessary short optical pulse source. Because conventional detectors of light, such as photodiodes are incapable of measuring such brief pulses, these sources were first characterized with the aid of autocorrelation techniques such as second harmonic generation <sup>10</sup> or two <sup>11</sup> or three photon fluorescence. However, these techniques do not unambiguously characterize the pulse shape. Streak cameras were subsequently used by several groups to examine individual pulses from this laser <sup>12-16</sup> allowing for the first time a direct measurement of the intensity profile,  $I(t)$ . It was discovered <sup>13</sup> that photoelectron time dispersion could be minimized by locating a planar, fine mesh, high potential electrode, called the extraction mesh, close to the tube photocathode, thereby achieving temporal resolutions of ca. 5 ps. Similar results were achieved by applying a high voltage pulse to the shutter grid element of a standard RCA C73435 image converter tube <sup>14</sup>. Shortly thereafter, streak cameras were used to monitor fast laser induced fluorescence <sup>17-27</sup>.

#### Streak Camera Operation

Figure 1 shows in schematic form some of the essential elements in the operation of a streak camera fluorometer. A mode-locked laser source provides the necessary short burst of light to excite the sample. A lens collects a portion of the resulting fluorescence and images the sample onto a slit which is in turn imaged onto the photocathode of the streak tube. Electrons are promptly emitted by the cathode by means of the photoelectric effect and are rapidly accelerated through a mesh and toward the anode. The extraction mesh is provided to minimize the velocity spread in the distribution of emitted photoelectrons. The resulting electron beam current as a function of time closely resembles the envelope function of the fluorescence,

$I(t)$ . An aperture in the anode allows the electron beam to pass, ultimately impinging on a phosphorescent screen. The focus cone provides an electrostatic lensing field which sharply images the slit onto the back phosphor screen. Indeed, if the slit is removed, a well formed image of the illuminated sample cell will be projected onto the phosphor. By dispensing with one spatial dimension through the use of a slit and by sweeping the electron beam across the phosphor screen by applying a linear voltage ramp to a set of deflection plates, a measure of time can be achieved. This occurs because those electrons leaving the photocathode at earlier times will arrive at the phosphor at one position while those that leave at later times will arrive at a different position and time is effectively transformed into spatial position. The resultant phosphorescence emitted by the screen at any spatial position,  $P(x)$ , is proportional to the electron beam current and consequently also to the fluorescence intensity,  $I(t)$ . Typically, the resulting phosphorescent spatial streak is intensified and subsequently photographed or electronically recorded.

The deflection plates are driven by a ramp generator triggered by a portion of the original excitation pulse. Typically, the deflection plates are biased to initially image the beam off screen. As the ramp is applied the beam sweeps onto, across and off the other side.

In assessing the performance of a streak camera, several parameters must be considered. These include, temporal resolution, streak velocity, spatial resolution, timing jitter, optical delay required, sensitivity, spectral characteristics and dynamic range. There are, of course, others but these are the most important and we will discuss each in turn.

The temporal resolution of a streak camera is determined by several factors. The first is commonly called the technical time resolution,  $\Delta\tau_T$ , and is determined by the speed,  $v_D$ , at which electrons are swept across the phosphor (on the order of  $10^9$  to  $10^{10}$  cm/sec) and the spatial resolution,  $L$ , of the image converter tube (typically 5 to 25 line pairs/mm).

$$\Delta\tau_T = \frac{1}{L v_D} \quad (1)$$

With deflection velocities approaching that of light and a spatial resolution of about 7 lp/mm, the technical time limit is in the subpicosecond range. As slower streak rates are used, this quantity can become quite large (~ns). In general, the spatial resolution is determined by the electrostatic lensing characteristics of the image converter tube. During the streak the dynamic spatial resolution is somewhat poorer than in the static mode. Equation (1) must be modified if the size of the magnified/demagnified image of the slit on the phosphor screen is larger than  $1/L$ . In this case, this quantity is substituted for  $1/L$ . Additional degradation of the technical time resolution <sup>may be caused by</sup> saturation effects in the streak system and limitations due to the spatial resolution of the intensifier and/or recording medium.

A second limiting factor is that due to photoelectron time dispersion,  $\Delta\tau_e$ . This effect, which is also called "chromatic time dispersion", arises because electrons are emitted from the cathode with a distribution of velocities and results in cathode to phosphor time of flight differences and subsequent loss of time resolution. This effect is small when the wavelength of the observed signal is near the photocathode red cutoff but becomes progressively more severe at shorter wavelengths. The electron time spread is given by the following relation:

$$\Delta\tau_e \approx \frac{\Delta v}{\mu E} \quad (2)$$

where  $\mu$  is the electron charge/mass ratio,  $\Delta v$  is the halfwidth of the distribution of initial electron velocities and  $E$  is the electric field strength at the cathode. It can be seen from Eq. 2 that  $\Delta\tau_e$  can be reduced significantly by applying large electric fields. This can be conveniently accomplished through the use of a high transmission metallic mesh placed in close proximity to the photocathode and applying a high voltage <sup>28</sup>. When this field approached 10kV/cm,  $\Delta\tau_e$  is reduced to subpicosecond values.

If one assumes that the functional form of the various contributions to the time dispersion are Gaussian <sup>14</sup> then the instrumental time resolution,  $\Delta\tau_{instr}$ , is given by

$$\Delta\tau_{instr} \approx [(\Delta\tau_T)^2 + (\Delta\tau_e)^2]^{1/2} \quad (3)$$

Instrumental time resolutions of the best currently available streak tube are in the range of 0.7 to 2 ps <sup>29,30</sup>. The Photochron II tube claims the highest resolution at 0.7 ps <sup>29,31</sup>. Designs are currently under development which would extend the limit to below 200 femtoseconds <sup>32,33</sup>. In addition, the time resolution of an experimental measurement will be degraded by group dispersion effects in the input collection optics and by the finite duration of the excitation pulse. If this contribution,  $\Delta\tau_e$ , is considered then the resolution of a measurement is approximately:

$$\Delta\tau_{meas}^2 \approx \Delta\tau_{instr}^2 + \Delta\tau_e^2 \quad (4)$$

Several important parameters, streak speed, optical delay required and timing jitter are directly related to the streak camera deflection system. Typically, a 1 to 10 kV voltage ramp is applied to the deflection plates, the risetime determining the streak speed. In practice, the fastest risetime (1 ns) is limited by the intrinsic capacitance and inductance of the deflection system which typically posses a natural frequency in the 100 to 200 MHz range. Use is normally made of a charged transmission line switched by a

krytron <sup>29</sup>, spark gap <sup>34</sup> or avalanche transistor string <sup>35</sup>. A portion of the excitation pulse is directed to a photodiode to generate a fast voltage pulse which triggers the ramp switch. Slower deflection speeds are accomplished through the use of RLC integrating networks, the exact parameter values determining the sweep rate. Because there is an inherent switch delay in the start of the ramp with respect to the incoming trigger signal, it is necessary to optically delay the arrival of the excitation pulse with respect to the trigger (as shown in Fig. 1) typical delay times being tens of nanoseconds even at the fastest deflection speeds. In addition, the required delay will also vary with the streak setting because additional time will be required to overcome the off-screen bias voltage. Most researchers find it convenient to maintain both an excessive fixed optical delay and a variable trigger electrical delay. As the sweep rate is modified, the electrical trigger delay can be adjusted accordingly by adding or subtracting lengths of cable. In addition to optical delay, the switch introduces jitter in the start of the streak. Trigger jitter can range from a picosecond to a nanosecond depending on the type of switch used. Typical jitter in commercial cameras is on the order of 100 to 350 ps. Since the temporal window on many cameras can be less than a nanosecond at the fastest streak rates such jitter can cause the camera to miss the event under observation. Certain applications, for example, low repetition rate single shot experiments where the sample is destroyed, require use of a low jitter switch. We discuss the subject of switches in somewhat more detail later in the section on signal averaging.

In principle, streak cameras are capable of single photoelectron detection and several commercial cameras experimentally approach this ideal to within an

order of magnitude. It is also important to employ high speed light collection optics to both collect fluorescence and image the slit onto the photocathode. Typically, commercial systems supply f/2 to f/3 optics, while some researchers have on occasion incorporated f/1 optics. The use of various photocathode material has allowed streak camera spectral sensitivity to span the broad range extending from the x-ray <sup>36,37</sup> and u.v. (gold photocathodes) to the near IR (S1 photoresponse). Commercial systems are available with the more commonly used photocathode spectral responses (S1, S5, S20, GaAs etc).

Another important quantity is the dynamic range. This parameter is appropriately defined, for a given time resolution, as the range over which the measured light level can be increased beyond a minimum required for an observable record without introducing either spatial and/or temporal degradation in the output record. This quantity is determined experimentally by measuring a short light pulse of known duration and determining the peak intensity at which the apparent half width increases approximately 20% and dividing that intensity by the background noise level of the recording medium. In practice, the range of intensity over which the performance of the camera is acceptable becomes more restricted as temporal resolution is improved. Typical streak tube dynamic ranges are 10 - 100 at 5 ps resolution and  $\geq 500$  at ns resolution.

Such degradation can arise from many sources. For instance, a rather gross spatial resolution deterioration occurs if the photocathode current density exceeds some critical value (typically  $10 \text{ mA/cm}^2$ ) for substantial periods of time ( $> \text{ns}$ ). This current density would occur in practice if only ten photoelectrons/ps were emitted from a  $100 \text{ }\mu\text{m}$  photocathode spot on average. A significant modification of the cathode-surface-potential then occurs which gives rise to aberration effects <sup>38</sup> (e.g. a diverging microlens) in the

electron lens system and subsequent defocusing ('blooming') of the image at the phosphor screen. This spatial image quality deterioration and subsequent loss of time resolution has long been observed in nanosecond and microsecond experiments. When such high photocathode current densities occur over shorter time intervals, the spatial blooming is normally not observed but an intensity-dependent electron transit-time spread occurs which is due to space-charge effects occurring near the photocathode <sup>39,40</sup>. In most applications of picosecond streak camera fluorometers, it is this mechanism that is primarily responsible for loss of dynamic range. In effect, the Coulombic repulsion due to the local space charge in the electron pulse will cause electrons in the lead to be accelerated while those in the rear of the packet will be decelerated. Other causes of dynamic range limitations include saturation of subsequent intensifier stages and the recording medium (e.g. use of film).

### RECORDING

There are two main recording schemes commonly in use today, photography and photoelectric recording. Photography was first employed to obtain streak records and current commercial streak cameras provide a film back option to allow a picture to be taken of the intensifier phosphor. Polaroid film is typically used for timing, determining appropriate intensity levels and for survey purposes while a much higher resolution emulsion may be used for recording data. Unfortunately, there are significant disadvantages associated with film recording that appear to outweigh the advantages. First, processing the film is often time consuming and does not provide an instant readout. Second, each piece of film is somewhat different and requires individual calibration, usually necessitating exposure of a portion of the film to light

which has passed through a step-density wedge. Third, film readout is indirect, requiring microdensitometry of the negatives. Fourth, the available dynamic range is limited (about 4 to 30). The main advantages of photography are its low initial cost and a clear two dimensional visualization of the streak. This latter point is important in some applications as for example use of the streak camera with a dispersive grating to display wavelength changes in fluorescence along the second dimension. Indeed, despite the dynamic range limitations of film, the two dimensional storage capability allows a greater number of bits of information to be recorded than that available using a vidicon/multichannel analyzer, for example. Fig. 2 is from Dneprovskii et al.<sup>41</sup> and illustrates the ability of the streak camera to provide a two dimensional representation of space and time, as well as, of course, light intensity. Here the dimension along the slit is used to monitor spatial beam profiles. As the light pulse traverses a sample of  $\text{CdS}_{0.4}\text{Se}_{0.6}$ , its leading edge is partially absorbed as coherent excitons are generated; this energy is eventually returned to the trailing edge by stimulated re-emission of the excitons. Consequently, the spatial and temporal profiles are modulated. A portion of the entering pulse (I) and transmitted pulse (II) are imaged onto the slit at different places. Successive scans parallel to the slit at various positions along the streak produce the display shown.

The replacement of photography by photoelectric recording<sup>42-45</sup>, for example multichannel image detection, allows the fluorescence profile to be displayed instantly on an oscilloscope and/or digitally stored for later computer analysis. This approach is linear, possesses adequate dynamic range ( $\geq 100$ ) and affords a simplicity of operation. So great are these advantages that this is currently the preferred mode of recording. Most streak camera fluorometers today are used with a vidicon/OMA combination or equivalent video camera/computer analysis system. Figures 3 and 4 are illustrative of the

capability of computer interfaced multichannel image detection. Commercial systems allow processing of raw streak data and correction of time base nonlinearities as well as other distortions (Fig. 3 from Barbara et al.<sup>46</sup>). In Fig. 4, Robinson et al.<sup>47</sup> employed a spectrograph to disperse the various fluorescence wavelengths along the slit direction. Successive time profiles at different wavelengths allow the researcher to determine the existence or absence of wavelength dependent effects.

Some care is necessary to insure that linearity is maintained. For example, an effect known as target lag, arising from the exponential charging characteristics of the vidicon target diodes cause the output to be extremely nonlinear unless a sufficient number of target scans ( $\geq 20$ ) are gathered<sup>44</sup>. Vidicons are also often used in a one dimensional mode; measuring and displaying the intensity of light imaged onto the detector head as a function of position (along the streak) and integrating light in the second dimension (along the slit). Consequently, it is important that the slit of the streak camera be aligned perpendicular to the streak direction and that the light sensitive channels of the OMA be set along the slit image or loss of spatial and temporal resolution will result.

#### CALIBRATION TECHNIQUES

The streak camera owes much of its present popularity to its ability to provide an accurate representation of the time variation of the luminescence under observation. Confidence in the performance of current cameras is due in large part to its proven linear behavior supported through careful calibration data. Early cameras exhibited nonnegligible nonlinear response to both intensity variations and time. Most of the causes (nonlinear deflection

voltage, intensifier pincushion effects, dynamic curvature of the streaked slit image, etc) for this have since been minimized by improved design. However, even today nonlinearities resulting from improper operation (intense light levels, nonlinear recording medium) or component failure can easily distort experimental data. Consequently, it remains prudent to calibrate instruments on a regular basis. Early attempts to calibrate streak cameras were often unnecessarily complicated. For example, step-density wedges placed over the streak camera slit were often used with a large diameter light source to calibrate the cameras response to intensity. Streak rates were determined by viewing the reflections of a calibrating pulse off of two or more glass slides. One such pulse delay device (PDD) <sup>34</sup> using 12 glass slides is shown in Fig. 5. Each reflection was focussed by a lens at different points along the length of the streak camera slit. The resulting comb of pulses, each separated by 160 ps, could be used to verify the magnitude and linearity of the streak rate. Arrangements such as this are somewhat cumbersome. Another approach consisted of viewing fluorescence from dyes exhibiting known exponential decays. A very simple yet accurate scheme <sup>25</sup> introduced by us in 1975 is now universally used. A test pulse is passed through an etalon consisting of two parallel flat mirrors, each having a front surface reflectivity of 50 to 95% and an AR coated rear surface. Emerging is a series of pulses each separated by the roundtrip time in the etalon,  $c/2L$ , and each pulse reduced in intensity from the previous pulse by the product of the mirror reflectivities. The resulting train has a known exponentially decaying envelope function which can be varied by insertion of density filters between the mirrors or by changing the spacing. Using this scheme, both intensity response and streak rate can be quickly calibrated. Fig. 6 shows a streak

camera/OMA readout of a comb of calibration pulses generated by passing the doubled output of a Nd:YAG laser (533 nm, ~26 ps) through an etalon with a round trip time of 100 ps.

### SIGNAL AVERAGING

In its usual operational format, luminescence data is obtained in a single streak. We saw earlier that the level of light viewed by a streak camera could not be increased arbitrarily since saturation effects occur in the photocathode, intensifier and recorder and subsequently distort the data. When detecting fluorescence, however, a common problem is one of not having enough light even after optimizing the input slit width and collection optics. Usually, the solution is to increase the intensity of the excitation laser. Unfortunately, however, this often leads to saturation or nonlinear effects occurring in the sample when the photon flux exceeds a critical value, usually in the range  $10^{13}$  to  $10^{18}$  photons/cm<sup>2</sup>. Operating at or below this critical excitation intensity level greatly restricts the ability of the streak system to adequately obtain data in a single scan and a tradeoff must be made between the signal to noise ratio and achievable time resolution. This point has apparently not been appreciated by a number of researchers and so we include a discussion here.

Consider first the following simple instructive example and derivation. An excitation impulse of magnitude  $I$ , in photons/cm<sup>2</sup>, is assumed incident on a thin absorbing sample of transmission  $T$  which subsequently fluoresces with efficiency  $\phi$  and characteristic exponential lifetime  $\tau_f$ . A lens is used to image (1:1) the light emission with collection efficiency,  $\eta_{opt}$ , onto a slit in contact with a photocathode. The slit has dimensions  $h$  (length) and  $w$  (width). Here it is also assumed that the reverse image of the slit onto the sample, also of dimensions  $h$  and  $w$ , is indeed smaller than the actual sample.

The number of photons,  $P_a$ , absorbed by the imaged sample region is simply  $Ihw(1-T)$ . The light,  $P_e$ , emitted into all solid angles during a short time interval,  $\Delta t$ , is given by  $P_a \phi \tau_f^{-1} (e^{-t'/\tau_f}) \Delta t$ , where  $t'$  is the time elapsed after excitation. The number of photoelectrons emitted by the photocathode during  $\Delta t$  is given by  $P_e \eta_{opt} \eta_{pc}$ , where  $\eta_{pc}$  is the photocathode quantum efficiency. If we ask, what is the corresponding minimum excitation impulse intensity,  $I_{min}$ , required to generate one photoelectron at say the 10% point in the fluorescence decay curve during a time interval corresponding to the desired time resolution,  $\tau_R$  (i.e.  $\Delta t = \tau_R$ ) then the answer may be obtained by setting  $P_e \eta_{opt} \eta_{pc}$  equal to 1,  $e^{-t'/\tau_f} = 0.1$  and solving for  $I$ .

$$I_{min} = \frac{10 \tau_f}{hw(1-T)\tau_R \phi \eta_{opt} \eta_{pc}} \quad (5)$$

Examination of equation (5) leads to several important implications. First detection of fluorescence in a single streak requires a minimum excitation intensity which depends inversely upon the desired time resolution. This follows logically since a sufficient number of photons must impinge on the streak camera photocathode during the time resolved interval to be detected. As the time resolution is improved, a greater photon flux is required eventually exceeding a value which the molecular system can tolerate. This molecular saturation ultimately limits the time resolution achievable. In specifying camera sensitivity manufacturers typically begin where equation (5) leaves off by providing data on the minimum number of photoelectrons,  $N$ , required to yield a detectable signal. For example, typically 10 photoelectrons (or ca. 100 photons impinging on the photocathode) will yield an electrical signal (assuming photoelectric recording) which exceeds the system noise level. However, from equation (5) we see that the slit parameters,  $h$  and  $w$ , and the collection optics efficiency,  $\eta_{opt}$ , are also critical.  $\eta_{opt}$ ,  $h$  and  $w$  must be made as large as possible. In the case of a

single collection lens with 1 to 1 imaging,  $n_{opt} = F^2 t / 64$ , where  $F$  and  $t$  are the f/number and transmission of the lens.  $h$  is determined by the recording spatial resolution along the slit.  $w$  is usually constrained by the desired time resolution. In most streak camera systems, light passing through the slit is actually relayed to the photocathode by a second lens system (see Fig. 1) matched to the collection lens. The subsequent magnification of the slit onto the photocathode is given by  $M_{opt}$  and magnification of the resulting image after intensification is given by  $M_{elec}$ . If the slit width is increased to the point where the instrumental time resolution is approximately equal to the technical time resolution, then  $\tau_R$  will be given by

$$\tau_R \approx M_{opt} M_{elec} R w \quad (6a)$$

$R$  is the streak rate. In terms of slit width, an expression for the excitation intensity required for an S/N of 1 at the 10% decay point is given by:

$$I_{min} \approx \frac{10 N \tau_f}{hw^2(1-T) M_{opt} M_{elec} \phi n_{opt} n_{pc} R} \quad (6b)$$

By using equation (6a), equation (6b) can be expressed instead in terms of the desired time resolution.  $M_{opt}$  is often less than unity to enhance the instrumental time resolution. However, this usually leads to a less efficient light collection system. Equation (6b) assumes that the recording system spatial resolution corresponds to the width of the slit image,  $M_{opt} M_{elec} w$ . The quantity  $N$  is greater than 1 because of internal streak camera losses and competition from noise sources. In the design shown in Fig. 1, a fraction of photoelectrons are lost due to geometrical aperturing of the extraction mesh as well as coupling losses to the intensifier stage, the latter being lost in either lens or fiber output coupling. In some designs a multichannel plate

intensifier is incorporated into the streak tube and there are associated aperturing losses in that case also. These losses cannot be compensated by the use of additional intensifier gain since the signal to noise of the system will usually be limited by the Poisson statistics of the small number of photoelectrons present in the streak tube at any given time. In practice, time resolutions of 10 ps typically require excitation intensity fluxes of  $10^{14}$  photons/cm<sup>2</sup> or greater for signal to noise ratios of 10 or better. A serious problem arises in many systems as one attempts to obtain higher time resolutions via single shot analysis; the intensity of the excitation source becomes so great that nonlinear optical effects, excited state saturation, stimulated emission and other artifacts result. An excellent example of this was discussed in Campillo et al.<sup>43</sup>. These authors studied the emission from chlorophyll molecules within the light collection or antenna apparatus of green plant chloroplasts. These molecules form networks of several hundred chlorophylls that collect light and funnel energy to a reaction center trap via a random walking Frenkel singlet exciton. The complex has a rather large absorption cross section ( $\sim 300 \text{ \AA}^2$ ) and intensities of  $>10^{13}$  photons/cm<sup>2</sup> result in multiple excitations and subsequent singlet-singlet exciton annihilation processes. This results in reduced fluorescence quantum efficiency and an anomalously shortened observed lifetime. The resulting nonexponential decay profiles are shown as a function of excitation intensity in figure 7. While most samples can tolerate higher photon fluxes than can plant chloroplasts, this drawback of single shot analysis places an inherent limitation preventing useful application of improved time resolution in weakly fluorescing samples.

A logical solution to the above limitation is to accumulate a great number of streaks at lower excitation intensities yet with superior time resolution and to sum these, the accumulated data thereby being effectively

signal averaged. However, achieving this requires that the electrical ramp which drives the deflection plates of the streak camera be accurately synchronized to the start of the fluorescence signal. Unfortunately, conventional techniques such as krytron or spark gap switches or avalanche transistor stacks commonly used for generating the sweep voltage result in significant pulse to pulse jitter (50-350 ps) as well as long term drift. This uncertainty in the start of the streak effectively negates the beneficial effect of signal averaging since the temporal resolution of the accumulated scans would be significantly degraded. Several approaches to this problem have been tried with good success: (1) use of an intense pulse arriving at the streak camera prior to the onset of fluorescence which serves as a temporal fiducial marker <sup>48</sup> and use of a computer to note the position of the pre-pulse, establish the true zero time of each shot and subsequently accumulate the corrected streaks, (2) use of a continuous repetitively mode-locked laser and a synchronously scanning streak camera <sup>49,50</sup> whose deflection plate voltage is phase locked to the recurring excitation source and results in substantially less jitter (5 ps) and (3) use of a specialized low jitter (2 ps) light activated switch <sup>51</sup> to initiate the deflection plate voltage thereby allowing direct accumulation of non-recurrent streaks.

The first technique above attempts to compensate for the jitter while the latter two attempt to eliminate it. The use of a fiducial pulse as a time marker, introduced by us <sup>48,52</sup> has the advantage of using standard deflection circuits and is currently used by many researchers. However, the technique requires either computer or human processing and the accumulation of more than a score of data shots is tedious. A recent modification <sup>53</sup> of the fiducial pulse technique is shown in Figure 8, which depicts C<sub>2</sub> swan band emission

following UV photolysis of gaseous acetylene at a pressure of several torr. Here a 532 nm fiducial pulse was split into two distinct marker pulses separated by 500 ps and directed via a second path to an adjacent part of the streak camera entrance slit. Dual traces, fluorescence and timing pulses, were recorded by a Nuclear Data vidicon system interfaced to a Nicolet minicomputer. Because of the weak emission, single shot fluorescence curves were noise dominated. Each streak trace and its corresponding reference were stored individually and were then shifted to a common timing mark and averaged. A risetime of 215 ps could be deduced by averaging 10 shots.

The synchronously scanning streak camera <sup>49,50</sup>, or "synchroscan" camera has been developed for use with recurrent lasers, that is, those producing a continuous train of ultrashort pulses each separated by nanoseconds, as for example CW passive<sup>54,55</sup> or synchronously pumped<sup>56-58</sup> dye lasers. By modifying the deflection circuitry to enable the camera to streak repetitively to correspond to the time between pulses in the train, it is possible to precisely superimpose successive images of the streaked fluorescence profiles. This effectively allows the integration of  $10^8$  fluorescence records in a recording time of 1 second and eliminates the need for image intensification. A steady image is formed which is clearly visible on the streak phosphor. This allows observation of weakly emitting species and the avoidance of high intensity effects in the sample.

Figure 9 shows a block diagram of the electrical layout of a synchroscan unit. An oscillator-power amplifier combination is coupled to the deflector plates of a streak tube to produce a sinusoidal deflection on the screen, the central linear portion of which is actually used. The resonant frequency of the oscillator/amplifier circuits are tuned to match the repetition frequency

of the laser in the range 70-200 MHz and are compatible with the natural frequency range of the deflection plates. The power amplifier was fed from a driver stage that could be operated either as an oscillator or amplifier, depending on the characteristics of the excitation laser. For example, when used with a CW synchronously pumped modelocked dye laser, where a continuous stable high frequency electrical signal was available from the argon laser mode-locker RF source, this is directly amplified in the driver stage to a level sufficient to fully load the output stage. When a passively mode-locked system is used, a portion of the light pulse train is directed to a photodetector which in turn produces the required electrical signal. When a burst of optical pulses is used, as for example from a pulsed mode-locked Nd:YAG laser, the photodetector output is then used to pull into synchronism the driver stage which is now operated as an oscillator and adjusted as closely as possible to the correct frequency.

Resolutions of ca. 5 ps using synchronously-pumped dye lasers at repetition rates of 140 MHz have been achieved using this technique <sup>49,50,59</sup>. In theory, this streaking method should yield subpicosecond jitter. Presently, the jitter is believed to be due to causes other than in the deflection system itself, for example, drift in the RF driving electronics, jitter in the repetition rate of the mode-locked CW lasers and variation in the durations of the dye laser pulses. Experimental dynamic range has also been improved from 30, for single shot measurements to over  $3 \times 10^3$  in this mode of operation <sup>60</sup>. The principle drawback to widespread use of the synchroscan approach lies in the availability of a number of straightforward sampling and nonlinear optical <sup>57</sup> techniques that may also be used with CW mode-locked lasers. By contrast, the streak camera, when used in a single sweep mode, appears superior to other techniques.

An example of the use of the synchroscan system is shown in Figure 10 from the work of Fujimoto et al. <sup>61</sup>. Using frequency doubled Rhodamine 6G laser pulses, Fujimoto et al. were able to demonstrate that the lifetime of the bound exciton in CuCl at 8° K is 130 ps. Even with excitation pulses containing only  $10^{-13}$  J, good signal to noise ratios were obtained. Operating at low excitation intensities allowed these authors to avoid nonlinear effects such as the previously discussed exciton-exciton interactions that occur in many solid state systems such as this.

A somewhat different scheme <sup>62,63</sup> has been considered in which a conventional camera is streaked at a low subharmonic (1-40 kHz) of the train frequency of a modelocked dye laser. The deflection voltage of the camera is derived from a step voltage generator built up with avalanche transistors or a high frequency electronic tube which charges the capacitance of the deflection plates and provides a sweep rate of ca. 200 ps/cm. Basically, this is very similar to the method used in single shot operation but with the deflection system designed to accomodate kHz rates of input pulses. Both synchroscan and this technique may be used with cavity dumped dye lasers. Cavity dumping reduces the excitation rate and allows investigation of fluorescence from samples with long recovery times.

Recently, near jitter-free (~2 ps) streak camera observation of light signals generated by non-recurrent laser pulses as outlined in (3) above has been achieved using a laser-activated switch employing either cryogenically cooled Si <sup>64,65</sup> or ambient temperature GaAs doped with Cr <sup>66</sup>. The latter material is attractive because of its high dielectric strength and its high resistivity ( $10^8 \Omega\text{-cm}$ ) enabling D.C. biasing at room temperature without thermal runaway. Figure 11 is from Knox and Mourou <sup>66</sup> and summarizes the manner in which the GaAs photoconductive switch is integrated into the sweep

circuitry. These researchers employed a 3mm gap biased at 0-5 kV D.C. which when illuminated by a portion of the  $1.06\mu\text{m}$  laser pulse conducts and charges the deflection plates through a current limiting resistor,  $R_C$ . As the deflection plates charge, the photoelectron beam is swept at nearly half the speed of light in a linear manner from one side of the streak tube phosphor, across and eventually off screen at the other side. After about a millisecond the plate voltage returns to initial bias level by discharging through the large bias resistor,  $R_B$ . There are several significant advantages associated with this scheme. First, and most importantly, is that the resultant short term jitter is a small fraction of the trigger laser pulse duration. For example, 30 ps pulses from a mode-locked Nd:YAG laser result in jitter of about 2 ps. Consequently, signal averaging can be performed using this technique to further increase the timing precision and signal-to-noise ratio. Figure 12 illustrates the latter, in a dramatic but typical way. The upper trace shows the luminescence from CdSe<sup>67</sup> obtained during a single streak. The signal-to-noise is too poor in this case to determine the decay time. However, after accumulating 300 streaks, an accurate estimate can be made of this parameter. Stavola et al<sup>65</sup> demonstrated that by averaging as few as 50 shots, a time delay of 0.4 psec between 30 psec pulses is resolvable to within  $\pm 0.05$  psec. They also showed that the long term timing drift present in other trigger/sweep circuits was negligible with this scheme. The second advantage is that the photoconductive switch can be triggered with fairly modest laser energies ( $<100\mu\text{J}$ ). This should be compared to the multi-mJ requirement of gas

or mylar spark gap<sup>68</sup> switches. Third, the fact that the photoelectron beam remains off screen for about a millisecond allows long lived ( $\geq$   $\mu$ sec) species to decay sufficiently before the retrace. Fourth, use of this scheme with signal averaging results in an enhanced dynamic range. There are some minor disadvantages associated with this technique. First, the switches are not commercially available and must be home-made. Second, the range of available streak rates is greatly restricted. Although the ramp speed can be varied somewhat by changing the DC bias voltage, it cannot be slowed to a value lower than permitted by the intrinsic carrier recombination time of the switch material. However, since the jitter associated with conventional schemes is primarily a problem only at the fastest streak rates the photoconductive switch is really required only at the highest streak camera resolutions and can be profitably employed in alliance with commercially available streak units. Finally, this scheme is not appropriate for rapid accumulation of data generated by bursts of recurrent pulses as, for example, from a modelocked train generated with a pulsed Nd<sup>3+</sup>:YAG laser. However, overall, the use of this switch greatly extends the capability of existing streak cameras and provides an exciting opportunity in future luminescence research.

## BIOLOGY

Picosecond Spectroscopy has played an important role in understanding the initial steps in several photobiological processes.<sup>69,70</sup> Interestingly, the early streak camera fluorescence literature (1974-1977) was almost entirely devoted to studying the role of exciton migration<sup>18-27,43,71-79</sup> in photosynthesis. The first steps in photosynthesis involve light absorption by

specialized antenna pigments (chlorophylls, caroteins, etc.) followed by efficient energy migration to a reaction center complex whereupon the excitation is utilized to drive the photosynthetic process. The various pigment species have complimentary overlapping absorption bands that together span the visible spectrum. Once excited, the accessory pigment molecules very quickly ( $\sim 1$  ps) transfer their energy via a nonradiative dipole-dipole interaction to a Chl a molecule. The Chl a's first excited singlet state has a lower energy than the singlet states of the antenna pigments and so the reverse jump is highly improbable. Possible, however, are further similar "Förster transitions between neighboring Chl a molecules and consequently the excited state, or Frenkel exciton, begins a random walk through the Chl a antenna matrix until it wanders near the reaction center complex whereupon it is quickly captured. The entire process, from initial pigment absorption to reaction center capture, although involving many hundreds of separate energy transfer steps, occurs in less than one nanosecond and has quantum yields for photon utilization approaching 100%.

The actual physico-chemical situation is fairly complicated and the exact organization of the antenna system was previously unknown. Photosynthesis in green plants takes place on a thin (ca. 10 nm) membrane called the thylakoid which is shaped like a flattened hollow sac. The major constituent of the thylakoid is chlorophyll which exists in a variety of chlorophyll-protein complexes. The various protein complexes, each composed of a dozen or so chlorophyll molecules, accessory pigments or other specialized photosynthetic material (cytochromes, ferredoxin, etc.) are the building blocks of the photosynthetic apparatus. The dimensions of these building blocks are

unfortunately too small to discern their precise organization using electron microscopy. Thus we must rely on indirect information such as that obtained with picosecond spectroscopic techniques. Repetitive structures, called quantasomes, measuring about 20 by 15 by 10 nm and arranged much like cobblestones cover the thylakoid membranes. These quantasomes are often identified with the photosynthetic unit (PSU), a hypothetical entity which contains all the functional material necessary to perform photosynthesis independently.

It is believed that in green plants there are at least two photosystems, PS I and PS II, which are in close proximity, each having their own distinct cooperative photochemistry. PS I, the smaller of the two units, upon red light absorption produces a strong reductant and a weak oxidant, whereas PS II, upon absorption of 'bluer' photons, produces a strong oxidant and a weak reductant. Electron flow from the weak reductant to the weak oxidant is coupled to the conversion of adenosine diphosphate and inorganic phosphate to adenosine triphosphate (ATP). ATP assists the strong reductant to reduce  $\text{CO}_2$  to a carbohydrate ( $\text{CH}_2\text{O}$ ), and the strong oxidant oxidizes  $\text{H}_2\text{O}$  to  $\text{O}_2$ . PSI and PSII are thought to be located on the outer and inner surfaces of the thylakoid, respectively.

Ultrafast streak camera measurements of fluorescence 18-27,43,71-91 from various molecular species can be readily employed to deduce information about the antenna apparatus of plants that is not presently obtainable by other means. The observed fluorescence would accurately probe the excited state density of the species under observation while wavelength dependent data track the various pathways. In particular, in green plants, the fluorescence decay

from Chl a is predominantly determined by the exciton migration time to the reaction center, which effectively quenches the Chl a excited state population. This rate can in turn be utilized to test various models under consideration. Further information may be obtained by studying the additional quenching mechanisms that come into play at higher excitation intensities. For example, by flooding the antenna network with additional excitons, Campillo et al.<sup>43,71</sup> have shown that the excitons have a high probability of interacting with each other via a singlet fusion scheme that effectively annihilates one of the excitons and leads to shorter decay times as in Figure 7. The manner in which excitons interact in vivo should strongly reflect the existence or non-existence of boundary conditions (puddle model), provide information on the coupling of the two photosystems and also assist in obtaining values for various rate coefficients.

Figures 13 and 14 are from Campillo et al.<sup>79</sup> and illustrate how fluorescence data from spinach chloroplasts at 77°K supports a modified tripartite model of antenna organization. Figure 13 depicts this model in which there are believed to be two types of light harvesting (LH) pigments; in one of these denoted by LH(1), the chlorophyll molecules are tightly coupled to the PSI pigment system with  $K \gg \beta_{II}$ ; i.e. the exciton lifetime is mainly determined by energy transfer to PSI, with  $K^{-1} \approx 140$  ps. The fluorescence yield from this system is low. The second type of LH pigments, LH(2) consists of chlorophyll molecules which are less tightly coupled to PSI (possible because of a large physical separation) and which decay mainly by the rate constant  $\beta_{II} \approx (800 \text{ ps})^{-1}$ . The fluorescence yield from this system is relatively high. The 735 nm emission is thus unaffected by exciton annihilation within LH(1) up to intensities of  $I \sim 10^{15}$  photons  $\text{cm}^{-2}$  per pulse when the

annihilation rate begins to compete with the rapid LH(1) → PSI transfer rate characterized by the rate constant K. This model is capable of accounting for all observations shown in Figure 14 as well as those presented in References 75 and 79.

Because of the complexity of the green plant apparatus many researchers have employed streak camera techniques in algae,<sup>73,81,82,88</sup> in photosynthetic bacteria<sup>74,76</sup> and in isolated light harvesting proteins.<sup>89-91</sup> This greatly facilitates interpretation of the data and has greatly increased the understanding of these systems.

Streak cameras have also been applied to other photochemically active biological systems. These include studies of the visual pigments Rhodopsin and Isorhodopsin<sup>92</sup> and the pseudo-photosynthetic protein, Bacteriorhodopsin<sup>93</sup>. Fluorescence from these molecules is difficult to observe because of the low quantum yields and because fluorescence from impurities in the sample can mask the intrinsic fluorescence. Fluorescence has also been observed and used as a probe in studies of dye molecules intercalated within DNA<sup>24</sup> or incorporated in aqueous micellar dispersions<sup>94,95</sup>.

#### CHEMICAL PHYSICS

Picosecond spectroscopy has found numerous applications in chemical physics. Molecular changes often occur in the subnanosecond time regime and excitation by picosecond lasers makes it possible to determine the evolution of a molecular system through its various energy states and transient chemical species. Researchers have employed picosecond streak camera fluorometry to study phenomena such as internal conversion,<sup>18</sup> vibrational decay,<sup>46</sup> intermolecular energy transfer,<sup>24,100-102</sup> solvent effects,<sup>103-104,106-110</sup> rotational diffusion,<sup>111-112</sup> conformational changes,<sup>17,63,113,114</sup> charge transfer phenomena,<sup>115-117</sup> photoejection, electron transfer and

solvation,<sup>118-119</sup> protonation and deprotonation,<sup>120-129</sup> excited state hydrogen bonded complexes,<sup>130-133</sup> excimer formation<sup>134-136</sup> and photochemistry<sup>53,137</sup>.

Shapiro et al.<sup>18</sup> measured the upper limit for vibrational state internal conversion in dimethyl POPOP and perylene molecules in the gaseous phase. The 353 nm pulses excited vibrational states high in the  $S_1$  manifold while the fluorescence was observed at 580 nm. The risetime was found to be less than 20 ps for dimethyl POPOP and less than 30 ps for perylene. Since the vapors were at 300°C, the collision rate between molecules could have been no more than  $10^8/s$ , about  $10^4$  times fewer collisions than in the liquid phase. Since fluorescence is commonly observed from the lowest vibrational state of  $S_1$ , the rapid risetime in the vapor was interpreted as direct evidence supporting rapid internal relaxation of the molecules, even in the absence of collisions. The ability of large dye molecules to relax internally independent of their surroundings is a manifestation of the fact that such molecules have a large number of vibrational and rotational modes so that the probability of mutual interactions among the modes is high. These interactions reduce the lifetime of any particular level, because any excess energy provided by the excitation wavelength can be rapidly redistributed over the large ensemble of densely packed levels.

Barbara et al.<sup>46</sup> studied the time and wavelength characteristics of s-tetrazine fluorescence in n-hexane excited by a 530 nm pulse at the  $v' = 1$  level. The decay of the excited state vibration has been monitored by comparing the risetime of the spectrally unresolved fluorescence to that of the (0,0) fluorescence at 560 nm. Vibrational relaxation was found to occur within 8 ps.

Several researchers have studied the resonant intermolecular transfer process between two dissimilar molecules. This type of transfer was treated by Förster<sup>99</sup> and results from dipole-dipole coupling between the two molecules. The rate of energy transfer is proportional to  $1/r^6$ , where  $r$  is the spacing between the two molecules, and hence is a sensitive function of concentration. A Förster radius,  $R_0$ , is defined as the interaction distance where the probability of energy transfer just equals the probability of the donor molecule losing its excitation through other mechanisms.  $R_0$  is calculable from the overlap of the acceptor absorption and donor emission spectra. Förster's equation describing the decay of the excited state molecules with time is given by:

$$n(t) = n_0 \exp \left[ -t/\tau - 0.846 \sqrt{\pi} N \frac{R_0^3}{R_g^3} (t/\tau)^{1/2} \right] \quad (7)$$

where  $\tau$  is the lifetime,  $N$  is the number of molecules within a sphere of radius  $R_g$ . At high concentrations the second term dominates. Shapiro et al.<sup>24</sup> found that the fluorescence lifetime of chlorophylls in chloroform showed the correct dependence of lifetime with concentration from 0.0038 to 0.1M. Porter and Tredwell<sup>100</sup> examined the transfer between rhodamine 6G and malachite green in a low viscosity solvent, ethanol. The donor fluorescence decay function was also found to be in agreement with equation (7) over a tenfold range of

acceptor concentrations ( $10^{-3}$  to  $10^{-2}$ ). Adams et al.<sup>101</sup> observed singlet-singlet resonance energy transfer from DQOCI (donor) to malachite green and to DQOCI in ethanolic solutions. They obtained  $R_0$  values of 45.6 Å for malachite green and 61.8 Å for DQOCI from the fluorescence decay curves. Departure from Förster kinetics was observed at the lowest acceptor concentrations employed. Sato et al.<sup>102</sup> employed Förster transfer as a probe of membrane formation. By monitoring the energy transfer between rhodamine 6G and 3,3'-diethylthiacarbocyanine iodide (DTC) in water, a normal decay versus concentration was found, as expected. However, when  $5 \times 10^{-3} M$  sodium lauryl sulfate, a substance that stimulates micellar growth, was added a departure from Förster theory was observed at a critical concentration. At that point the local concentration of DTC appeared to increase about 90-fold suggesting dye-enriched micelle formation occurred.

Fluorescence from a dye molecule is greatly affected by the environment in which it is placed. In solution, the yield and lifetime can be readily affected by parameters such as viscosity, polarity, pH, temperature, hydrogen bond donor or acceptor strength. As a practical matter, understanding these processes can be important in a number of applications, for example, in probing the structure of biological molecules. Researchers seeking to improve laser performance are searching for ways to increase dye fluorescence yield while others seeking better mode-locking dyes are searching for ways to decrease yield and the accompanying fast decay. Several researchers have studied the effect of viscosity on lifetime as well as the effect of atomic substitution. Fleming et al.<sup>103</sup> studied the photophysics of fluorescein and three of its halogenated derivatives, eosin, erythrosin and rose bengal in aqueous and simple alcoholic solvents. In these systems, the fluorescence

lifetime is primarily determined by the intersystem ( $S_1 - T_1$ ) crossing rate. As the solvent changes from i-Propanol to  $H_2O$  or there is increased substituent halogenation ("heavy atom effect") of the parent, fluorescein, the fluorescence maxima shift to the blue and the lifetimes are observed to decrease markedly. This is consistent with both the increased  $S_1 - S_0$  spectral blue shift and a smaller  $S_1 - T_1$  energy gap which enhances the intersystem crossing rate. The solvent effect was further studied by Yu et al.<sup>104</sup> who observed the lifetime of erythrosin in a water-acetone solution as a function of concentration. The fluorescence lifetime was observed to decrease linearly as the concentration of water increased. This group also studied the effect of solvent viscosity,  $\eta$ , on the decay rate of malachite green and found that the lifetime varied as  $\eta^{3/2}$  in the range  $1 < \eta < 60$  poise (p). This is consistent with the model of Förster and Hoffmann<sup>105</sup> who postulate that the increase in fluorescence is due to the inhibition of the rotational motion of the phenyl rings of the dye molecules in a viscous medium. As a consequence, the rate of internal conversion and fluorescence lifetime should show a strong viscosity dependence.

Mialocq et al.<sup>106</sup> studied the photobleaching and absorption recovery as well as fluorescence of pinacyanol. In a viscous solvent, such as glycerol, the recovery time of  $330 \pm 30$  ps was approximately equal to the fluorescence lifetime,  $302 \pm 29$  ps. In light alcohols, such as methanol or isopropanol, the recovery time was less than 10 ps indicating very efficient internal conversion between the two singlet states involved. Sibbett et al.<sup>107-109</sup> investigated a number of polymethine dyes of the cyanine family in variety of solvents and over a fair range of viscosities (0.5 - 250 cp). Although the

cyanine dyes examined did not possess a structural form necessary to be included in the Förster theoretical model of viscosity dependent fluorescence lifetime, efficient loss of excitation energy within the dye should occur through partial rotation of the aromatic rings about the linking aliphatic chain. The measured lifetimes were found to follow a  $2/3$  or  $1/3$  power dependence of the viscosity.

Heisel et al.<sup>63</sup> measured the fluorescence decays of pinacyanol in glycerol ( $\tau = 280$  ps) and a 50/50 mixture of glycerol and ethanol ( $\tau = 143$  ps). Huppert et al.<sup>110</sup> studied the dual-fluorescence kinetics of p-dimethylaminobenzonitrile in several alcohols. The  $b^*$  state emission was found to rise promptly and funnel into the  $a^*$  state. This rate followed the solvent viscosity.

In most fluorescence measurements, the exciting pulse is laser derived and is polarized. However, because of this whenever the lifetime of the emission occurs on the same timescale as molecular rotation, as is often the case in liquids, then it is necessary to correct for polarization effects of the emitted light. Any rotation of the molecule between the time it absorbs and emits light affects the angle between the polarization vectors of absorption and emission. Consequently, the emission,  $I_{11}(t)$ , polarized parallel to the exciting pulse polarization decays somewhat faster than the population of the emitting state. Conversely, the emission,  $I_{\perp}(t)$ , polarized perpendicular to the exciting pulse also has a complicated profile. Observing unpolarized emission (i.e.  $I_{11} + I_{\perp}$ ) after having excited with polarized light will not completely eliminate the interference effects occurring between the two polarizations. However, it can be shown that the correct fluorescence decay is given by  $I_{11}(t) + 2I_{\perp}(t)$ . Thus if an analyzer is used and set at a

magic angle,  $\alpha = 54.7^\circ$  (from  $\tan^2 \alpha = 2$ ), then such effects are negligible. A number of researchers, however, rely on fluorescence depolarization to yield rotational relaxation data. A parameter, called the time-dependent polarization anisotropy, is experimentally measurable and can be related to various theoretical models. It is defined by the quantity,

$$r(t) = \frac{I_{11}(t) - I_{\perp}(t)}{I_{11}(t) + 2I_{\perp}(t)} \quad (8)$$

Of major interest is whether or not orientational relaxation of molecules can be described by the Stokes-Einstein-Debye relationship,  $\tau_{OR} = \eta V(kT)^{-1}$  which assumes hydrodynamic or 'stick' boundary conditions. Fleming et al.<sup>111</sup> utilized polarization spectroscopy to study eosin and rose bengal in a variety of solvents. Both the fluorescence decay curve and the rotational correlation function derived from the experimental data decayed as pure exponentials.

Many molecules undergo conformational changes after absorbing light including some having importance in ultrafast spectroscopy. For example, the photoisomer of DODCI plays an important role in the mode-locking of rhodamine dye lasers, especially at the longer wavelengths. This fact was verified by Arthurs et al.<sup>17</sup> who studied DODCI under conditions of mode-locking. They determined that after excitation an equilibrium is established between the two forms and that both display fluorescence lifetimes of  $330 \pm 40$  ps. Sumitani et al.<sup>113</sup> and Heisel et al.<sup>63,114</sup> studied trans-stilbene. The trans-cis geometrical isomerization of stilbene is a rather fundamental form of photochemical reaction. Sumitani et al. studied the temperature dependence

of the fluorescence lifetimes of trans-stilbene and observed a smooth sigmoidal relation, quite similar to the temperature dependence of the quantum yield. The results indicate that the relative rate is constant from 77 to 295°K. Heisel et al.<sup>114</sup> observed two components in the decay of the emission. The slow component was attributed to a return to the trans-geometry after photoisomerization. The rate constant for photoisomerization to excited twisted stilbene shows an Arrhenius temperature dependence, with an activation energy of 2.6 kcal/mole and a frequency factor of  $1.2 \times 10^{12} \text{ s}^{-1}$ . The reverse process has a rate constant 500 times smaller.

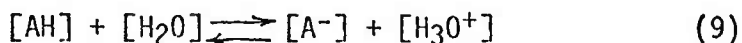
Another class of excited-state interactions involves the transfer of an electron between a donor molecule D and an acceptor A, one of which is in an electronically excited state, to produce a new species  $(A^- - D^+)^*$ , called an excited state charge transfer complex or exciplex. The excited molecule may be the electron donor or acceptor. Before electron transfer can occur the donor and acceptor must diffuse to within an appropriate separation distance. Consequently, environmental factors play an important role. Certain geometrical orientations are required to form the exciplex in nonpolar solvents whereas in highly polar solvents there is direct electron transfer resulting in an ion pair. Eisenthal et al.<sup>115-117</sup> studied several cases of exciplexes resulting from intramolecular conversion. In the case of the intramolecular exciplex anthracene- $(\text{CH}_2)_3$ -N,N-dimethylaniline in acetonitrile,<sup>116</sup> two processes occur. First is a very rapid ( $7 \pm 1 \text{ ps}$ ) electron transfer for molecules in extended conformations, producing solvated ion pairs without passing through the exciplex state. Second, folded conformers yield exciplexes within 2 ps, having a lifetime of  $580 \pm 30 \text{ ps}$ . This component emits in the 500-600 nm region and is shown in Figure 15. The dual fluorescence of p-(dimethylamino) benzonitrile (DMABN) in propanol solution was also studied.<sup>117</sup> Two emitting

states were observed to reach equilibrium with a rate of ca. 20 ps. The forward reaction rate (20 ps) is the time required for the molecule to relax conformationally to a charge-transfer geometry. Figure 16 shows the DMABN fluorescence at 350 nm and the rise of the CT complex at 480 nm.

Besides electron transfer from one molecular species to another, photoejection can occur resulting in an excess electron remaining in the liquid.<sup>118-119</sup> The electrons are thought to be solvated by initially being trapped in already existent molecular solvent clusters that form relatively shallow potential wells. Once the electron is localized, the surrounding solvent dipoles reorient themselves about the electron, deepening the potential well and leading to the formation of the solvated electron. Monitoring the steps involved in the localization of the quasi-free electron in the solvent yields information on the structure and relaxation properties of the liquid as well as the nature of the electron-solvent cluster. The trapped and solvated electrons possess distinct absorption bands and typically, this process is followed through absorption spectroscopy. However, Auerbach et al.<sup>119</sup> have monitored the fluorescence from toluidenyl naphthalene sulfonate (TNS) in water/ethanol solvent mixtures. Their data suggests that in the excited state, TNS in water has a preexisting local solvent structure that promotes the electron transfer to the solvent. Evidence based on the dynamics of solvent exchange in mixed solvent systems indicates that this structure consists of approximately twelve water molecules.

There has been considerable interest in using streak camera fluorometry to study excited state protonation and deprotonation kinetics. This has been stimulated by a novel technique, the laser "pH Jump," which enables the researcher to rapidly vary the hydrogen ion concentration of a solution using

laser excitation. This in turn can be used to initiate ground state acid or base catalyzed reactions and to follow subsequent reactions. It's useful to review several acid-base concepts, here. A typical reversible acid reaction is described by the equation



Here AH is an acid that gives up a proton to water to form a hydronium ion,  $\text{H}_3\text{O}^+$ , and an anion,  $\text{A}^-$ . pH in this case is simply  $-\log_{10}[\text{H}_3\text{O}^+]$ , where the bracket indicates the concentration in moles/liter. Thus a pH of 2 indicates that the concentration of hydronium ions is  $10^{-2}$  moles/liter. Equation 9 can be described by a characteristic acid equilibrium constant, K defined as:

$$K = \frac{[\text{A}^-] \cdot [\text{H}_3\text{O}^+]}{[\text{AH}]} \quad (10)$$

If the amount of one of the constituents is varied, the others will adjust to keep K constant. pK is defined as the  $-\log_{10}K$  and is a useful chemical shorthand for indicating the strength of an acid or base. For the reaction given in (9), a pK of 8 would indicate a weak acid, whereas a pK of 1 would indicate a strong acid. Physically, when the pH of a solution is adjusted so that it equals the pK of the acid, then  $[\text{AH}] = [\text{A}^-]$ .

There is a strong link between the acid-base properties of a molecule and its electronic structure. Thus a change in electronic structure, say by

excitation after light absorption, should produce a concomitant change in acid-base properties. Indeed in many compounds the acid dissociation constant ( $pK_a$  value) varies between the ground and electronically excited states. Somewhat surprisingly, the changes in  $pK$  value can be many orders of magnitude. For example, 2-naphthol-6-sulfonate is a weak acid in its ground state but in its first excited singlet state it is a strong acid, showing a  $pK$  change of 7. Fluorene, an aromatic hydrocarbon, shows a  $pK$  change of 29 upon excitation. Some compounds such as phenanthrene, become less acidic in the excited state. This phenomenon is characteristic of bases as well as acids.

Intense picosecond pulses allow considerable concentrations of electronically excited molecules to be prepared. Thus appreciable changes in the concentration of  $H^+$  (or  $H_3O^+$ ), and by definition  $pH$ , can be brought about on a very rapid time scale. The change in solution  $pH$  allows other ground state acid-base catalyzed reactions to be initiated. Thus a reaction which is not photochemical in nature can be initiated using an ultrafast laser. Since the majority of solution phase reactions are either acid or base catalyzed, including most reactions of biological importance, this  $pH$  jump technique offers a general, widely applicable method for rapid initiation of solution phase chemistry.

Campillo et al.<sup>120,121</sup> were the first to demonstrate a  $pH$  jump using the compounds 2-naphthol and 2-naphthol-6-sulfonate in water solution. By exciting these species with 266 nm radiation, they were able to induce the  $pH$  to jump from 7 to 4. The protonated form of each species emitted in a different spectral region than its corresponding anion. Consequently, by measuring the time history of both anionic and acidic species under a variety of experimental conditions and using a kinetic scheme which includes terms for the fluorescence lifetimes and quenching, the complete kinetics of excited state protonation

were obtained. For 2-naphthol-6-sulfonate,  $k_f = (1.02 \pm 0.2) \times 10^9 \text{ s}^{-1}$  and  $k_b = (9 \pm 3) \times 10^{10} \text{ L mol}^{-1} \text{ s}^{-1}$ . Here  $k_f$  is the deprotonation rate and  $k_b$  is the backward protonation rate. Smith et al.<sup>122</sup> also observed an ultrafast pH jump in 2-naphthol-3,6-disulfonate and 8-hydroxy 1,3,6 pyrene trisulfonate. The rates of proton ejection were found to be  $3.1 \times 10^{10} \text{ s}^{-1}$  and  $3.2 \times 10^{10} \text{ s}^{-1}$ , respectively. Thistlethwaite and Woolfe<sup>123</sup> studied the fluorescence decay of aqueous salicylamide and also interpreted the complex fluorescence spectrum and kinetics in terms of excited state proton transfer. Campillo et al.<sup>124</sup> measured the rate constant for protonation of electronically excited coumarin 102 in water to be  $(1.4 \pm 0.4) \times 10^{10} \text{ L mol}^{-1} \text{ s}^{-1}$ . In this case, the solution becomes much more basic upon electronic excitation. Gutman and Huppert<sup>125</sup> demonstrated a pH jump in a space enclosed by liposomes. This has potential use in biological studies such as ATP synthesis where the reaction is driven by a proton gradient. If the pH jump is limited to one side of a proton impermeable membrane, a proton motive force will result. The resulting  $\Delta\mu\text{H}^+$  jump will be identical to the magnitude of the pH jump. Since their  $\Delta\text{pH}$  was of the order of 3-4 they estimated that the resulting  $\Delta\mu\text{H}^+$  was 180-240 mV. Shizuka et al.<sup>128</sup> studied proton transfer reactions in the excited state of 1-aminopyrene in  $\text{H}_2\text{O}$  (or  $\text{D}_2\text{O}$ )-acetonitrile mixtures. The proton dissociation rates  $k^{\text{H}^+}$  and  $k^{\text{D}^+}$  were measured to be  $1.8 (\pm 0.4) \times 10^9 \text{ s}^{-1}$  and  $1.2 (\pm 0.3) \times 10^9 \text{ s}^{-1}$ , respectively. Eisenthal et al.<sup>129</sup> reported an excited state double proton transfer on excitation of 7-azaindole dimer. In nonpolar hydrocarbon solvents such as hexane, high concentrations of 7-azaindole form dimers. Upon excitation with 266 nm radiation, there occurs a double proton transfer within the dimer yielding a tautomer forming within 5 psec.

Shapiro and Winn<sup>130,131</sup> studied the temporal behavior of the spectral emission of coumarin 102 in several liquids as a function of temperature. In addition to protonation they also observed the formation of an excited state

complex (CA)\* between the excited state coumarin molecules, C\* and solvent molecules, A, through the kinetics of the disappearance of a blue edge emission and the formation of a red edge emission. They also observed interesting spectral dynamical behavior in acridine<sup>131-133</sup>. Here again, this behavior depended sensitively on the temperature and solvent and were interpreted in terms of the hydrogen bonding characteristics of the solvents.

Excited and ground state aromatic hydrocarbons in solution often form excimers which can be identified by their characteristic fluorescence. In most cases, the fluorescence is emitted from a sandwich-type excimer in which the  $\pi$  orbitals of aromatic chromophores overlap as in the case of pyrene. Tagawa et al.<sup>134</sup>, however, observed two distinct excimers of poly(N-vinylcarbazole). The first is the sandwich-type while the second (emitting at 375 nm) is formed within 10 ps of a 10 ps electron pulse. The sandwich type excimer (emitting at 420 nm) takes several nanoseconds to form. Migita et al.<sup>136</sup> studied the intramolecular heteroexcimer formation processes in the excited state of p-(CH<sub>3</sub>)<sub>2</sub>N-C<sub>6</sub>H<sub>4</sub>-(CH<sub>2</sub>)<sub>3</sub>-(9-anthryl) as well as p-(CH<sub>3</sub>)<sub>2</sub>N-C<sub>6</sub>H<sub>4</sub>-(CH<sub>2</sub>)<sub>3</sub>-(1-pyrenyl) in hexane and 2-propanol. Kobayashi<sup>135</sup> observed the formation process of anthracene excimers in chloroform.

Somewhat surprisingly, only one group to date has applied streak camera fluorometry to the study of gas phase photolysis products. Craig et al.<sup>53</sup> followed the formation of the C<sub>2</sub> Swan system emission following 266 nm photolysis of acetylene and observed a 215 ps risetime (see Fig. 8). This experiment clearly demonstrates that the streak camera is capable of following the temporal development of a variety of emissive fragments.

## Solid State

The physics of solids is rich in luminous phenomena occurring on a picosecond time scale.<sup>97</sup> Researchers have studied exciton migration<sup>48,138</sup> and subsequent interactions<sup>138</sup> at low<sup>61,140</sup> and high excitation intensities,<sup>139</sup> electron spin relaxation,<sup>142,143</sup> excimer effects<sup>144</sup> and energy transfer in both bulk media<sup>19</sup> and from molecular monolayers to a solid.<sup>145</sup>

Campillo et al.<sup>138</sup> studied exciton-exciton interactions in tetracene at 170K using high excitation intensities. From the variation of the decay rate of singlet exciton emission as a function of laser intensity, they were able to measure a singlet-singlet annihilation rate,  $\lambda_{SS}$ , of  $10^{-7}\text{cm}^3\text{s}^{-1}$  and an exciton diffusion rate,  $D_S$ , of  $4 \times 10^{-2}\text{cm}^2\text{s}^{-1}$ . In a later study they doped tetracene with pentacene and studied the kinetics of electron energy transfer from host to guest. The guest fluorescence risetime was observed to be the same as the decay time of the host, while the simple exponential character of the host fluorescence was consistent with a diffusion model for singlet exciton migration from host to guest. Kobayashi et al.<sup>139</sup> studied the decay kinetics of free excitons, bound excitons and excitonic molecules in CdS at 4.2°K. By varying the level of excitation they were able to determine that the P band (at 490.5nm) is due to bimolecular emission from free excitons, that bound excitons are generated from free excitons through a monomolecular process and that excitonic molecules are formed through bimolecular processes. Fujimoto et al.<sup>61,140</sup> studied luminescent processes in CuCl using a low power synchronously pumped dye laser excitation source and a synchroscan streak camera. This enabled these researchers to perform time-resolved investigations of bound exciton luminescence in CuCl at 8°K in the absence of competing biexciton effects. The luminescence was filtered to allow observation of the I line at 390nm which is due to the radiative decay of an exciton bound to a neutral

acceptor. The luminescence profile, shown in Fig. 10, indicates that the bound exciton is formed within 10ps and decays within 130ps.

Pellegrino and Alfano<sup>141</sup> studied the 720-850nm photoluminescence kinetics of GaAs at 100°K. Using 530nm excitation, the luminescence kinetics reflect the intervalley transfer of electrons from  $\Gamma$ , to and from the upper valleys along the L and X direction. The emission profile is complex, displaying a rise of 5ps and a decay time of ca. 25ps. Seymour and Alfano<sup>142</sup> studied the spin relaxation and recombination kinetics in GaAs using polarization spectroscopy. A partial spin alignment of the conduction-band electrons is created when the crystal is illuminated with circularly polarized light. As these spin aligned electrons radiatively decay to the valence-band and shallow-acceptor states, the resulting luminescence is partially circularly polarized, reflecting the degree of spin alignment of the recombining electrons. The experimental results are displayed in Fig. 17. The spin relaxation time and initial spin alignment are separately determined in these measurements. Gobel et al.<sup>143</sup> also observed luminescence from GaAs and observed Mott transitions from the electron-hole plasma to the excitonic state. This transition is smooth and does not show a phase separation.

Kobayashi<sup>144</sup> studied the formation of excimer excitons in pyrene and perylene crystals. Kobayashi found that excimers formed in both crystals in less than 20ps and concluded that the sum of the time constants for conformational change of an energy-donating pair and excimer-energy transfer is about 20ps. Nakashima et al.<sup>145</sup> studied energy transfer processes between monolayers of rhodamine B on surfaces of single crystals of anthracene, phenanthrene and naphthalene. Fluorescence decays were biexponential indicating two types of transfer process, one due to electron-transfer

from the crystal to excited rhodamine B and the other due to two dimensional Förster-type energy transfer. Campillo et al.<sup>19</sup> monitored the fluorescence from components of commercial scintillator materials.

#### OTHER APPLICATIONS

Walden and Winefordner<sup>146</sup> have critically reviewed the suggestion of employing streak camera fluorometry in quantitative analysis of trace species in liquids, the characteristic molecular lifetimes yielding information that supplements spectral identification. However, their attempts proved unsatisfactory in many of the mixtures they tried because of chemical, solvent and optical interferences.

In this paper we have reviewed streak camera usage in laser fluorescence spectroscopy. However, the streak camera has proven invaluable and is widely used in providing direct visualization of mode-locked laser pulses,<sup>1</sup> synchrotron radiation,<sup>50</sup> Cerenkov emission from Linear Electron Accelerators,<sup>147</sup> nonlinear optical effects,<sup>148,149</sup> mode-propagation in optical fibers<sup>150</sup>, implosion of laser fusion microspheres and explosive detonations.<sup>3</sup> Coverage of these subjects is, unfortunately, beyond the scope of this paper. However, we would like to draw the readers attention to an exciting related application of streak cameras, ultrafast transient absorption studies.<sup>151-155</sup> This is typically implemented in the following way. Fluorescence of an appropriate wavelength and having a lifetime of several nanoseconds is generated in a dye solution and serves as a quasi-CW probe light source in the picosecond time region. The probe light is passed through the sample and is observed with a streak camera. Any transient absorptions induced in the sample by a second intense actinic light pulse will be evident in the level of transmitted probe light. Use of multichannel image recorder of the streak camera output and subsequent computer interfacing allows

a direct scope display of the optical density of the sample versus time.

#### ACKNOWLEDGEMENTS

The authors of this paper were fortunate to have been at the Los Alamos Scientific Laboratory during the early years of streak camera development where we had access to a variety of experimental and commercial streak cameras. The availability of these and associated equipment enabled us to carry out the first extensive use of streak cameras in fluorescence spectroscopy. We thank K. Boyer for his encouragement and support. Special thanks are also due A.J. Lieber and H.D. Sutphin, both formerly of the LASL streak camera development program and to our former associates, R.C. Hyer and K.R. Winn. S.L.S. thanks the U. S. Air Force Office of Scientific Research for partial support.

## REFERENCES

1. D. J. Bradley, Chapter 2 of Ultrashort Light Pulses, S. L. Shapiro, ed., Springer-Verlag, Berlin, New York (1977), p 18.
2. C. B. Johnson, "Photoelectronic Streak-Tube Technology Review", Proc. of the S.P.I.E., Vol. 94, 13 (1976).
3. A.E. Huston, "High-Speed Photography and Photonic Recording," J. Phys. E (GB), 11, 601 (1978).
4. N. H. Schiller, Y. Tsuchiya, E. Inuzuka, Y. Suzuki, K. Kinoshita, K. Kamiya, H. Iida and R. R. Alfano, "An Ultrafast Streak Camera System: Temporal disperser and Analyzer, Optical Spectra, June 1980, p 55.
5. J. S. Courtney-Pratt, "A New Method for the Photographic Study of Fast Transient Phenomena," Research, 2, 287 (1949).
6. J. S. Courtney-Pratt, "A New Photographic Method for Studying Fast Transient Phenomena", Proc. Roy. Soc., A204, 27 (1950).
7. E. K. Zavoiskii and S. D. Fanchenko, "Studies of Very Fast Light Processes," Doklady Akad. Nauk SSSR 100, 4, 661 (1955).
8. E. K. Zavoiskii and S. D. Fanchenko, "Physical Fundamentals of Electron-Optical Chronography, Sov. Phys. Doklady 1, 285 (1956).
9. Some authors employ the term "Electron-optical chronoscopy"
10. J. A. Armstrong, "Measurement of Picosecond Laser Pulse Widths," Appl. Phys. Lett, 10, 16 (1967).
11. J. A. Giordmaine, P. M. Rentzepis, S. L. Shapiro and K. W. Wecht, "Two-Photon Excitation of Fluorescence by Picosecond Light Pulses," Appl. Phys. Lett., 11, 216, (1967).
12. A. A. Maljutin and M. Ya Schelev, "Investigation of the Temporal Structure of Neodymium-Laser Emission in the Mode Self-Locking Regime," JETP Lett, 9, 266 (1969).
13. D. J. Bradley, B. Liddy and W. E. Sleat, "Direct Measurement of Ultrashort Light Pulses With a Picosecond Streak Camera," Optics Comm., 2, 39 (1971).
14. M. Ya. Schelev, M. C. Richardson and A. J. Alcock, "Image Converter Streak Camera with Picosecond Resolution", Appl. Phys. Lett., 19, 354 (1971).
15. S.D. Fanchenko, B.A. Frolov, "Picosecond Structure of the Emission of a Laser with a Nonlinear Absorber," Sov. Phys. JETP Lett. 16, 101 (1972).

16. M.M. Butslav, B.A. Demidov, S.D. Fanchenko, V.A. Frolov, R.V. Chikin, "Observation of Processes of Picosecond Duration by Electron-Optical Chronography," *Dokl. Akad. Navk SSSR* 209, 1060 (1973).
17. E. G. Arthurs, D. J. Bradley and A. G. Roddie, "Picosecond Measurements of 3,3'-Diethyloxadicarbocyanine Iodide and Photoisomer Fluorescence", *Chem. Phys. Lett.*, 22, 230 (1973).
18. S. L. Shapiro, R. C. Hyer and A. J. Campillo, "Polyatomic Molecular Relaxation in the Absence of Collisions", *Phys. Rev. Lett.* 33, 516-8 (1974).
19. A. J. Campillo, S. L. Shapiro and R. C. Hyer, "Fluorescence Risetime of NE 102 Scintillator", *Nucl. Instr. and Methods* 120, 533-4 (1974).
20. A.J. Campillo, V.H. Kollman and S.L. Shapiro, "Ultrafast Streak Camera" (Letter to the Editor), *Science*, 189, 410 (1975).
21. A. J. Campillo, R. C. Hyer, V. Kollman, S. L. Shapiro and H. D. Sutphin, "Fluorescence Lifetimes of Alpha and Beta-Carotenes", *Biochim. et Biophys. Acta*, 376, 219-221 (1975).
22. V.Z. Pashchenko, A.B. Rubin and L.B. Rubin, "Pulse Fluorometer Measurement of the Duration of the Fluorescence of Chlorophyll Excited by a Mode-Locked Laser", *Sov. J. Quant. Electron.*, 5, 730 (1975).
23. V. H. Kollman, A. J. Campillo and S. L. Shapiro, "Photosynthetic Studies with a 10 psec Resolution Streak Camera", *Biophys. Biochem Res. Comm.*, 63, 917-20 (1975).
24. S. L. Shapiro, A. J. Campillo and V. Kollman, "Energy Transfer in Photosynthesis: Pigment Concentration Effects and Fluorescent Lifetimes", *FEBS Lett.*, 54, 358-61 (1975).
25. S. L. Shapiro, A. J. Campillo, V. H. Kollman and W. B. Goad, "Exciton-Transfer in DNA", *Optics Comm.*, 15, 308-310 (1975).
26. V.Z. Pashchenko, S.P. Protasov, A.B. Rubin, K.N. Timofeev, L.M. Zamazova and L.B. Rubin, "Probing Kinetics of Photosystem I and Photosystem II Fluorescence in Pea Chloroplasts on a Picosecond Pulse Fluorometer," *Biochim. Biophys. Acta.*, 408, 143 (1975).
27. G.S. Beddard, G. Porter, C.J. Tredwell and J. Barber, "Fluorescence Lifetimes in the Photosynthetic Unit," *Nature (London)* 258, 166 (1975).
28. E. H. Eberhardt, "The Use of An Accelerator Mesh to Increase the Resolution and Response Speed of Dissectors and Multiplier Phototubes", Research Memo No. 437, ITT Industrial Laboratories, Fort Wayne, Indiana (1966).
29. D. J. Bradley and W. Sibbett, "Subpicosecond Chronoscopy", *Appl. Phys. Lett.*, 27, 382 (1975).

30. Y. Tsuchiya, E. Inuzuka, M. Koishi and M. Miwa, "Performance and Application of a 2 Picosecond Streak Camera System", Proceedings of the Conference "Electro-Optics/Laser International 82 UK Brighton, England, March 1982.
31. Certain commercial equipment, instruments, or materials are identified in this paper in order to adequately specify the experimental procedure or to provide examples of current technology. In no case does such identification imply recommendation or endorsement by either the National Bureau of Standards or the U. S. Naval Research Laboratory, nor does it imply that the materials or equipment identified are necessarily the best available for the purpose.
32. D. J. Bradley, K. W. Jones and W. Sibbett, "Picosecond and Femtosecond Streak Cameras: Present and Future Designs", Phil. Trans. R. Soc. Lond. A298, 281-285 (1980).
33. H. Niu, W. Sibbett and M. R. Baggs, "Theoretical Evaluation of the Temporal and Spatial Resolutions of Photochron Streak Image Tubes", Rev. Sci. Instr. 53, 563 (1982).
34. M. Ya. Schelev, M. C. Richardson and A. J. Alcock, "Operation of a Grid-Shuttered Image Converter Tube in the Picosecond Region", Rev. Of Sci. Instrum. 43, 1819 (1972).
35. S.W. Thomas and L.W. Coleman, "Laser-Triggered Avalanche-Transistor Voltage Generator for a Picosecond Streak Camera," Appl. Phys. Lett., 20, 83 (1972).
36. C.F. McConaghy and L.W. Coleman, "Picosecond X-ray Streak Camera," Appl. Phys. Lett. 25, 268 (1974).
37. D. J. Bradley, A. G. Roddie, W. Sibbett, M. H. Key, M. J. Lamb, C. L. S. Lewis, P. Sachsenmair, "Picosecond X-ray Chronoscopy," Opt. Comm., 15, 231 (1975).
38. R. Kalibijian, "High-Intensity Laser-beam Effects on the Spatial Resolution of a Streak Camera Tube", J. A. P., 46, 4875-86 (1975).
39. D. Bradley, S. F. Bryant, J. R. Taylor and W. Sibbett, "Intensity Dependent Time-Resolution and Dynamic Range of Photochron Streak-Cameras", Rev. Sci. Instrum., 49, 215-219 (1978).
40. H. Niu and W. Sibbett, "Theoretical Analysis of Space-Charge Effects in Photochron Streak Cameras", Rev. Sci. Instrum., 52, 1830-1836 (1981).
41. V.S. Dneprovskii, V.N. Chumash and E.V. Zimenko, "Coherent Interaction of Picosecond Frequency-Tunable Light Pulses with Excitons in a Semiconductor," Appl. Phys. 25, 157 (1981).
42. L. A. Lompre, G. Mainfray and J. Thebault, "Instant Recording of the Duration of a Single Mode-locked Nd:YAG Laser Pulse", Appl. Phys. Lett., 26, 501-503 (1975).

43. A. J. Campillo, V. H. Kollman and S. L. Shapiro, "Intensity Dependence of the Fluorescence Lifetime of in vivo Chlorophyll Excited by a Picosecond Light Pulse", *Science*, 193, 227-229 (1976).
44. D. J. Bradley, S. F. Bryant and W. Sibbett, "Intensity Dependent Time Resolution and Dynamic Range of Photochron Picosecond Streak Cameras, II Linear Photoelectric Recording", *Rev. Sci. Instrum.*, 51, 824-831 (1980).
45. Y. Takagi, M. Sumitani and K. Yoshihara, "High Speed Image Processor for Picosecond Time Resolved Spectroscopy", *Rev. Sci. Instrum.*, 52, 1003-09 (1981).
46. P.F. Barbara, E.E. Brus and P.M. Rentzepis, "A Picosecond Time-Resolved Fluorescence Study of s-Tetrazine Vibrational Relaxation in Solution," *Chem. Phys. Lett.* 69, 447 (1980).
47. G.W. Robinson, T.A. Caughey, R.A. Auerbach and P.J. Harman, "Coupling an Ultraviolet Spectrograph to a SC/OMA for Three Dimensional ( $\lambda, I, t$ ) Picosecond Fluorescence Measurements," Chapter 9 of *Multichannel Image Detectors*, Y. Talmi, Ed., ACS Symposium Series 102, American Chemical Society (1979).
48. A. J. Campillo, S. L. Shapiro, and C. E. Swenberg, "Picosecond Measurements of Exciton Migration in Tetracene Crystals Doped with Pentacene", *Chem. Phys. Lett.*, 52, 11 (1977).
49. M. C. Adams, W. Sibbett and D. J. Bradley, "Linear Picosecond Electron-Optical Chronoscopy at a Repetition Rate of 140 MHz", *Optics Comm.*, 2, 273 (1978).
50. A. E. Huston and K. Helbrough, "The Synchroscan Picosecond Streak Camera System", *Phil. Trans. R. Soc. Lond.* A298, 287 (1980).
51. G. Mourou and W. Knox, "A Picosecond Jitter Streak Camera", *Appl. Phys. Lett.*, 36, 623 (1980).
52. A. J. Campillo, S. L. Shapiro, N. E. Geacintov and C. E. Swenberg, "Single-Pulse Picosecond Determination of 735 nm Fluorescence Risetime in Spinach Chloroplasts", *FEBS Lett.*, 83, 316 (1977).
53. B. B. Craig, W. L. Faust, L. S. Goldberg and R. G. Weiss "UV Short-Pulse Fragmentation of Isotopically Labeled Acetylene: Studies of Emission with Subnanosecond Resolution", *J. Chem. Phys.*, 76, 5014 (1982).
54. E. P. Ippen, C. V. Shank and D. Dienes, "Passive Mode Locking of the CW Dye Laser," *App. Phys. Lett.*, 21, 348 (1972).
55. F. O'Neill, "Picosecond Pulses from a Passively Mode-Locked CW Dye Laser," *Opt. Comm.*, 6, 360 (1972).
56. C. K. Chan and S. O. Sari, "Tunable Dye Laser for Production of Picosecond Pulses," *App. Phys. Lett.* 25, 403 (1974).

57. H. Mahr and M. D. Hirsch, "An Optical Up-Conversion Light Gate with Picosecond Resolution," *Optics. Comm.*, 13, 96 (1975).
58. J. M. Harris, R. M. Chrisman and R. E. Lyle, "Pulse Generation in a CW Dye Laser by Mode-Locked Synchronous Pumping," *Appl. Phys. Lett.* 26, 16 (1975).
59. M. C. Adams, "Repetitive Picosecond Chronoscopy with Mode-Locked CW Dye Lasers", Ph.D. thesis, Imperial College, London (1979).
60. J. R. Taylor, M. C. Adams and W. Sibbett, "Investigation of Viscosity Dependent Fluorescence Lifetime Using Synchronously Operated Picosecond Streak Camera", *Appl. Phys.*, 21, 13 (1980).
61. J. G. Fujimoto, T. K. Yee, and M. M. Salour, "Picosecond Spectroscopy of Bound Excitations in CuCl Using a Synchronously Operating Streak Camera", *Appl. Phys.*, 39, 12 (1981).
62. F. Heisel, J. A. Mieke and B. Sipp, "Applications of Synchronously Pumped and Cavity-Dumped Dye-Laser Associated with Streak Camera Operated at the Repetitive Mode to Time-Resolved Spectroscopy", *Il Nuovo Cimento*, 63B, 221 (1981).
63. F. Heisel, J. A. Mieke and B. Sipp, "Characteristics and Performances of a Streak Camera Operating in Repetitive Mode", *Rev. Sci. Instrum.*, 52, 992 (1981).
64. G. Mourou and W. Knox, "High-Power Switching with Picosecond Precision", *Appl. Phys. Lett.* 35, 492-495 (1979).
65. M. Stavola, G. Mourou and W. Knox "Picosecond Time Delay Fluorimetry Using a Jitter-Free Streak Camera", *Optics Comm.*, 34, 404-408 (1980).
66. W. Knox and G. Mourou, "A Simple Jitter-Free Picosecond Streak Camera", *Optics Comm.*, 37, 203-206 (1981).
67. G. Mourou, W. Knox and S. Williamson, "Advances in Picosecond Optoelectronics, *Proc. of S.P.I.E.*, 322, 107 (1982).
68. A.J. Lieber, H.D. Sutphin and C.B. Webb, "Subpicosecond Proximity-Focused Streak Camera for X-ray and Visible Light," *Proc. of S.P.I.E.*, 94, 7 (1976).
69. A.J. Campillo and S.L. Shapiro, "Picosecond Relaxation Measurements in Biology," Chapter 7 of Ultrashort Light Pulses, S.L. Shapiro, Ed. (Springer, Berlin, 1977).
70. R.R. Alfano, Ed., Biological Events Probed by Ultrafast Laser Spectroscopy (Academic Press, New York, 1982).

71. A. J. Campillo, S. L. Shapiro, V. H. Kollman, K. R. Winn, and R. C. Hyer, "Picosecond Exciton Annihilation in Photosynthetic Systems", *Biophys. J* 16, 93 (1976).
72. A. J. Campillo and S. L. Shapiro, "Use of Picosecond Lasers for Studying Photosynthesis", *Proc. S.P.I.E.*, 94, 89 (1976).
73. L. Harris, G. Porter, J. A. Synowiec, C. J. Tredwell, and J. Barber, "Fluorescence Lifetimes of *Chlorella Pyrenoidosa*," *Biochim. Biophys. Acta* 449, 329 (1976).
74. A. J. Campillo, R. C. Hyer, T. G. Monger, W. W. Parson and S. L. Shapiro, "Light Collection and Harvesting Processes in Bacterial Photosynthesis Investigated on a Picosecond Time Scale", *Proc. Natl. Acad. Sci. USA* 74, 1997 (1977).
75. N. E. Geacintov, J. Breton, C. Swenberg, A. J. Campillo, R. C. Hyer and S. L. Shapiro, "Picosecond and Microsecond Pulse Laser Studies of Exciton Quenching and Exciton Distribution in Spinach Chloroplasts at Low Temperatures," *Biochim. Biophys. Acta* 461, 306 (1977).
76. V. Z. Paschenko, A. A. Kononenko, S. P. Protasov, A. B. Rubin, L. B. Rubin and N. Ya. Uspenskaya, "Probing the Fluorescence Emission Kinetics of the Photosynthetic Apparatus of *Rhodospseudomonas Sphaeroides* Strain 760-1, on a Picosecond Fluorometer", *Biochim. et Biophys. Acta* 461, 403 (1977).
77. G. Porter, J. A. Synowiec and C. J. Tredwell, "Intensity Effects on the Fluorescence of In Vivo Chlorophyll", *Biochim. Biophysica Acta*, 459, 329 (1977).
78. G. F. Searle, W. J. Barber, L. Harris, G. Porter and C. J. Tredwell, "Picosecond Laser Study of Fluorescence Lifetimes in Spinach Chloroplast Photosystem I and Photosystem II Preparations", *Biochim. Biophys. Acta* 459, 390 (1977).
79. A. J. Campillo, S. L. Shapiro, N. E. Geacintov and C. E. Swenberg, "Single-Pulse Picosecond Determination of 735 nm Fluorescence Risetime in Spinach Chloroplasts, *FEBS Lett.* 83, 316 (1977).
80. A. J. Campillo and S. L. Shapiro "Picosecond Fluorescence Studies of Exciton Migration and Annihilation in Photosynthetic Systems. A Review", *Photochem. Photobiol.* 28, 975 (1978).
81. G. Porter, C. J. Tredwell, G. F. W. Searle, and J. Barber, "Picosecond Time-Resolved Energy Transfer in *Porphyridium Cruentum*, Part I. In the Intact Alga", *Biochim. Biophys. Acta* 501, 232 (1978).
82. G. F. W. Searle, J. Barber, G. Porter and C. J. Tredwell, "Picosecond Time-Resolved Energy Transfer in *Porphyridium Cruentum*, Part II. In the Isolated Light Harvesting Complex (Phycobilisomes) *Biochim. et Biophys. Acta* 501, 246 (1978).

83. J. Barber, G. F. W. Searle, and C. J. Tredwell, "Picosecond Time Resolved Study of  $MgCl_2$  - Induced Chlorophyll Fluorescence Yield Changes from Chloroplasts", *Biochim. Biophys. Acta* 501, 174 (1978).
84. A. J. Campillo and S. L. Shapiro, "Light Collection and Exciton Dynamics in Photosynthetic Membranes," *Picosecond Phenomena*, C.V. Shank, E.P. Ippen, S.L. Shapiro (Springer, Berlin, 1978), 140-148.
85. C. J. Tredwell, J. Synowiec, G. F. W. Searle, G. Porter and J. Barber, "Picosecond Time Resolved Fluorescence of Chlorophyll In Vivo", *Photochem. Photobiol.* 28, 1013 (1978).
86. G. F. W. Searle, C. J. Tredwell, J. Barber and G. Porter, "Picosecond Time-Resolved Fluorescence Study of Chlorophyll Organization and Excitation Energy Distribution in Chloroplasts from Wild-Type Barley and a Mutant Lacking Chlorophyll b", *Biochem. Biophys. Acta.* 545, 496 (1979).
87. S.S. Brody, G. Porter, C.J. Tredwell, J. Barber, "Picosecond Energy Transfer in *Anacystis Nidulans*," *Photobiochem. Photobiophys.* 2, 11 (1981).
88. S. S. Brody, C. Treadwell, J. Barber, "Picosecond Energy Transfer in *Porphyridium Cruentum* and *Anacystis Nidulans*," *Biophys. J.* 34, 439 (1981).
89. D. Wong, F. Pellegrino, R. R. Alfano and B. A. Zilinskas, "Fluorescence Relaxation Kinetics and Quantum Yield from the Isolated Phycobiliproteins of the Blue-Green Alga *Nostoc Sp.* Measured as a Function of Single Picosecond Pulse Intensity, I.", *Photochem. and Photobiol.* 33, 651 (1981).
90. F. Pellegrino, D. Wong, R. R. Alfano and B. A. Zilinskas, "Fluorescence Relaxation Kinetics and Quantum Yield from the Isolated Phycobiliproteins of the Blue-Green Alga *Nostoc Sp.* Measured as a Function of Single Picosecond Pulse Intensity, I.", *Photochem. and Photobiol.* 34, 691 (1981).
91. "T. M. Nordlund and W. H. Knox, Lifetime of Fluorescence From Light-Harvesting Chlorophyll a/b Proteins", *Biophys. J.*, 3, 193 (1981).
92. A. G. Doukas, P. Y. Lu and R. R. Alfano, "Fluorescence Relaxation Kinetics from Rhodopsin and Isorhodopsin", *Biophys. J.* 35, 547 (1981).
93. S. L. Shapiro, A. J. Campillo, A. Lewis, G. J. Perreault, J. P. Spoonhower, R. K. Clayton, and W. Stoeckenius, "Picosecond and Steady State, Variable Intensity and Variable Temperature Emission Spectroscopy of Bacteriorhodopsin", *Biophys. J.* 23, 384 (1978).
94. M. A. J. Rogers, "Picosecond Fluorescence Studies of Rose Bengal in Aqueous Micellar Dispersions", *Chem. Phys. Lett.* 78, 509 (1981).
95. M.A.J. Rogers, "Picosecond Fluorescence Studies of Xanthene Dyes in Anionic Micelles in Water and Reverse Micelles in Heptane," *J. Phys. Chem.*, 85, 3372 (1981).

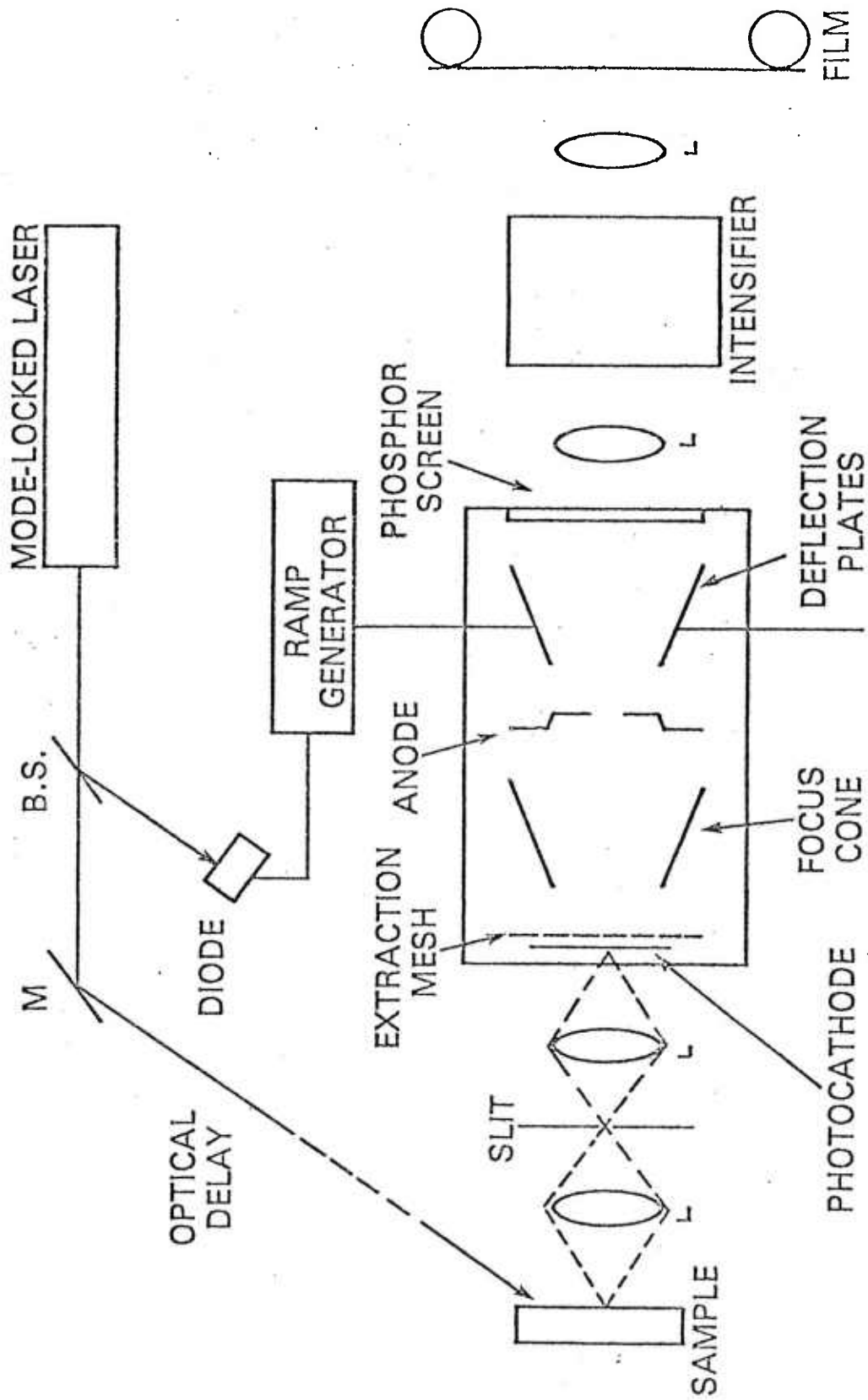
96. K.B. Eisenthal, "Picosecond Relaxation Processes in Chemistry," Chapter 6 of Ultrashort Light Pulses, S.L. Shapiro, ed. Springer-Verlag, Berlin (1977).
97. D. von der Linde, "Picosecond Interactions in Liquids and Solids," Chapter 5 of Ultrashort Light Pulses, S.L. Shapiro, ed., Springer-Verlag, Berlin (1977).
98. G.A. Kenney-Wallace, "Picosecond Relaxation Processes in Liquids," *Phil. Trans. R. Soc. Lond.* A299, 309 (1980).
99. Th. Förster, "Die Viskositätsabhängigkeit der Fluoreszenzquantenausbeuten einiger Farbstoffsysteme," *Z. Naturforschg.* 4a, 321 (1949).
100. G. Porter and C.V. Tredwell, "Picosecond Time Resolved Energy Transfer Between Rhodamine 6G and Malachite Green," *Chem. Phys. Lett.* 56, 278 (1978).
101. M.C. Adams, D.J. Bradley, W. Sibbett and J.R. Taylor, "Real-Time Picosecond Measurements of Electronic Energy Transfer from DODCI to Malachite Green and DQOCI," *Chem. Phys. Lett.* 66, 428 (1979).
102. H. Sato, Y. Kusumoto, N. Nakashima, and K. Yoshihara, "Picosecond Study of Energy Transfer Between Rhodamine 6G and 3,3'-Diethylthiacarbocyanine Iodide in the Premicellar Region: Förster Mechanism with Increased Local Concentration," *Chem. Phys. Lett.* 71, 326 (1980).
103. G.R. Fleming, A.W.E. Knight, J.M. Morris, R.J.S. Morrison and G.W. Robinson, "Picosecond Fluorescence Studies of Xanthene Dyes," *J. Am. Chem. Soc.*, 99, 4306 (1977).
104. W. Yu, F. Pellegrino, M. Grant and R.R. Alfano, "Subnanosecond Fluorescence Quenching of Dye Molecules in Solution," *J. Chem. Phys.* 67, 1766 (1977).
105. Th. Förster, G. Hoffmann, "Experimentelle und Theoretische Untersuchung des Zwischenmolekularen Übergangs von Elektronenanregungsenergie," *Z. Phys. Chemie NF*, 75, 63 (1971).
106. J.C. Mialocq, J. Jaraudias and P. Goujon, "Picosecond Spectroscopy of Pinacyanol (1,1'-Diethyl-2,2'-Monocarbocyanine Chloride)," *Chem. Phys. Lett.*, 47, 123 (1977).
107. J.R. Taylor, M.C. Adams and W. Sibbett, "Investigation of Viscosity Dependent Fluorescence Lifetime Using a Synchronously Operated Picosecond Streak Camera," *Appl. Phys.* 21, 13 (1980).

108. D. Welford, W. Sibbett and J.R. Taylor, "Dual Component Fluorescence Lifetime of Some Polymethine Saturable Absorbing Dyes," *Optics Comm.* 34, 175 (1980).
109. W. Sibbett, J.R. Taylor and D. Welford, "Substituent and Environmental Effects on the Picosecond Lifetimes of the Polymethine Cyanine Dyes," *IEEE J. of Quan. Electron.*, QE-17, 500 (1981).
110. D. Huppert, S.D. Rand, P.M. Rentzepis, P.F. Barbara, W.S. Struve, Z.R. Grabowski, "Dynamics of the Dual Fluorescences of p-Dimethylaminobenzonitrile," *J. of Photochemistry*, 18, 89 (1982).
111. G.R. Fleming, J.M. Morris and G.W. Robinson, "Direct Observation of Rotational Diffusion by Picosecond Spectroscopy," *Chemical Physics* 17, 91 (1976).
112. R.J. Seymour, P.Y. Lu and R.R. Alfano, "Picosecond Polarization Kinetics of Photoluminescence of Semiconductors and Dyes," *Picosecond Phenomena II*, R.M. Hochstrasser, W. Kaiser, C.V. Shank, Eds. (Springer-Verlag, Berlin, 1980) 111.
113. M. Sumitani, N. Nakashima, and K. Yoshihara, "Temperature Dependence of Fluorescence Lifetimes of Trans-Stilbine," *Chem. Phys. Lett.*, 51, 183 (1977).
114. F. Heisel, J.A. Mieke and B. Sipp, "Picosecond Analysis of Trans-Stilbine Fluorescence," *Chem. Phys. Lett.*, 61, 115 (1979).
115. K.B. Eisenthal, M.K. Crawford, C. Dupuy, W. Hetherington, G. Korenowski, M.J. McAuliffe, and Y. Wang, "Photodissociation, Short-Lived Intermediates and Charge Transfer Phenomena in Liquids," *Picosecond Phenomena II*, R.M. Hochstrasser, W. Kaiser, C.V. Shank, Eds., (Springer-Verlag, Berlin, 1980) 220.
116. M.K. Crawford, Y. Wang and K.B. Eisenthal, "Effects of Conformation and Solvent Polarity on Intramolecular Charge Transfer: A Picosecond Laser Study," *Chem. Phys. Lett.*, 79, 529 (1981).
117. Y. Wang, M. McAuliffe, F. Novak and K.B. Eisenthal, "Picosecond Dynamics of Twisted Internal Charge-Transfer Phenomena," *J. Phys. Chem.* 85, 3736 (1981).
118. G.A. Kenney-Wallace, L.A. Hunt and K.L. Sala, "Picosecond Electron Relaxation and Photochemical Dynamics," *Picosecond Phenomena II*, R.M. Hochstrasser, W. Kaiser, C.V. Shank, Eds., (Springer-Verlag, Berlin 1980), 203.
119. R.A. Auerbach, J.A. Synowiec and G.W. Robinson, "Dynamical Evidence for Preferential Structure in Electron Photoejection from Arylaminoanthralene Sulfonates," *Picosecond Phenomena II*, R.M. Hochstrasser, W. Kaiser, C.V. Shank, Eds., (Springer-Verlag, Berlin, New York, 1980), 215.

120. A.J. Campillo, J.H. Clark, S.L. Shapiro, K.R. Winn, "Picosecond Studies of Excited State Proton Transfer Reactions: The Laser pH Jump," Picosecond Phenomena, C.V. Shank, E.P. Ippen and S.L. Shapiro, Eds., (Springer-Verlag, Berlin, 1978), p. 319.
121. J.H. Clark, S.L. Shapiro, A.J. Campillo and K.R. Winn, "Picosecond Studies of Excited-State Protonation and Deprotonation Kinetics. The Laser pH Jump," J. Am. Chem. Soc. 101, 746 (1979).
122. K.K. Smith, K.J. Kaufmann, D. Huppert and M. Gutman, "Picosecond Proton Ejection: An Ultrafast pH Jump," Chem. Phys. Lett., 64, 522 (1979).
123. P.J. Thistlethwaite and G.F. Woolfe, "Kinetic Evidence for Excited State Proton Transfer in Salicylamide," Chem. Phys. Lett. 63, 401 (1979).
124. A.J. Campillo, J.H. Clark, S.L. Shapiro, K.R. Winn and P.K. Woodbridge, "Excited-State Protonation Kinetics of Coumarin 102," Chem. Phys. Lett., 67, 218 (1979).
125. M. Gutman and D. Huppert, "Rapid pH and  $\Delta\mu\text{H}^+$  Jump by Short Laser Pulse," J. Biochem. Biophys. Methods, 1, 9 (1979).
126. S.L. Shapiro, K.R. Winn and J.H. Clark, "Excited-State Proton-Transfer Kinetics in 1-Naphthol, 1-Naphthol Sulfonates, and Organometallic Complexes," Picosecond Phenomena II, R.M. Hochstrasser, W. Kaiser, C.V. Shank, Eds. (Springer-Verlag, Berlin, 1980), p. 227.
127. D. Huppert, E. Kolodny and M. Gutman, "Picosecond Proton Transfer," Picosecond Phenomena II, R.M. Hochstrasser, W. Kaiser, C.V. Shank, Eds., (Springer-Verlag, Berlin, 1980), p. 242.
128. H. Shizuka, K. Tsutsumi, H. Takeuchi and I. Tanaka, "Proton Transfer Reactions in the Excited State of 1-Aminopyrene by Picosecond/Streak Camera and Nanosecond Spectroscopy," Chemical Physics 59, 183 (1981).
129. K.B. Eisenthal, K. Gnadig, Wm. Hetherington, M. Crawford and R. Micheels, "Picosecond Laser Studies of Electron-Hole Interactions and Double Proton Transfer," Picosecond Phenomena, C.V. Shank, E.P. Ippen and S.L. Shapiro, Eds., (Springer-Verlag, Berlin 1978), 34.
130. S.L. Shapiro and K.R. Winn, "Picosecond Time-Resolved Spectral Shifts in Emission: Dynamics of Excited State Interactions in Coumarin 102," Chem. Phys. Lett. 71, 440 (1980).
131. S.L. Shapiro and K.R. Winn, "Picosecond Studies of Temperature and Solvent Effects on the Fluorescence from Coumarin 102 and Acridine," Picosecond Phenomena II, R.M. Hochstrasser, W. Kaiser, C.V. Shank, Eds., (Springer-Verlag, Berlin, 1980), p. 237.
132. S.L. Shapiro and K.R. Winn, "Temperature Dependence of the Fluorescence Decay of Acridine Measured with Picosecond Techniques," J. Chem. Phys. 73, 1469 (1980).

133. S.L. Shapiro and K.R. Winn, "Picosecond Kinetics of Acridine in Solution," *J. Chem. Phys.* 73, 5958 (1980).
134. S. Tagawa, M. Washio and Y. Tabata, "Picosecond Time-Resolved Fluorescence Studies of Poly (N-Vinylcarbazole) Using a Pulse-Radiolysis Technique," *Chem. Phys. Lett.* 68, 276 (1979).
135. T. Kobayashi, "Picosecond Spectroscopic Study on Excimer Formation in Solution and in Crystalline Phase," *Picosecond Phenomena II*, R.M. Hochstrasser, W. Kaiser, C.V. Shank, Eds., (Springer-Verlag, Berlin, 1980), 339.
136. M. Migita, T. Okada, N. Matoga, N. Nakashima, K. Yoshihara, Y. Sakata and S. Misumi, "Picosecond Time-Resolved Fluorescence Studies of Intramolecular Heteroexcimers," *Chem. Phys. Lett.* 72, 229 (1980).
137. G.R. Fleming, J.M. Morris, R.J. Robbins, G.J. Woolfe, P.J. Thistlethwaite and G.W. Robinson, "Nonexponential Fluorescence Decay of Aqueous Tryptophan and Two Related Peptides by Picosecond Spectroscopy," *Proc. Natl. Acad. Sci. USA* 75, 4652 (1978).
138. A.J. Campillo, R.C. Hyer, S.L. Shapiro and C.E. Swenberg, "Exciton Interactions in Crystalline Tetracene Studied by Single Picosecond Pulse Excitation," *Chem. Phys. Lett.* 48, 495 (1977).
139. T. Kobayashi, Y. Segawa and S. Namba, "Picosecond Decay Kinetics of CdS Luminescence Studied by a Streak Camera," *Solid State Comm.* 31, 253 (1979).
140. J.G. Fujimoto and M.M. Salour, "Ultrafast Picosecond Chronography," *Proc. of S.P.I.E.*, 322, 137 (1982).
141. P. Pellegrino and R.R. Alfano, "Video Imaging Systems in Picosecond Laser Spectroscopy," in *Multichannel Image Detectors*, Y. Talmi, ed., (American Chemical Society, 1979), 231.
142. R.J. Seymour and R.R. Alfano, "Time-resolved Measurement of the Electron-Spin Relaxation Kinetics in GaAs," *Appl. Phys. Lett.* 37, 231 (1980).
143. E.O. Gobel, P.H. Liang, D. von der Linde, "Picosecond Luminescence Spectroscopy of Highly Excited GaAs," *Solid State Comm.* 37, 609 (1981).
144. T. Kobayashi, "The Observation of the Excimer Formation Process in Pyrene and Perylene Crystals Using a Picosecond Ruby Laser and Streak Camera," *J. Chem. Phys.* 69, 3570 (1978).
145. N. Nakashima, K. Yoshihara and F. Willig, "Time-Resolved Measurements of Electron and Energy Transfer of Rhodamine B Monolayer on the Surface of Organic Crystals," *J. Chem. Phys.* 73, 3553 (1980).
146. G.L. Walden, J.D. Winefordner, "A Streak Camera System for Time Resolved Fluorimetry," *Spectrosc. Lett.* 13, 793 (1980).

147. J.C. Sheppard, R.H. Pantell, R.A. Gearhart, R.H. Miller, L.F. Chase, K.M. Monahan, B.A. Watson, "Picosecond Resolution of a Cerenkov Cell-Streak Camera Arrangement for Monitoring Charged Particle Bunches," *Rev. Sci. Instrum.* 51, 1634 (1980).
148. A.J. Campillo, R.A. Fisher, R.C. Hyer and S.L. Shapiro, "Streak Camera Investigation of the Self-Focusing Onset in Glass," *Appl. Phys. Lett.* 25, 408 (1974).
149. R.S. Adrain, E.G. Arthurs and W. Sibbett, "Tunable Picosecond Transient Stimulated Raman Scattering in Ethanol," *Optics Comm.* 15, 290 (1975).
150. J. P. Willson, W. Sibbett and P. G. May, "Synchroscan Streak Camera Measurements of Mode-Propagation in Optical Fibers", *Picosecond Phenomena III*, K. B. Eisenthal, R. M. Hochstrasser, W. Kaiser and A. Laubereau, Eds., (Springer-Verlag, Berlin, 1982).
151. A. Muller, J. Schulz-Hennig and H. Tashiro, "Ultrafast Absorption Spectroscopy of Polymethine Laser Dyes Using a Streak Camera," *Z. Phys. Chemie NF*, 101, 361 (1976).
152. A. Muller, J. Schulz-Hennig and H. Tashiro, "Excited State Absorption of 1,3,3,1',3,3'-Hexamethylindotricarbocyanine Iodide: A Quantitative Study by Ultrafast Absorption Spectroscopy," *Appl. Phys.* 12, 333 (1977).
153. K. Yoshihara, A. Namiki, M.S. Sumitani and N. Nakashina, "Picosecond Flash Photolysis of CIS - and trans-stilbine Observation of an Intense Intramolecular Charge - resonance Transition," *J. Chem. Phys.* 71, 2892 (1979).
154. Y. Wang, M.K. Crawford, M.J. McAuliffe and K.B. Eisenthal, "Picosecond Laser Studies of Electron Solvation in Alcohols," *Chem. Phys. Lett.*, 74, 160 (1980).
155. Y. Liang, D.K. Negus, R.M. Hochstrasser, M. Gunner and P.L. Dulton, "Picosecond Kinetic Absorption Studies of an Iron Porphyrin and Bacteriochlorophyll Using a Streak Camera," *Chem. Phys. Lett.* 84, 236 (1981).



### STREAK TUBE

Figure 1. Schematic of typical streak camera fluorometer.

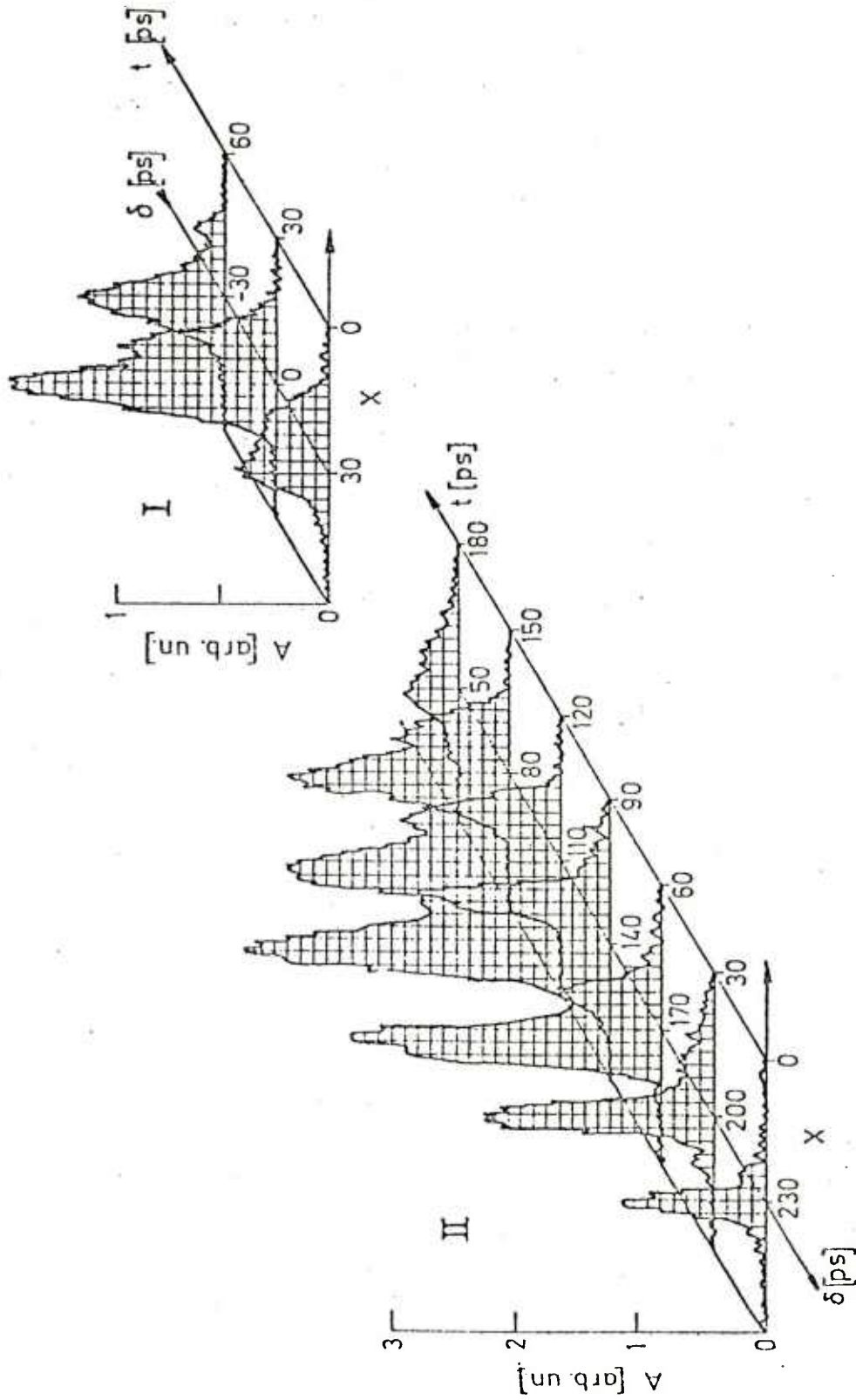


Figure 2. By utilizing the streak camera input slit dimension to represent spatial extent, the complex time dependence of a beam's spatial profile can be obtained (from Dneprovskii et al., Ref. 41).

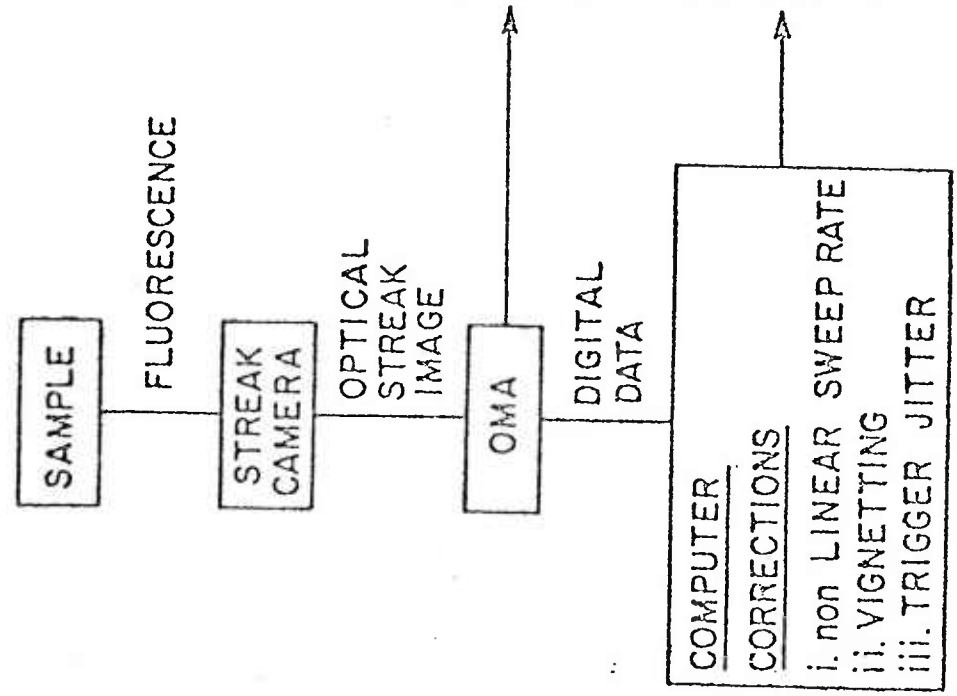
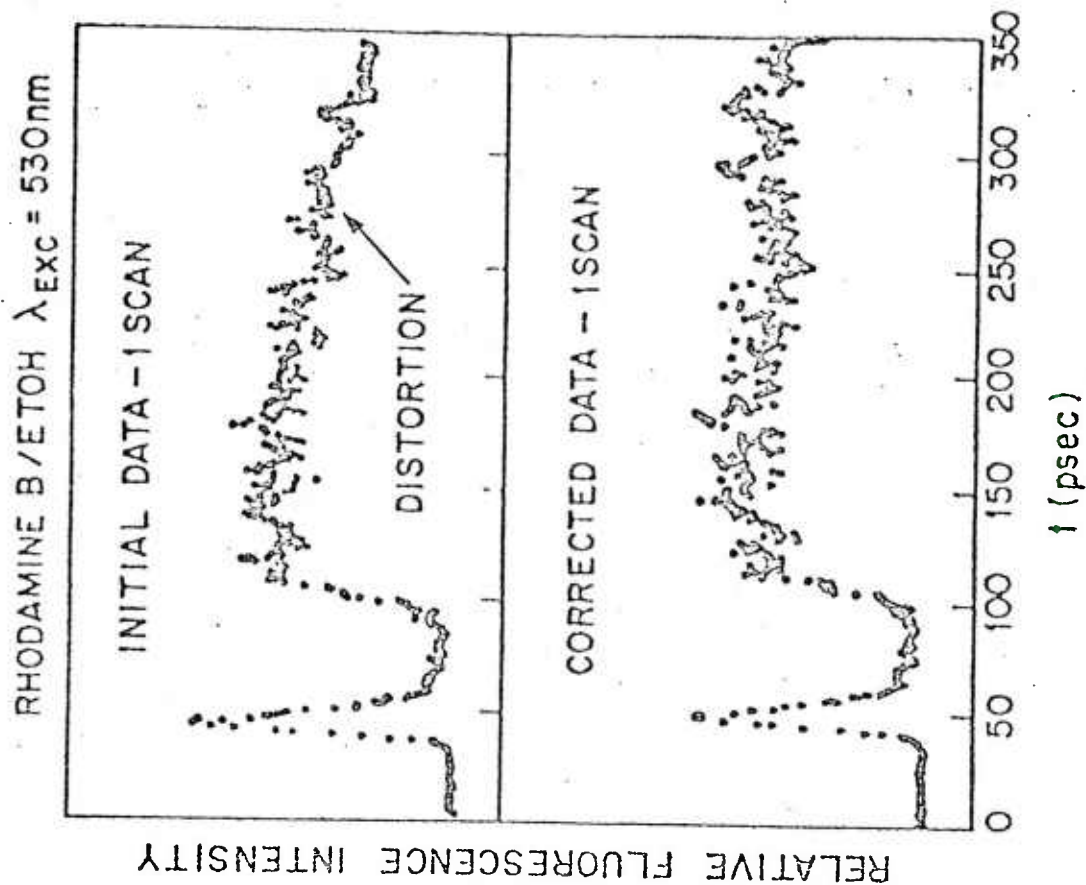


Figure 3. A streak camera/data processing system is used to collect time resolved fluorescence from a  $5 \times 10^{-4}$  rhodamine-B solution in ethanol. The raw data shown in upper right picture contains a 30% streak time base nonlinearity as well as other distortions. After computer correction, a corrected scan is displayed (lower right). In this figure individual OMA channel spacing is 0.8ps (from Barbara et al., Ref. 46).

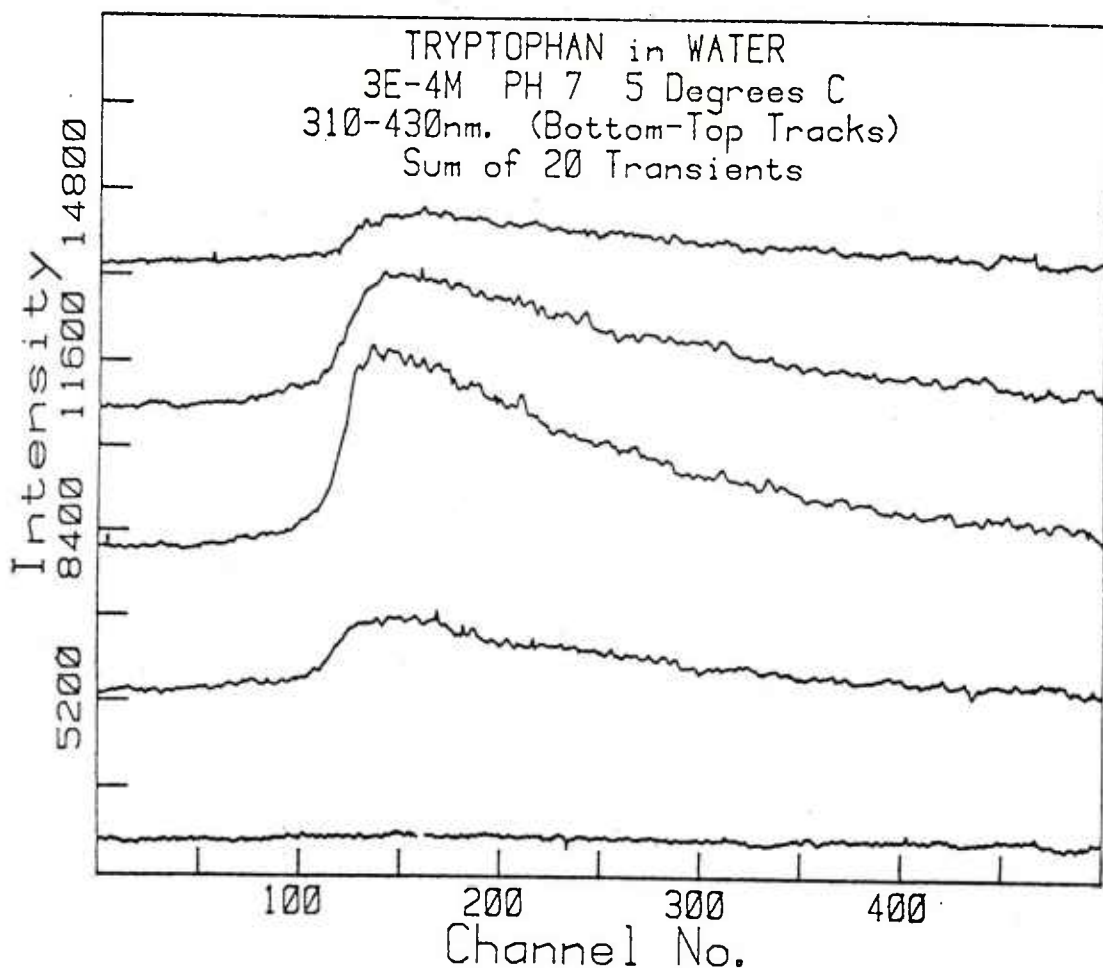


Figure 4. Time and wavelength resolved fluorescence of tryptophan ( $3 \times 10^{-4}M$ ) in water at  $5^{\circ}C$ . Each curve is an average of 20 single shots. This figure illustrates the ability of a multichannel image detector/computer to simultaneously collect and display several tracks across a complex two dimensional streak (from Robinson et al., Ref. 47).

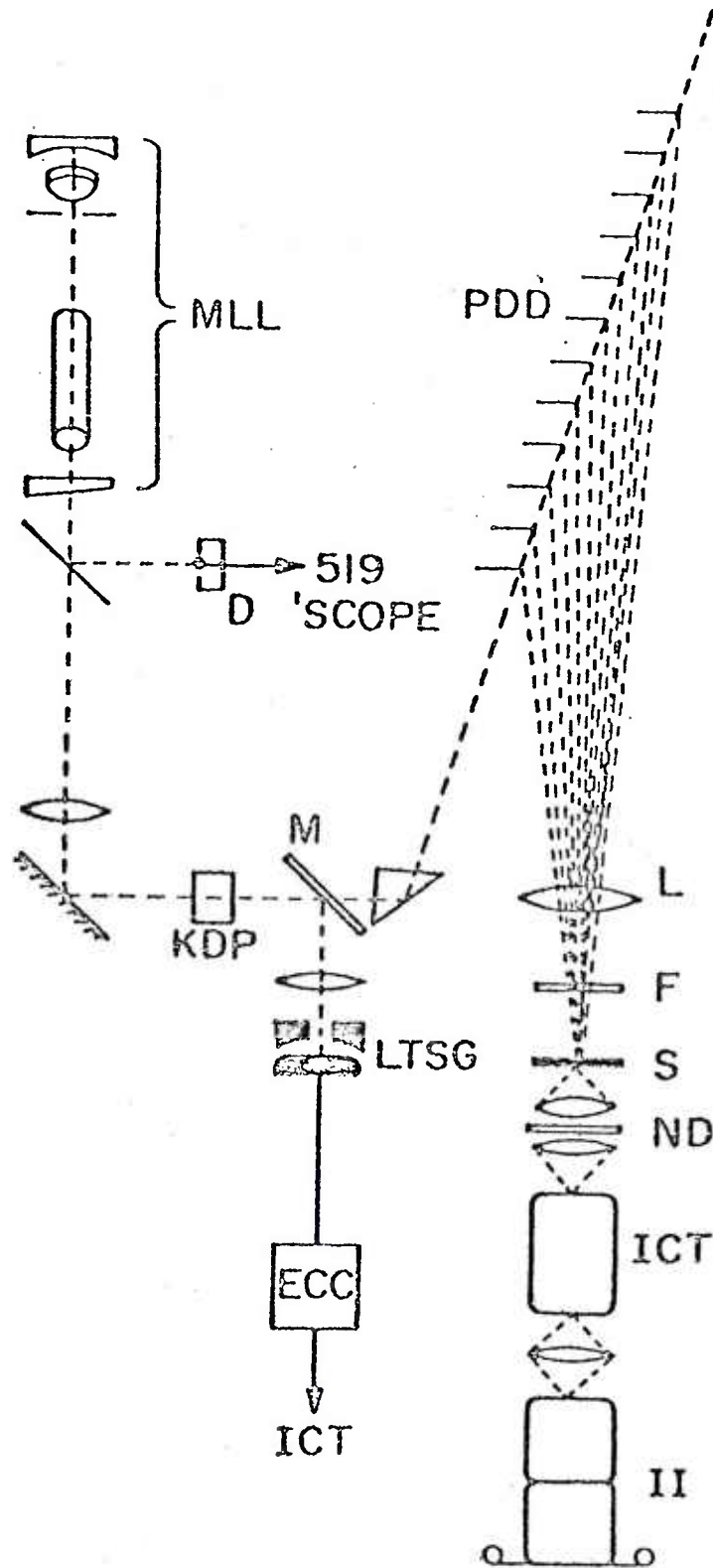


Figure 5. Diagram of experimental pulse delay device (PDD) used to calibrate streak camera. See text for details (from Schelev et al., Ref. 34).

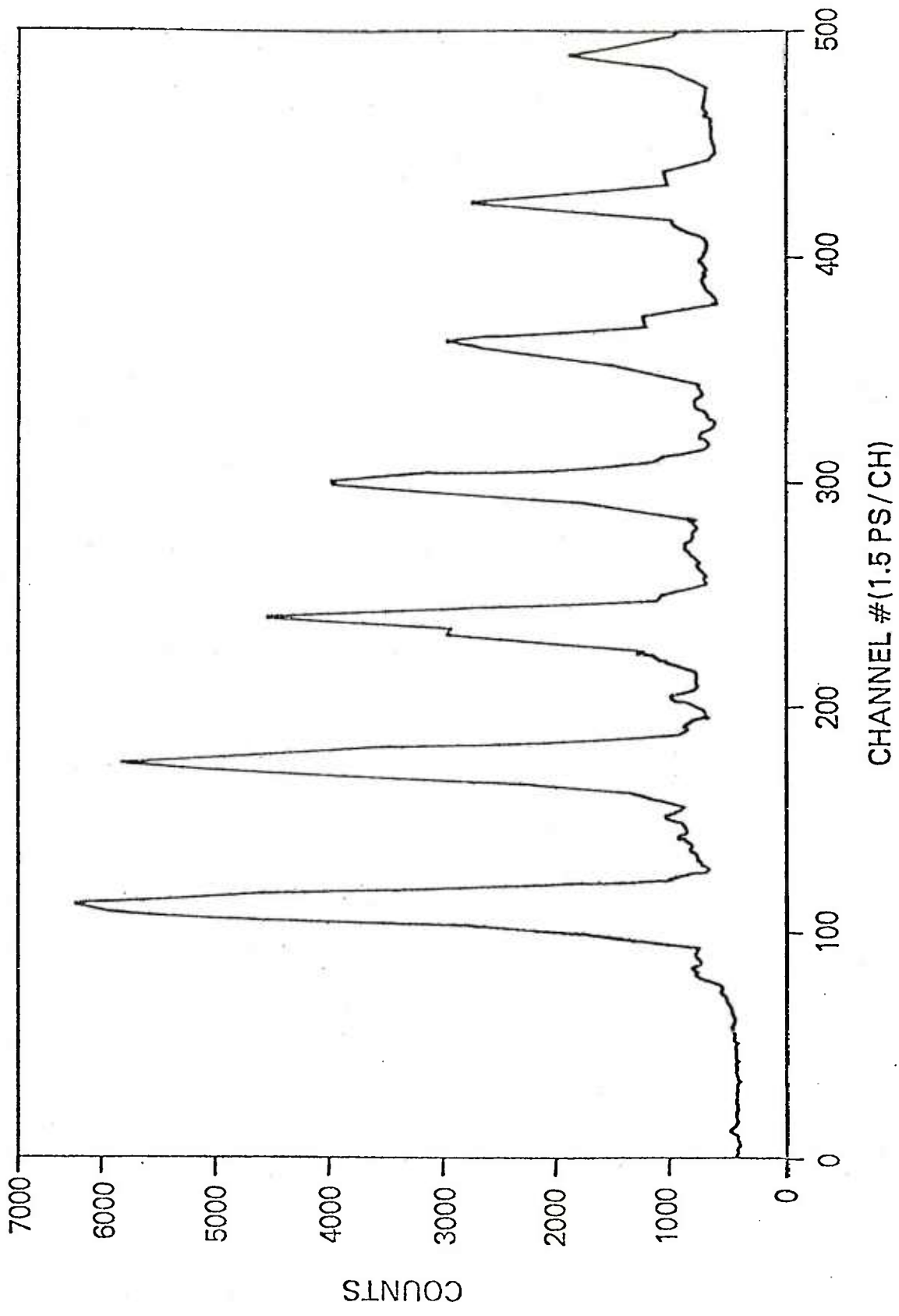


Figure 6. Display of a train of calibration pulses through two parallel mirrors. Spacing between pulses is ca. 100ps.

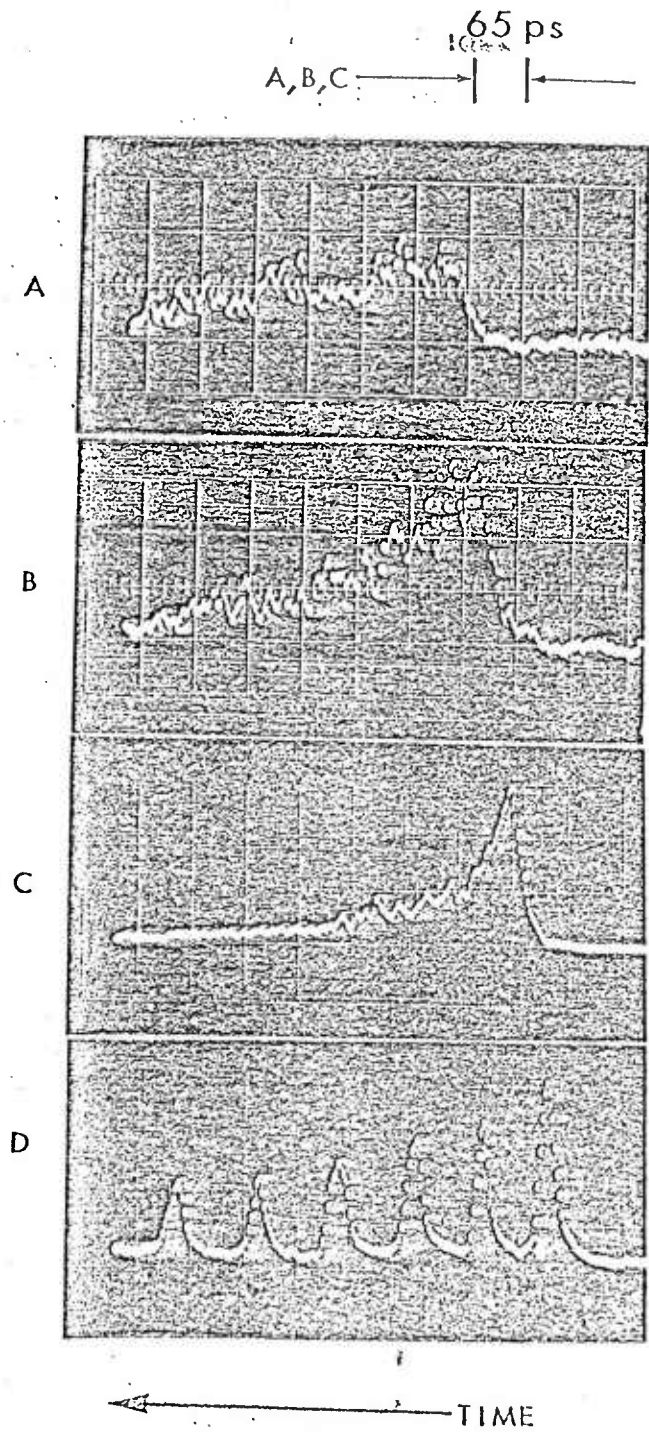


Figure 7. OMA-oscilloscope displays of 700 nm fluorescent streaks from *C. pyrenoidosa* excited with a single 20psec, 530nm pulse. Excitation intensities are (A)  $10^{14}$  (B)  $3 \times 10^{14}$  and (C)  $\approx 3 \times 10^{15}$  photon/cm<sup>2</sup>. The variation in fluorescence lifetime with intensity is consistent with singlet-singlet exciton processes occurring within the photosynthetic antenna apparatus. (D) Train of calibration pulses (from Campillo et al., Ref. 43).

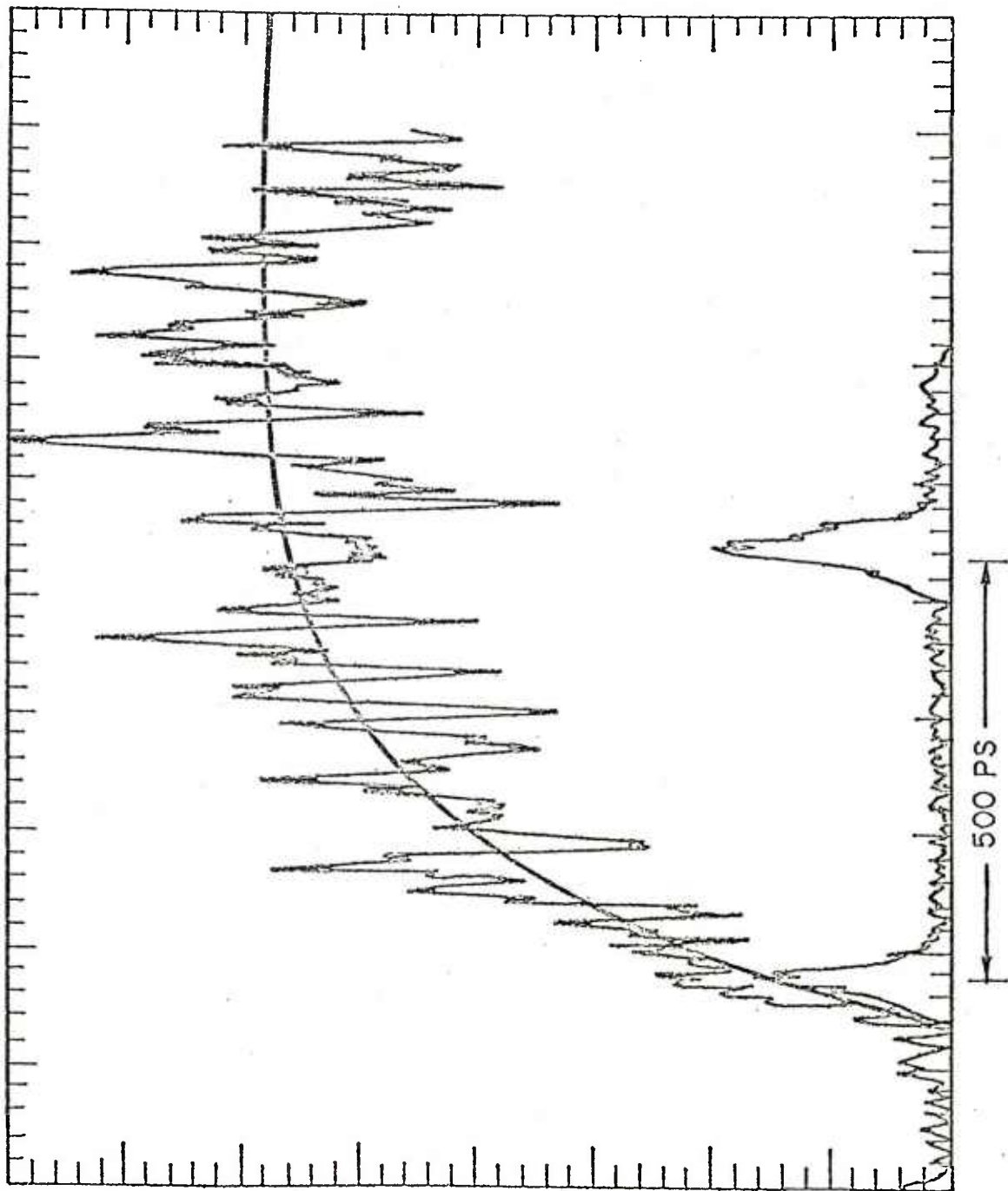


Figure 8. Streak camera record of the rise of C<sub>2</sub> Swan emission after 266nm photolysis of acetylene at a few torr; the average of 10 pulses. Also shown are a model curve with time constant 215ps, and second-harmonic reference pulses at a pair separation of 500ps (from Craig et al., Ref. 53).

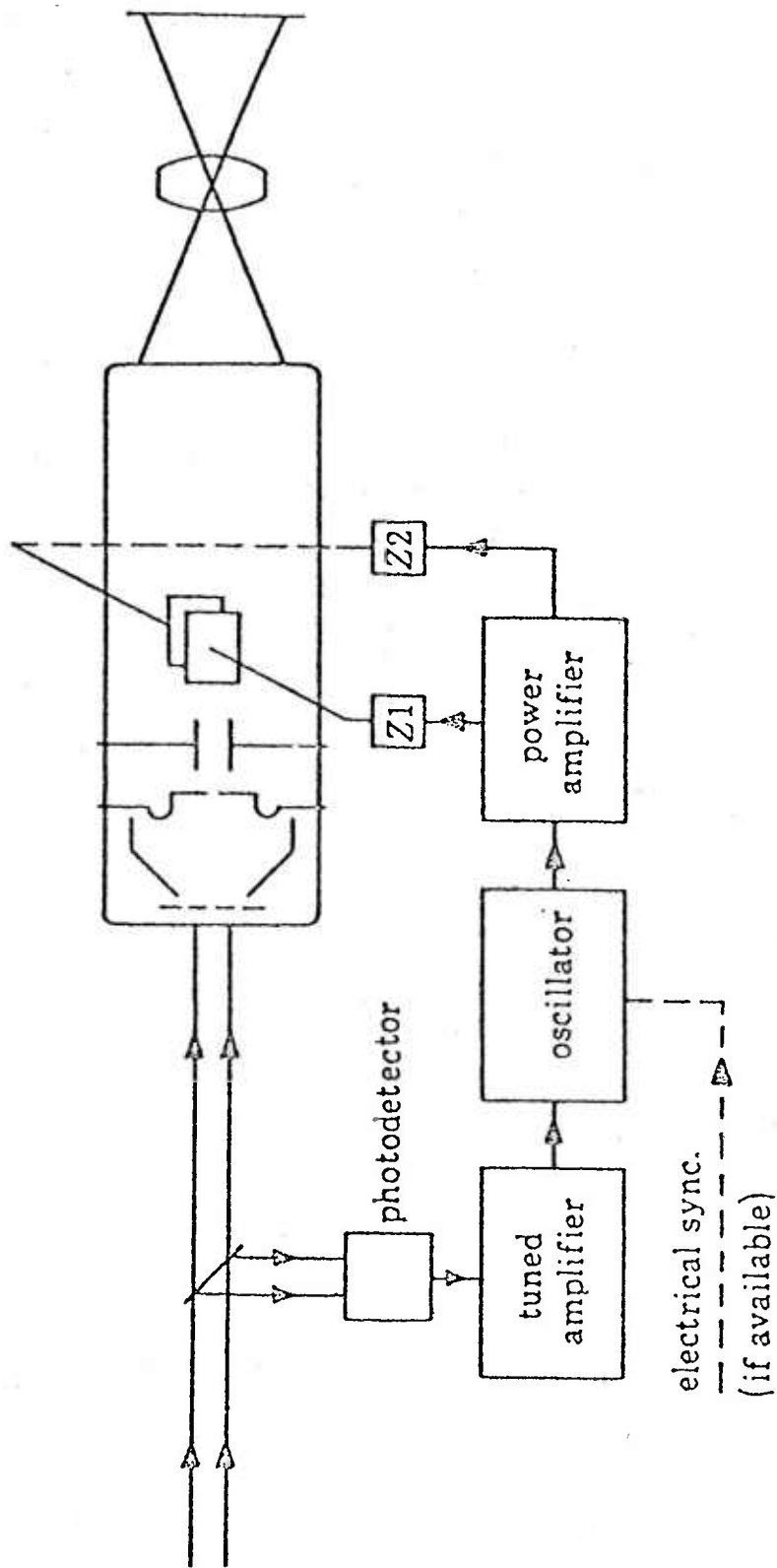


Figure 9. Block diagram of the synchroscan deflection scheme (from Huston and Helbrough, Ref. 50).

— I LINE  
..... UV EXCITATION PULSE

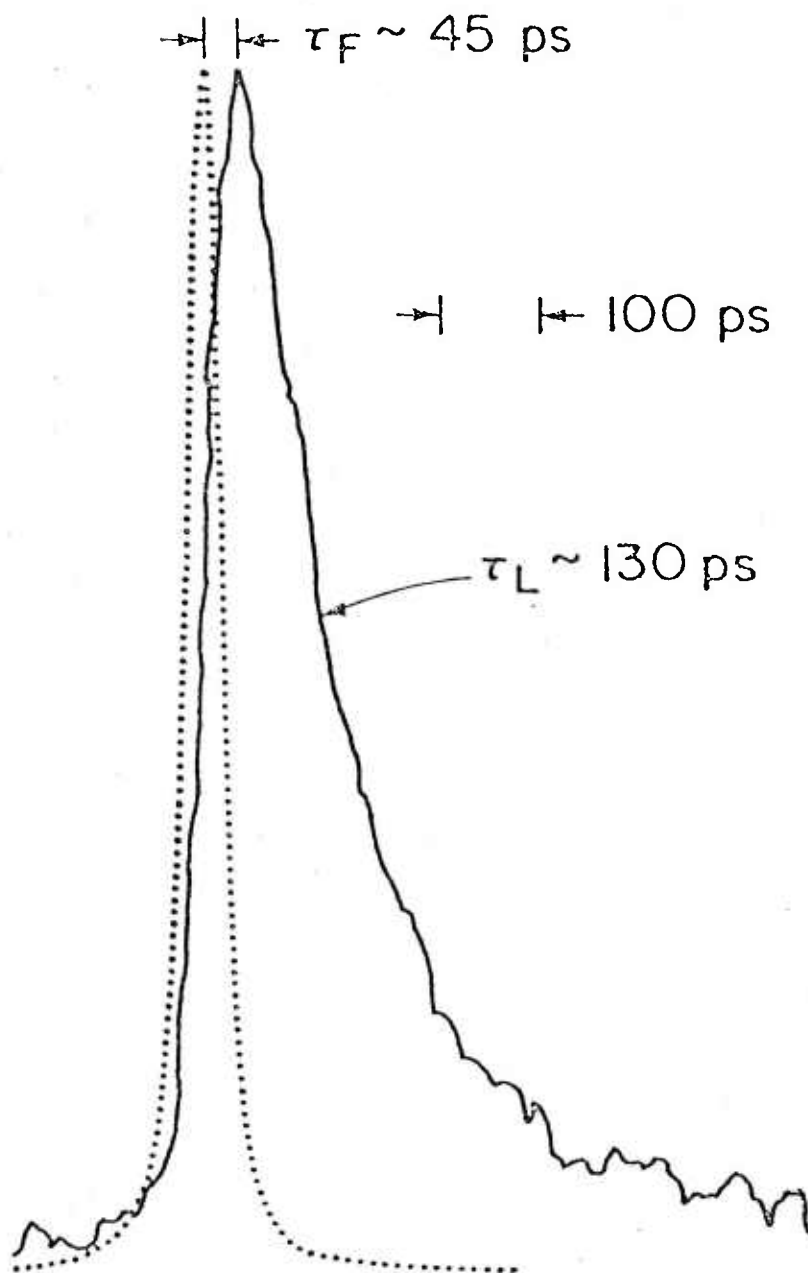


Figure 10. Time dependence of the I line luminescence from CuCl at 8°K (solid line) and UV laser excitation (dashed line). Data obtained with sychroscan streak camera (from Fujimoto et al., Ref. 61).

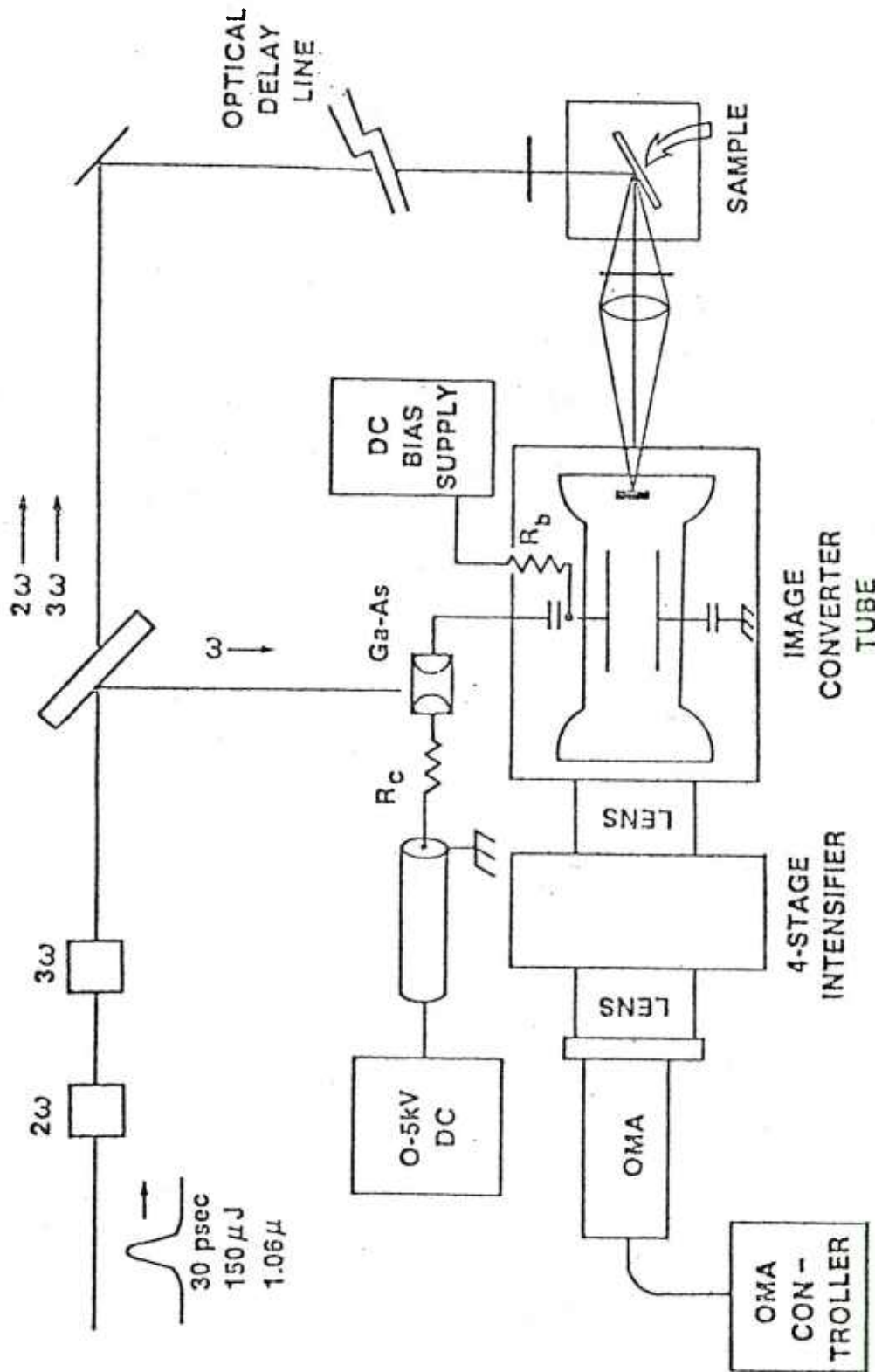


Figure 11. Schematic of optical experiment employing a low jitter GaAs:Cr photoconductive switch and associated streak camera deflection system (from Knox et al., Ref. 66).

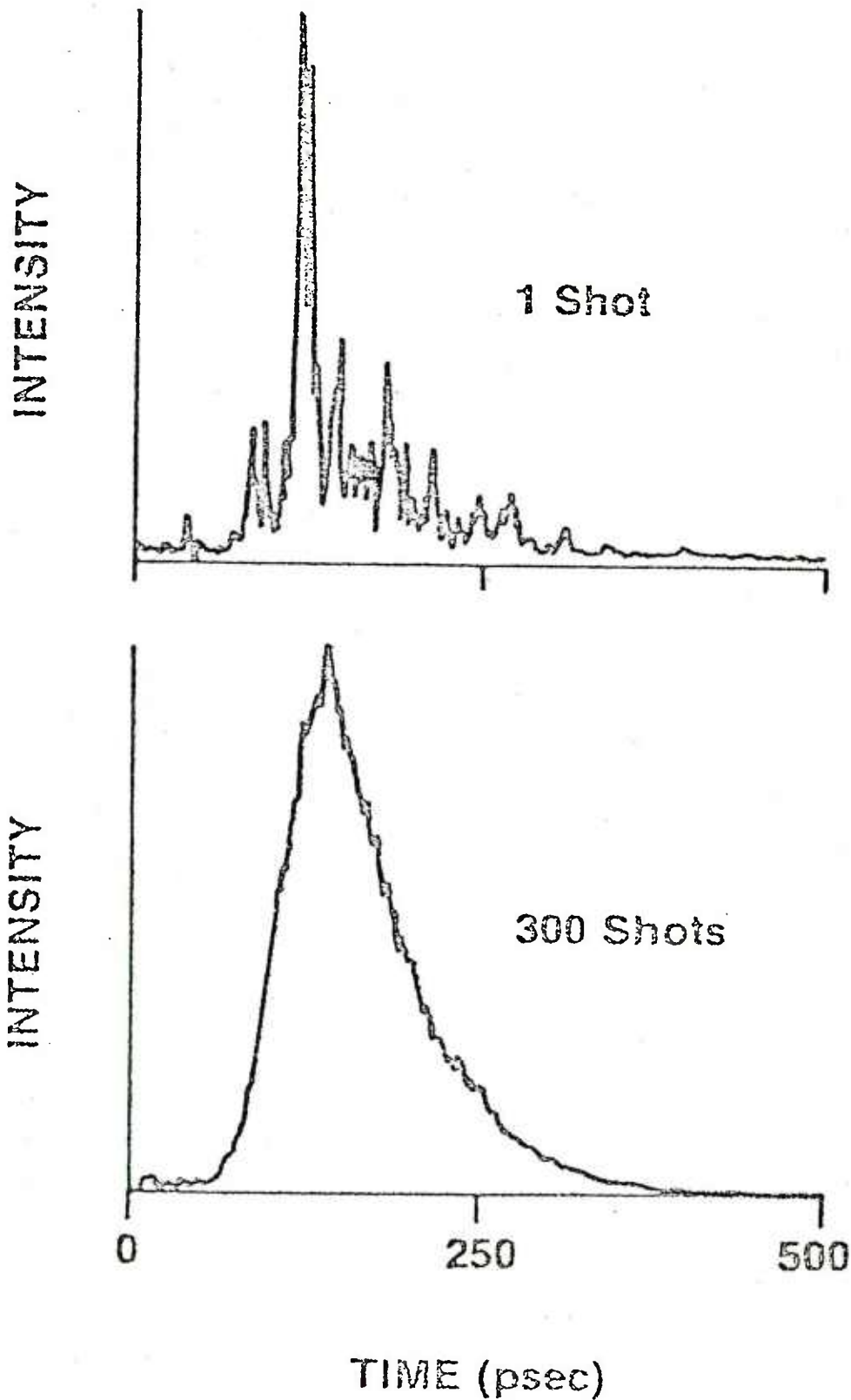


Figure 12. CdSe luminescence at 170°C. Upper trace is data taken during a single streak sweep. Lower trace is the average of 300 shots accumulated using the low jitter deflection scheme shown in Fig. 11 (from Mourou et al., Ref. 67).

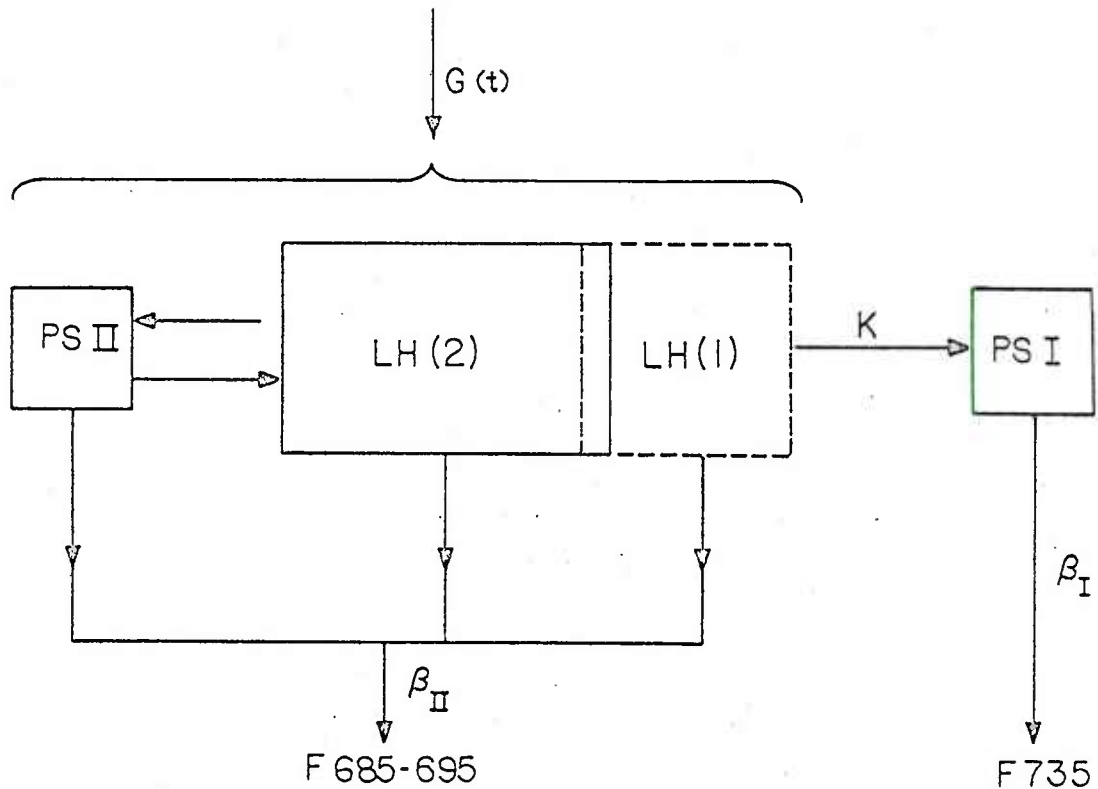


Figure 13. On the basis of streak camera measurements this modified tripartite fluorescence model of the antenna apparatus of green plants was proposed. The source term  $G(t)$ , excites both the light harvesting aggregate, LH, and the photosystem II (PSII) chlorophylls. Fluorescence emission corresponding to LH, PSII and photosystem I (PSI) are at 685, 695 and 735nm. The light harvesting pigment system is presumed to consist of two fractions: in LH(1) the light harvesting pigments are closely associated with PSI and energy transfer occurs with rate constant  $K$ ; in LH(2) the pigments are not closely connected to PSI and excitons decay mainly with the rate constant  $\beta_{II}$ . The decay rate of the 735nm fluorescence, which reflects the exciton density in PSI, is denoted by  $\beta_I$  (from Campillo et al., Ref. 52).

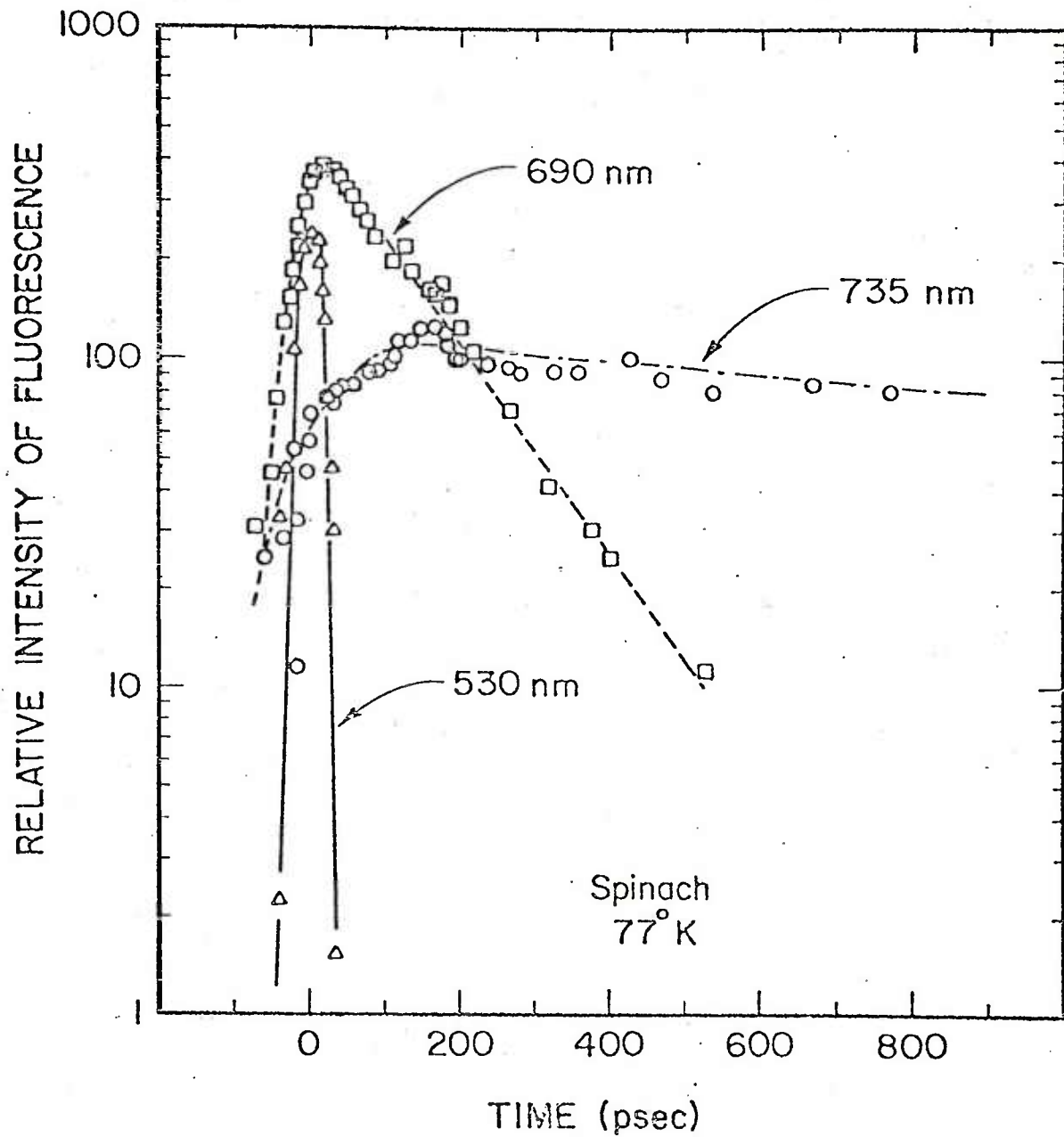


Figure 14. Time resolved fluorescence from spinach chloroplasts at a temperature of 77°K and an incident intensity of  $2 \times 10^{14}$  photons  $\text{cm}^{-2}$ . The 735nm fluorescence is signal averaged data obtained by accumulating 180 shots using a temporal fiducial pulse arriving prior to the arrival of the fluorescence (from Campillo et al., Ref. 52).

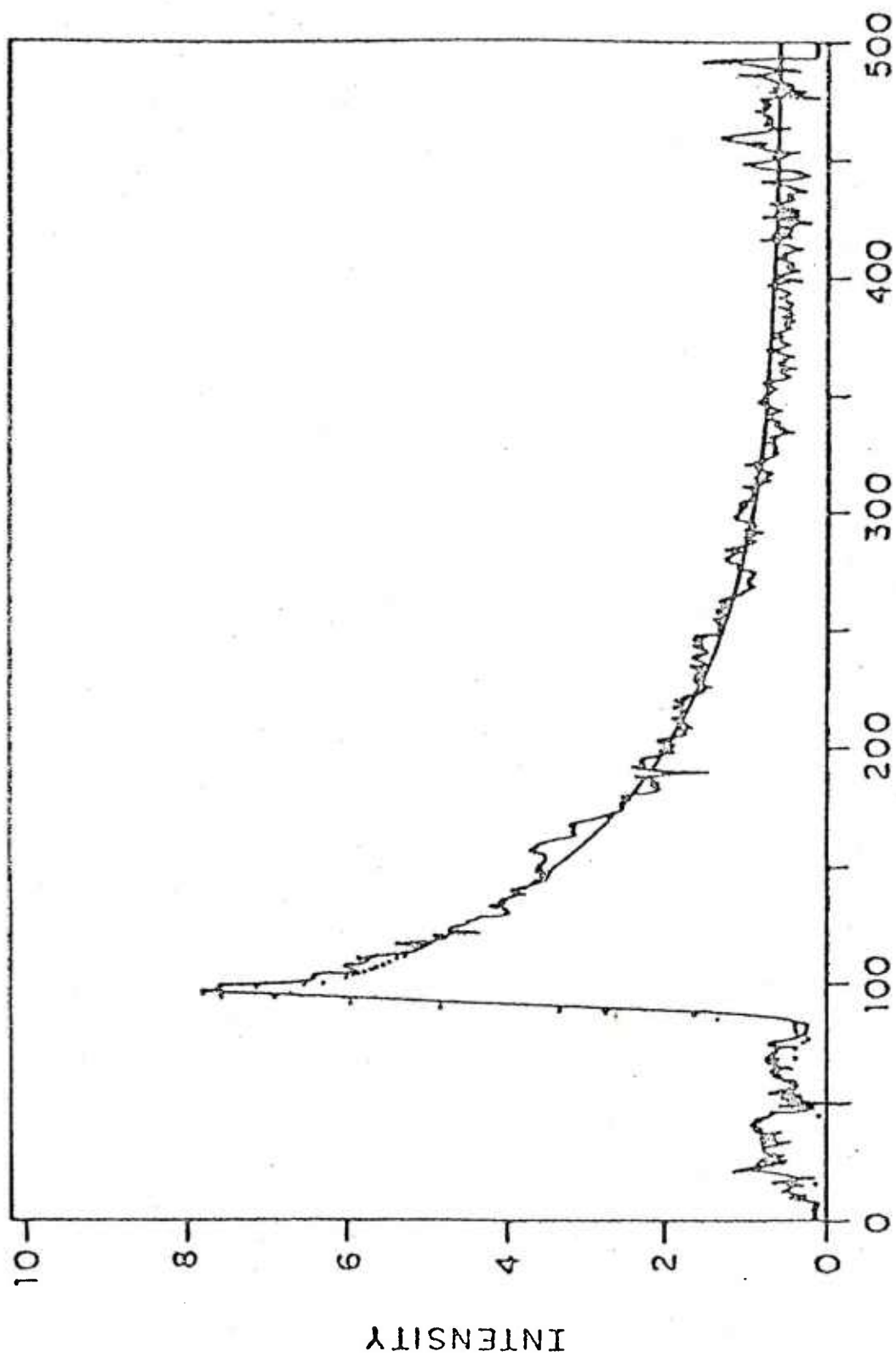


Figure 15. Fluorescence of the excited charge transfer (CT) complex in acetonitrile ( $2.5 \times 10^{-3} M$ ). The smooth curve is a theoretical fit to the experimental data (from Crawford et al., Ref. 116).

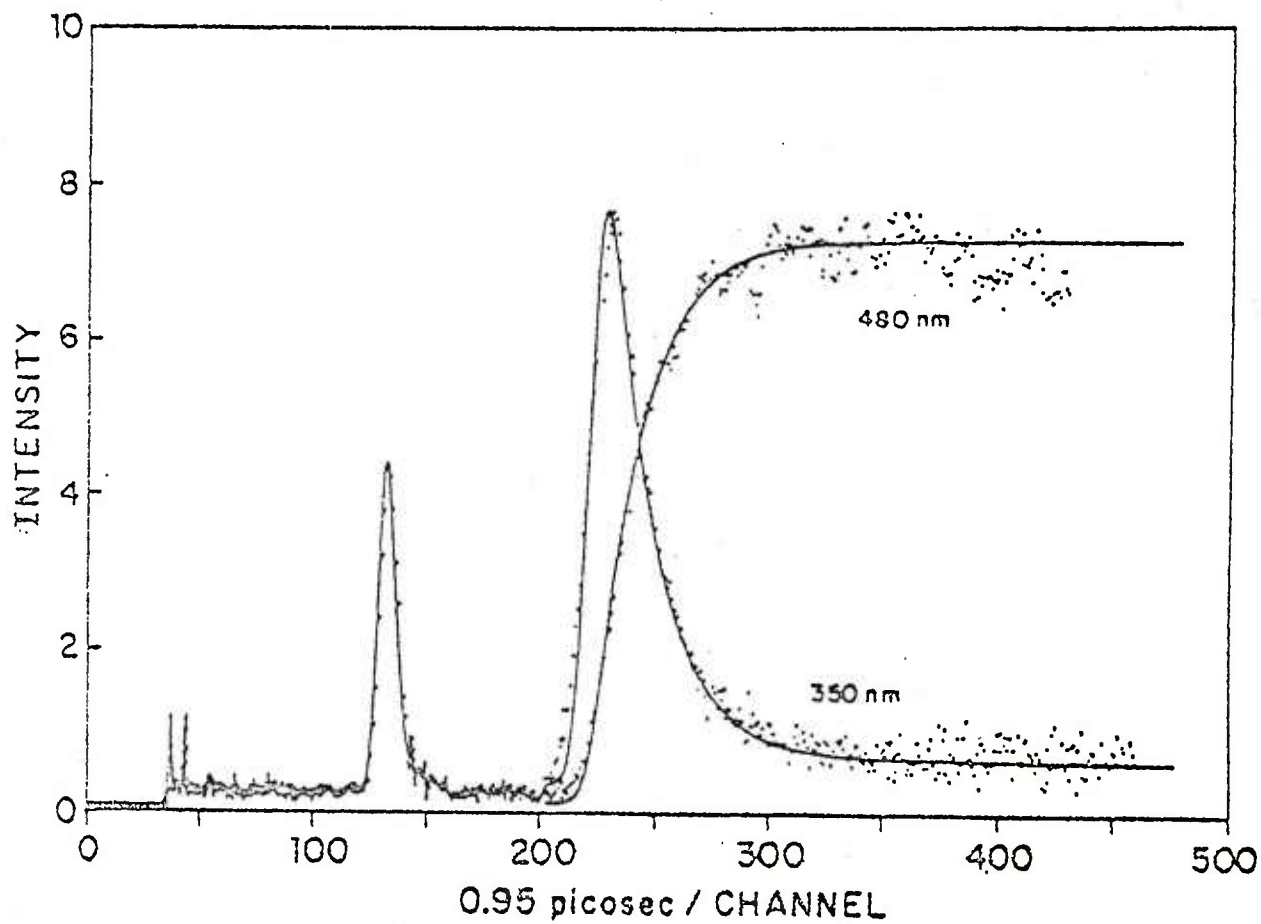


Figure 16. The dual fluorescence of DMABN in propanal is shown. The solid curve is the theoretical calculation and the points are experimental data. The prepulse at channel 140 is a time marker (from Wang et al., Ref. 117).

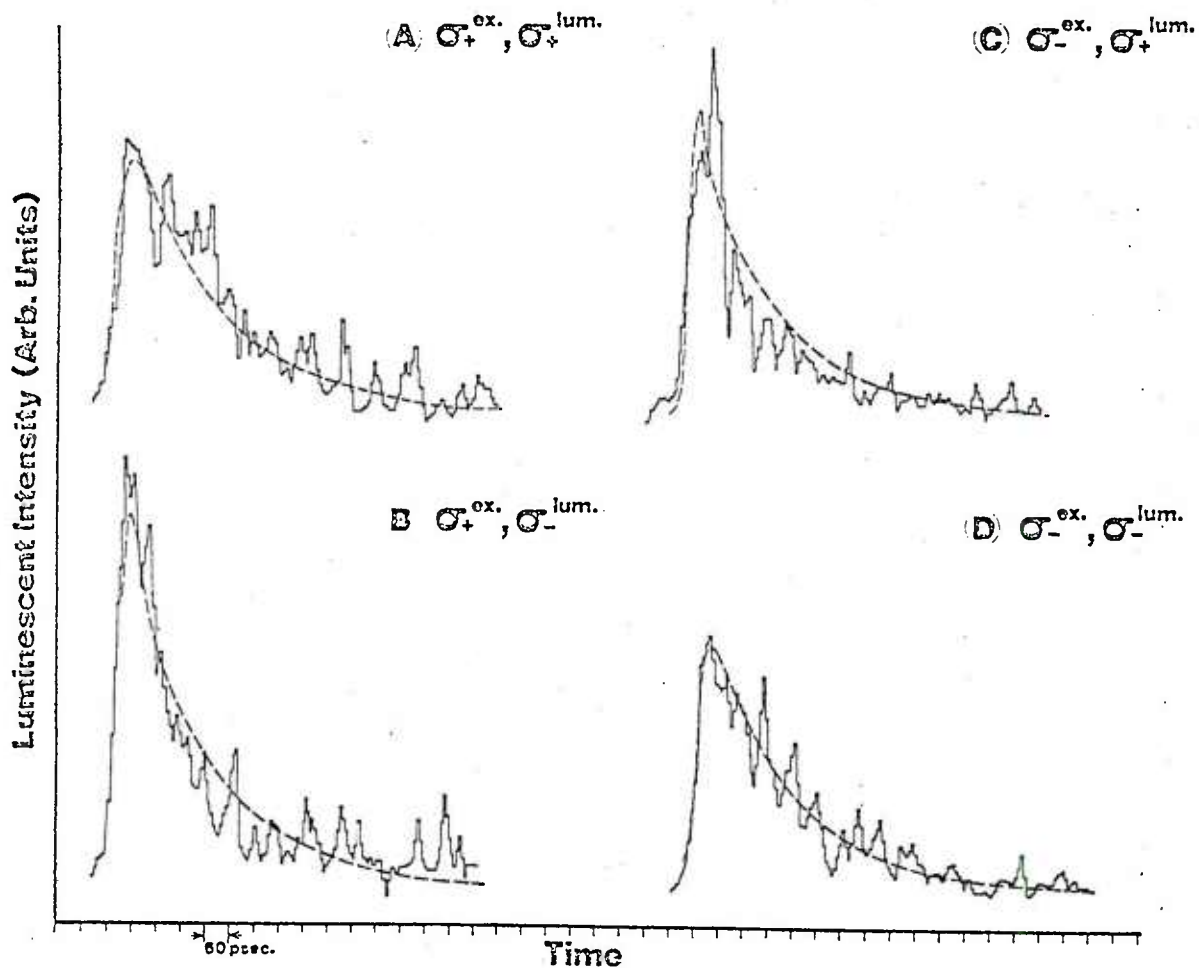


Figure 17. Luminescent decay kinetics for p-type GaAs (Zn doped,  $N_A = 7 \times 10^{17} / \text{cm}^3$ ). 2A and 2B are for left- ( $\sigma_+^{\text{ex}}$ ) and 2C and 2D are for right-circular-polarized excitation ( $\sigma_-^{\text{ex}}$ ). 2A and 2C are the right-circular-polarized luminescence ( $\sigma_-^{\text{lum}}$ ) and 2B and 2D are the left-circular-polarized luminescence ( $\sigma_+^{\text{lum}}$ ). The solid curve is the experimental data output from the streak camera. The broken curve is calculated from rate equations (from Seymour and Alfano, Ref. 142).

DELAYED FORMATION OF EMISSIVE CN AND C<sub>2</sub>  
FRAGMENTS FOLLOWING SHORT-PULSE UV EXCITATION  
OF ISOTOPICALLY LABELED CH<sub>3</sub>CN

B.B. Craig, W.L. Faust,  
Naval Research Laboratory  
Washington, DC 20375

and

R.G. Weiss  
Department of Chemistry  
Georgetown University  
Washington, DC 20057

We have studied fragment emission in the spectral range 200 to 900nm, following photolysis of CH<sub>3</sub>CN (0.27-10torr) by short UV pulses (25ps, 266nm). The dominant components of emission are the CN B<sup>2</sup>Σ<sup>+</sup>→X<sup>2</sup>Σ<sup>+</sup> violet system and the C<sub>2</sub> d<sup>3</sup>Π<sub>g</sub>→a<sup>3</sup>Π<sub>u</sub> Swan system, which appear with pressure-dependent rates. The rise and fall of the fragment waveforms have been characterized by simple exponential time constants. The CH<sub>3</sub>CN pressure-dependence of the rate constants for fragment formation supports the existence of a precursor state or states, which decay spontaneously (collision-free) with characteristic lifetimes to CN B<sup>2</sup>Σ<sup>+</sup> and to C<sub>2</sub> d<sup>3</sup>Π<sub>g</sub>. Collisionally assisted fragment formation from and/or simple quenching of the precursors proceed with very large bimolecular rate constants (13 x 10<sup>-10</sup>cm<sup>3</sup> s<sup>-1</sup> for CN B<sup>2</sup>Σ<sup>+</sup>). A secondary minor channel of CN B<sup>2</sup>Σ<sup>+</sup> production is shown to be from CN A<sup>2</sup>Π<sub>j</sub>. We have employed isotopic parents to characterize several distinct source channels of fragmentation. Two unimolecular channels of CN B<sup>2</sup>Σ<sup>+</sup> production are recognized, one involving retention of the C-N bond and another consistent with an isomerization process; a common precursor exhaustion time is indicated. A mechanistic interpretation is developed.

## I. Introduction

There is an extensive literature on the photodissociation of XCN-type ( $X = \text{H}, \text{CH}_3, \text{halogen}, \text{etc.}$ ) compounds (1-9). The well-characterized CN radical  $B^2\Sigma^+ \rightarrow X^2\Sigma^+$  and  $A^2\Pi_1 \rightarrow X^2\Sigma^+$  fluorescence systems have provided particularly useful probes of primary photochemical processes and of the details of energy partitioning among product degrees of freedom (7,8,10-13). In VUV (2-9) and in more recent multiphoton IR (14) and UV (15-17) studies CN  $B^2\Sigma^+$  has been postulated as a primary fragmentation product of several cyano-bearing parents. Ashfold and Simons (8), through an analysis of the vibrational and rotational energy distribution within the CN  $B^2\Sigma^+$  fragment, proposed the existence of a "long-lived" dissociative intermediate in the VUV photolysis of  $\text{CH}_3\text{CN}$ . The nature and lifetimes of such energetic intermediates have remained elusive. However, a deeper understanding of these species is important because of their potential role in fast exothermic reactions.

In the present study, we have examined the temporal development of emissive fragments produced by short-pulse UV excitation (25ps, 266nm) of low pressure (0.27-10torr)  $\text{CH}_3\text{CN}$ . In contrast to our studies of  $\text{C}_2\text{H}_2$  (18), where prompt unimolecular and delayed intermolecular pathways of fragment production were identified,  $\text{CH}_3\text{CN}$  yields no prompt diatomic products; all emissive fragments appear with pressure-dependent rates. The dominant components of emission are the CN  $B^2\Sigma^+ \rightarrow X^2\Sigma^+$  violet system and the  $\text{C}_2$   $d^3\Pi_g \rightarrow a^3\Pi_u$  Swan system. With isotopic labeling we have gained further insight into the mechanistics of the photodissociation pathways.

## II. Experimental

The apparatus has been described previously (19,20). UV pulses (25ps, 266nm) of up to 12mJ energy were focused into a static gas sample cell. Emission was collected through a side window and dispersed in a one-meter Czerny Turner spectrometer. A Varian VPM-154M crossed-field photomultiplier (GaAs photocathode) coupled to a Tektronix digital oscilloscope provided a detection system of net risetime 0.6ns and spectral range 200-900nm. Data were processed with a Tektronix 4052 computer system.

CH<sub>3</sub>CN was Burdick & Jackson spectrophotometric grade, used as supplied. Identical results were obtained with Fisher ACS grade solvent, which had been distilled from P<sub>2</sub>O<sub>5</sub> under N<sub>2</sub>, collecting the mid-fraction bp. 81-82°C. Isotopic forms of CH<sub>3</sub>CN were supplied by Merck, Inc. NMR analysis, by the supplier, was used to determine the exact isotopic content. All samples were thoroughly degassed prior to use by several freeze-pump-thaw cycles. Pressures were measured with a Wallace-Tiernan gauge (0-50torr).

### III. Results

Following multiphoton UV excitation of CH<sub>3</sub>CN, we have identified a variety of diatomic emissive fragments. The strongest components of emission were the CN B<sup>2</sup>Σ<sup>+</sup>→X<sup>2</sup>Σ<sup>+</sup> violet system (350-460nm) and the C<sub>2</sub> d<sup>3</sup>Π<sub>g</sub>→a<sup>3</sup>Π<sub>u</sub> Swan system (430-670nm). Weak NH A<sup>3</sup>Π→X<sup>3</sup>Σ (310-370nm), CH A<sup>2</sup>Δ→X<sup>2</sup>Π (430-490nm) and CH C<sup>2</sup>Σ<sup>+</sup>→X<sup>2</sup>Π (314.5nm) were also detected. We have assigned a very weak red emission (600-900nm) to the CN A<sup>2</sup>Π<sub>i</sub>→X<sup>2</sup>Σ<sup>+</sup> transition. In contrast to ArF laser multiphoton dissociation of C<sub>2</sub>N<sub>2</sub> (16) and ClCN (15), no emission from higher energy CN states was observed. Continuum emission was minimal, and atomic emission was restricted to a few lines, e.g. C (247.6nm), H (656.3nm) and C<sup>+</sup> (283.7nm).

Uniformly, diatomic fragment populations are generated with pressure-dependent rates. The rise of the emission was readily examined with the fast photomultiplier/digital oscilloscope system. Detailed investigations were undertaken to characterize temporally the formation and decay of the CN B<sup>2</sup>Σ<sup>+</sup> and C<sub>2</sub> d<sup>3</sup>Π<sub>g</sub> populations. In each of these systems the (0,0) vibrational head afforded a relatively favorable signal level.

#### 1. Dependence of CN B<sup>2</sup>Σ<sup>+</sup> waveforms upon CH<sub>3</sub>CN pressure.

Figure 1 shows typical (0,0) violet emission waveforms obtained from 3torr of CH<sub>3</sub>CN. For pressures below 10torr and for low UV pulse energies (0.4-6.0mJ) the B state waveforms are relatively well fit by simple biexponential curves. Pressure-dependent rate constants, k<sub>1</sub><sup>v</sup> (v'=0) and k<sub>2</sub><sup>v</sup> (v'=0), were determined. However, even under these conditions, there

exists a definite excess component of protracted violet emission; the intensity is ca. 3-5% of the main peak (Fig 1a). This long-lived component reflects a persistent minor channel of B state generation. At pressures of 14 and 20 torr, and for high UV pulse energy (12mJ), the late violet emission is quite pronounced.

Figure 2 and Fig 3 illustrate the pressure-dependence of  $k_1^v$  ( $v'=0$ ) and  $k_2^v$  ( $v'=0$ ) up to 10 torr of  $\text{CH}_3\text{CN}$ . These data were obtained with pulse energies in the range 0.4-6.0mJ. Although the excitation energy was systematically decreased from low to high pressure, the data are believed to represent the limit of low pulse energy. In fitting the waveforms we have respected the rise and initial decay, but not the late "excess" (Fig 1a). This treatment best isolates the rise of the B state population produced by the dominant generative mechanism, with minimal interference from the minor secondary process (the latter will be shown to be correlated with the  $\text{CN } A^2\Pi_i$  state, sect. III.4). The agreement of the zero-pressure  $k_2^v$  ( $v'=0$ ) value ( $57 \pm 5\text{ns}$ ) with the known radiative lifetime of  $\text{CN } B^2\Sigma^+$  (21,22), relieves the potential ambiguity in such biexponential curves; clearly  $k_1^v$  reflects formation of  $\text{CN } B^2\Sigma^+$  and  $k_2^v$  its destruction. Figure 3 then implies that the B state is formed from some precursor state, with a zero pressure rate constant of  $5.0 \pm 0.6 \times 10^7 \text{s}^{-1}$  (i.e. a precursor lifetime of 20ns); the precursor is quenched with a very large bimolecular rate constant,  $13 \pm 2 \times 10^{-10} \text{cm}^3 \text{s}^{-1}$ .

In a less extensive study  $v' > 0$  violet band waveforms were recorded. To obtain adequate signal-to-noise we accumulated data from 300 laser pulses at 385.6nm, where transitions from  $v'=1,2$  and 3 overlap.  $k_1^v$  ( $v'=1,2,3$ ) and  $k_2^v$  ( $v'=1,2,3$ ) values were obtained for only four pressures, but the following points are clear. The rate of B state appearance shows no marked vibrational dependence either in intercept or in slope (Fig 2). For the decay constant,  $k_2^v$ , the intercept again shows a common value for  $v'=1,2,3$  and for  $v'=0$  (Fig 3). However, the higher  $v'$  have a distinctly larger bimolecular rate constant for quenching by  $\text{CH}_3\text{CN}$  (cf.  $3.9 \pm 0.2 \times 10^{-10} \text{cm}^3 \text{s}^{-1}$  for  $v'=1,2,3$  and  $2.2 \pm 0.2 \times 10^{-10} \text{cm}^3 \text{s}^{-1}$  for  $v'=0$ ). This is in contrast with the recent work

of Lurie and El-Sayed (17), where no vibrational preference (for  $v'=0$  and  $v'=1$ ) was observed for B state quenching by  $\text{CH}_4$ .

## 2. Dependence of $\text{C}_2\text{d}^3\Pi_g$ waveforms upon $\text{CH}_3\text{CN}$ pressure.

At 1torr, the intensity of the Swan system is about 35% of that for the violet system. Emission waveforms obtained at the (0,0) band head exhibit a pressure-dependence similar to those of the violet emission. The curves are well accommodated by simple biexponential forms (rate constants  $k_1^S$  and  $k_2^S$ ); they show no late term excess signal. The extrapolated zero-pressure lifetime of the Swan emission is then  $123 \pm 10\text{ns}$ , which agrees well with the literature value of  $119 \pm 5\text{ns}$  (23). In an analogous plot to that shown in Fig 2, we obtain a unimolecular decay constant of  $3.0 \pm 0.6 \times 10^{-7}\text{s}^{-1}$  for the precursor (i.e. a lifetime of 33ns) and a quenching constant of  $19 \pm 1 \times 10^{-10}\text{cm}^3 \text{s}^{-1}$ .

## 3. Effect of additive gases on the risetime of $\text{CN B}^2\Sigma^+$ and $\text{C}_2 \text{d}^3\Pi_g$

An attempt was made to investigate the effect of additive gases on the rates of rise of both the B state and  $\text{C}_2^*$  emissions. An inherent difficulty in such a study is that any added gases are themselves subject to photolysis by the UV excitation pulse. Two gases which yield minimal emission upon laser excitation are  $\text{CH}_4$  and Ar. A limited investigation was made at a fixed  $\text{CH}_3\text{CN}$  pressure of 3torr and a total gas pressure of up to 12.5torr.

Ar has essentially no effect on the initial rate of B state or of  $\text{C}_2^*$  appearance. However, added  $\text{CH}_4$  caused an increase in both  $k_1^V$  ( $v'=0$ ) and  $k_1^S$  with precursor quenching constants about 1/3 of those observed for  $\text{CH}_3\text{CN}$ . It is unresolved whether the essential feature of the collision partner is associated with internal vibrations or with a capacity for reactive collisions.

#### 4. Evidence for CN $A^2\Pi_i$ emission

In several studies (4,26) CN  $A^2\Pi_i$  ( $v' > 10$ ) has been postulated as a precursor of the B state. Collisionally induced internal conversion is thought to occur between near iso-energetic levels:



This motivated a careful assessment of low-level red emission. A very weak (ca. 2% of the violet system) structured continuum emission, extending throughout the red, was assigned to the CN  $A^2\Pi_i \rightarrow X^2\Sigma^+$  transition. Our observations at 2 and 5 torr are consistent with the known long radiative lifetime (24,25) and with a moderate rate of quenching (cf. 25). However, there is clear vibrational dependence; this is likely to be due to collisional vibrational relaxation or interaction with the X state.

The poor signal-to-noise of the red system prevented a detailed study of its risetime. For 2 torr of  $\text{CH}_3\text{CN}$  the emission waveform at 630nm (10,5) has no discernible delayed maximum and shows no rapidly decaying component which could correlate with the formation of the B state. Clearly, CN  $A^2\Pi_i$  is not directly responsible for the dominant fast pressure-dependent CN  $B^2\Sigma^+$  production. However, at several pressures we did observe a concomitance of the late term violet band component and the red system (10,5) decay. It appears then that A state radicals are the source of the minor channel producing CN  $B^2\Sigma^+$ , as was suggested by Luk and Bersohn for ICN (4).

## 5. Fragmentation studies with isotopically-labeled CH<sub>3</sub>CN

With the use of isotopically labeled CH<sub>3</sub>CN it is possible to investigate the atomic heritage of C<sub>2</sub> d<sup>3</sup>Π<sub>g</sub> and CN B<sup>2</sup>Σ<sup>+</sup>. To resolve spectrally distinct isotopic forms it is necessary to study Δv≠0 sequences. The heads of the Swan system in the Δv=+1 sequence for <sup>12</sup>C<sub>2</sub>, <sup>12</sup>C<sup>13</sup>C and <sup>13</sup>C<sub>2</sub> are well-known from the work of Dhumwad and Narasimham (27). The corresponding information for the <sup>12</sup>C<sup>14</sup>N, <sup>13</sup>C<sup>14</sup>N, <sup>12</sup>C<sup>15</sup>N isotopes of the violet system in the Δv=-1 sequence was acquired in the current work through point-by-point scanning at intervals of 0.2nm. Labeled atoms enable fractional assignment of emissive fragments according to distinct sources; e.g. C<sub>2</sub><sup>\*</sup> may contain two carbon atoms from the same parent or from different ones. Such determinations were made from temporal integrals of waveforms, which have relatively good signal-to-noise.

It was found that at 5torr, about 50% of C<sub>2</sub><sup>\*</sup> is generated in a process which specifically preserves fraternal C-C pairs. In contrast, at least 80% of CN B<sup>2</sup>Σ<sup>+</sup> is parent-respecting. Furthermore, within this 80% we have recognized two components of B state production: one in which the parent C-N bond is preserved (60-70%), consistent with C-C cleavage, and another channel in which the methyl carbon is associated with the nitrogen atom, necessitating a rearrangement or isomerization process. Other fragments are produced via atomic exchange (between distinct parent molecules); we believe that such fragment populations are generated according to a random scrambling model, i.e. without preference between methyl and cyano carbons. For C<sub>2</sub><sup>\*</sup> this channel is thought to be analogous to that observed for C<sub>2</sub>H<sub>2</sub> (18).

It is difficult to exploit labeled parents in the pursuit of distinctly different risetimes associated with the various source channels. The signal-to-noise is poor because the (0,0) head cannot be used and because the B state signal is distributed among the isotopic forms. Nevertheless, for  $^{12}\text{CH}_3^{13}\text{CN}$  and  $^{13}\text{CH}_3^{12}\text{CN}$  we have acquired, through extensive averaging, waveforms at the  $^{12}\text{CN}^*$  (0,1) band head; these are free of underlying rotation. Clearly, such  $^{12}\text{CN}^*$  can not be generated through identical reaction pathways, for the two labeled isotopes. However, waveforms obtained at 2 torr and 0.5 torr exhibit the same pressure-dependent risetimes. This strongly suggests that the different source channels have a common precursor.

#### IV. Discussion

In contrast to the results for  $\text{C}_2\text{H}_2$  (18), no prompt components of fragment emission were observed for  $\text{CH}_3\text{CN}$  parent. We have established the existence of pressure-dependent formation processes for both  $\text{CN } B^2\Sigma^+$  and  $\text{C}_2 d^3\Pi_g$ , from  $\text{CH}_3\text{CN}$ . The well-defined characteristic times for exponential production of observed species are considered to describe exhaustion of precursor species. However, the character and the identity of the intermediates remain unresolved. It is clear that the intermediates are present as a minority, relative to the population of undisturbed parents:  $\text{CH}_3\text{CN}$  possesses no single quantum absorption at 266 nm, and two quantum excitation to a Rydberg R state (133 nm) at our flux level proceeds with <1% efficiency (18). Thus reactions of the intermediates with parent  $\text{CH}_3\text{CN}$  are characterized by pseudo first order rate constants,  $k_1^V$  and  $k_1^S$ . These rate constants may reflect simple quenching of the intermediates, competitive with the spontaneous unimolecular process. Alternatively, they may represent a second fragment formation channel, which is collisionally assisted. Discrimination between these two cases will require a careful analysis of relative yields. Although the pathway from excited parent to emissive fragments may pass through several intermediates, our technique recognizes only the residence time of the intermediate associated with the rate-determining step.

The zero-pressure rate constant of  $5.0 \pm 0.6 \times 10^7 \text{ s}^{-1}$  (Fig 2) for spontaneous unimolecular decay of the B state intermediate corresponds to a precursor lifetime of 20ns. The corresponding precursor lifetime for  $\text{C}_2 \text{ d}^3\Pi_g$  generation is 33ns. Identically equal zero-pressure lifetimes would imply a common precursor for both unimolecular Swan and violet components. Similarly identical rate constants for  $\text{CN B}^2\Sigma^+$  and  $\text{C}_2 \text{ d}^3\Pi_g$  formation,  $13 \times 10^{-10} \text{ cm}^3 \text{ s}^{-1}$  and  $19 \times 10^{-10} \text{ cm}^3 \text{ s}^{-1}$  respectively, would imply a common precursor for the collisional Swan and violet components. The isotope experiments establish that nearly 50% of  $\text{C}_2^*$  fails to respect the parent C-C bond. It is conceivable that if the formation process representative of fraternal  $\text{C}_2^*$  could be isolated, it would indeed yield rate parameters identical to those of the B state. The values of the bimolecular rate constants for precursor destruction are substantially larger than those representative of diffusion-mediated processes (ca.  $10^{-10} \text{ cm}^3 \text{ s}^{-1}$ ). Suprathermal fragment velocities, Rydberg states, or ionic species, affording long-range Coulomb forces, could account for the large cross sections implied in the observed rate constants.

A secondary minor channel of B state production has been shown to occur via  $\text{CN A}^2\Pi_1$ . Another source, in principle, is a highly excited ground state radical,  $\text{CN X}^2\Sigma^+(\nu>14)$ . However, transition between X and B is made difficult by the unfavorable Franck Condon factor (ca.  $10^4$  smaller than that of  $\text{A} \rightarrow \text{B}$ ) (4). High lying vibrational levels of B, which cascade down to the observed  $\nu'=0$  to 5 levels, can also be excluded as precursors to the major B state channel; no emission from  $\nu'=10,11,12$  was observed, although the oscillator strengths for the  $\Delta\nu=0$  transitions are similar to those of the low lying transitions (28). We are forced then to consider more complex intermediate species.

No single photon absorption for  $\text{CH}_3\text{CN}$  is known at 266nm. Consequently, we believe that  $2h\nu$  ( $214\text{kcal mol}^{-1}$ ) excitation occurs to the  $n=3$  R lowest Rydberg state (29). The pertinent thermodynamic thresholds for decomposition are:  $\text{CH}_2\text{CN} + \text{H}$ ,  $93\text{kcal mol}^{-1}$ ;  $\text{CH}_3 + \text{CN } X^2\Sigma^+(v=0)$ ,  $122\text{kcal mol}^{-1}$ ;  $\text{CH}_3 + \text{CN } A^2\Pi_i(v'=0)$ ,  $147\text{kcal mol}^{-1}$ ; and  $\text{CH}_3 + \text{CN } B^2\Sigma^+(v'=0)$ ,  $196\text{kcal mol}^{-1}$ . In a study of a series of XCN compounds, Okabe and Dibeler measured a relatively small quantum yield of  $\text{CN } B^2\Sigma^+$  emission from  $\text{CH}_3\text{CN}$  with incident excitation of 121.6nm ( $235\text{kcal mol}^{-1}$ ) (5). They suggested that the B state fluorescence yield decreased with the complexity of the molecule, reflecting an increased number of dissociation pathways. Further, our observation of  $\text{CN } B^2\Sigma^+$  emission up to  $v'=5$  ( $28.5\text{kcal mol}^{-1}$  above  $v'=0$ ) is incompatible with  $2h\nu$  excitation. In view of these considerations we believe that formation of the B state at the  $2h\nu$  level is not a major dissociative channel. By analogy with  $\text{C}_2\text{H}_2$  (18) and as previously advocated for excitation at 184.9nm (1), H atom elimination is favored as the primary step at the  $2h\nu$  level, although the initial excitation occurs within the  $\pi$  electron system. However, population of the A state (which generates the late term B state component), and of the X state also are energetically allowed. Indeed, production of X state with subsequent excitation to higher states, which cascade down to the emissive B state, could account for the primary B state channel. The lack of emission from higher CN states (observed in other work (15,16)) tends to disfavor this mechanism. Furthermore, such a scheme would provide no account of fraternal  $\text{C}_2^*$  nor of any relationship between  $k_1^V$  and  $k_1^S$ .

For the cyanomethyl radical,  $\cdot\text{CH}_2\text{CN}$ , produced at the  $2h\nu$  level, further excitation probably occurs via  $\pi-\pi^*$  resonant absorptions (cf.  $\text{C}_2\text{H}_2$  (18), secondary excitation of  $\cdot\text{C}_2\text{H}$ ). Production of a Rydberg state, which may have undergone successive H eliminations, would account for the large experimentally observed precursor quenching constants.  $\text{CN } B^2\Sigma^+$  and  $\text{C}_2 d^3\Pi_g$  formation (through C-C or C-N cleavage) could occur at the 2 or  $3h\nu$  level of  $\cdot\text{CH}_2\text{CN}$  (depending upon the internal energy remaining after the primary H elimination). Isomerization of the excited parent or of  $\cdot\text{CH}_2\text{CN}$  allows a mechanism for intramolecular  $\text{CN } B^2\Sigma^+$  production in which the methyl carbon is associated with the nitrogen atom. The isomerization may proceed via a cyclic

or azirine-type intermediate. Direct fragmentation from a symmetric cyclic intermediate is not dominant. Such a process would yield, for example, in  $^{12}\text{CH}_3^{13}\text{CN}$  equivalent amounts of  $^{12}\text{CN}^*$  and  $^{13}\text{CN}^*$ , whereas our observations distinctly prefer  $^{13}\text{CN}^*$ .

## V. Conclusion

Following multiphoton UV excitation of  $\text{CH}_3\text{CN}$  we have identified parallel, pressure-dependent production of  $\text{CN } B^2\Sigma^+$  and  $\text{C}_2 d^3\Pi_g$ . With the use of isotopically labeled parents we have recognized distinct processes which arise essentially from intramolecular and from intermolecular pathways. For  $\text{CN } B^2\Sigma^+$  the intramolecular formation accounts for over 80% of the emissive fragments. There are two source channels: one corresponding to parent C-C cleavage and another in which the methyl carbon is associated with the nitrogen atom. The different source channels for  $\text{CN } B^2\Sigma^+$  are not characterized by distinct rates of rise; this is consistent with a common or similar precursor. Evidently isomerization is possible at some point in the reaction pathway. Fraternal  $\text{C}_2 d^3\Pi_g$  may share the same intermediate. In addition,  $\text{CN } B^2\Sigma^+$  has a minor long-lived component, which is produced from  $\text{CN } A^2\Pi_j$ .

## References

1. D.E. McElcheran, M.H.J. Wijnen, and E.W.R. Steacie, *Can. J. Chem.* 36, 321 (1958).
2. D.D. Davis and H. Okabe, *J. Chem. Phys.* 49, 5526 (1968).
3. A. Mele and H. Okabe, *J. Chem. Phys.* 51, 4798 (1969).
4. C.K. Luk and R. Bersohn, *J. Chem. Phys.* 58, 2153 (1973).
5. H. Okabe and V.H. Dibeler, *J. Chem. Phys.* 59, 2430 (1973).
6. G.A. West and M.J. Berry, *J. Chem. Phys.* 61, 4700 (1974).
7. M.N.R. Ashfold and J.P. Simons, *J. Chem. Soc. Faraday Trans. II*, 73, 858 (1977).
8. M.N.R. Ashfold and J.P. Simons, *J. Chem. Soc. Faraday Trans. II*, 74, 1263 (1978).
9. L.C. Lee, *J. Chem. Phys.* 72, 6414 (1980).
10. M. Sabety-Dzvonik and R. Cody, *J. Chem. Phys.* 64, 4794 (1976).
11. A.P. Baronavski and J.R. McDonald, *Chem. Phys. Lett.* 45, 172 (1977).
12. J.B. Halpern and W.M. Jackson, *J. Phys. Chem.* 86, 973 (1982).
13. A.M. Renlund, H. Reisler, and C. Wittig, *Chem. Phys. Lett.* 78, 40 (1981).
14. M.L. Lesiecki and W.A. Guillory, *J. Chem. Phys.* 69, 4572 (1978).
15. W.M. Jackson, J.B. Halpern and C.S. Lin, *Chem. Phys. Lett.* 55, 254 (1978).
16. W.M. Jackson and J.B. Halpern, *J. Chem. Phys.* 70, 2373 (1979).
17. J.B. Lurie and M.A. El-Sayed, *Chem. Phys. Lett.* 70, 251 (1980).
18. B.B. Craig, W.L. Faust, L.S. Goldberg and R.G. Weiss, *J. Chem. Phys.* in press.
19. B.B. Craig, W.L. Faust, L.S. Goldberg, P.E. Schoen and R.G. Weiss, "Picosecond Phenomena Vol 2" eds. R.M. Hochstrasser, W. Kaiser, and C.V. Shank (Springer-Verlag, Berlin, 1980) p. 253.
20. B.B. Craig, W.L. Faust, L.S. Goldberg, J.M. Schnur, P.E. Schoen, and R.G. Weiss, "Fast Reactions in Energetic Systems" eds. C. Capellos and R.F. Walker (D. Reidel, Dordrecht, 1981) p. 419.

21. H.S. Liszt and J.E. Hesser, *Astrophys. J.*, 159, 1101 (1970).
22. W.M. Jackson, *J. Chem. Phys.* 61, 4177 (1974).
23. J.R. McDonald, A.P. Baronavski, and V.M. Donnelly, *Chem. Phys.* 33, 161 (1978).
24. M. Jeunehomme, *J. Chem. Phys.* 42, 4086 (1965).
25. C. Conley, J.B. Halpern, J. Wood, C. Vaughn and W.M. Jackson, *Chem. Phys. Lett.* 73, 224 (1980).
26. M.N.R. Ashfold and J.P. Simons, *Chem. Phys. Lett.* 47, 65 (1977).
27. R.K. Dhumwad and N.A. Narasimham, *Can. J. Phys.* 46, 1254 (1968).
28. R.J. Spindler, *J. Quant. Spectrosc. Radiat. Transfer* 5, 165 (1965).
29. R.S. Stradling and A.G. Loudon, *J. Chem. Soc. Faraday Trans. II*, 73, 623 (1977).

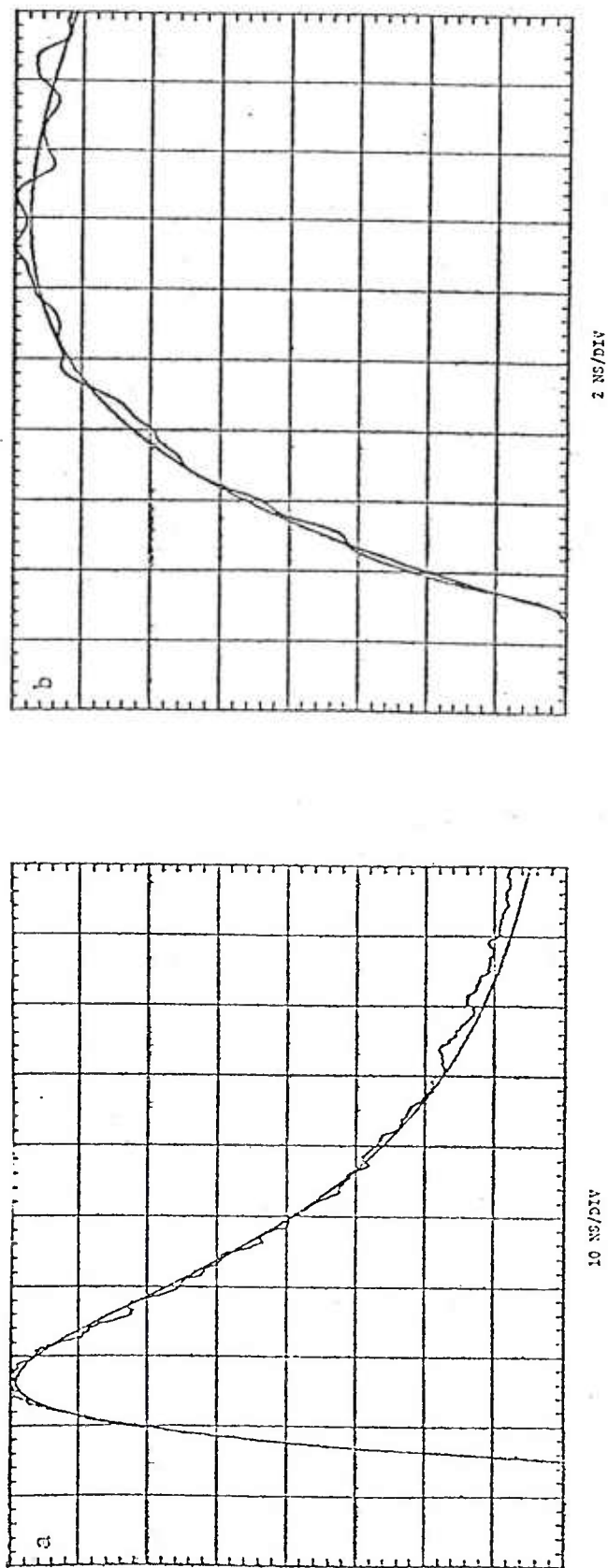


Figure 1

Oscilloscope traces (signal average of 64 laser pulses) of the CN  $B^2\Sigma^+$  emission monitored at 388.3nm ( $(0,0)$  transition) for 3torr of  $CH_3CN$ . Also shown are typical model biexponential curves. (a), 10ns/div. Note the late term excess signal, attributable to the minor secondary formation channel. (b), 2ns/div.

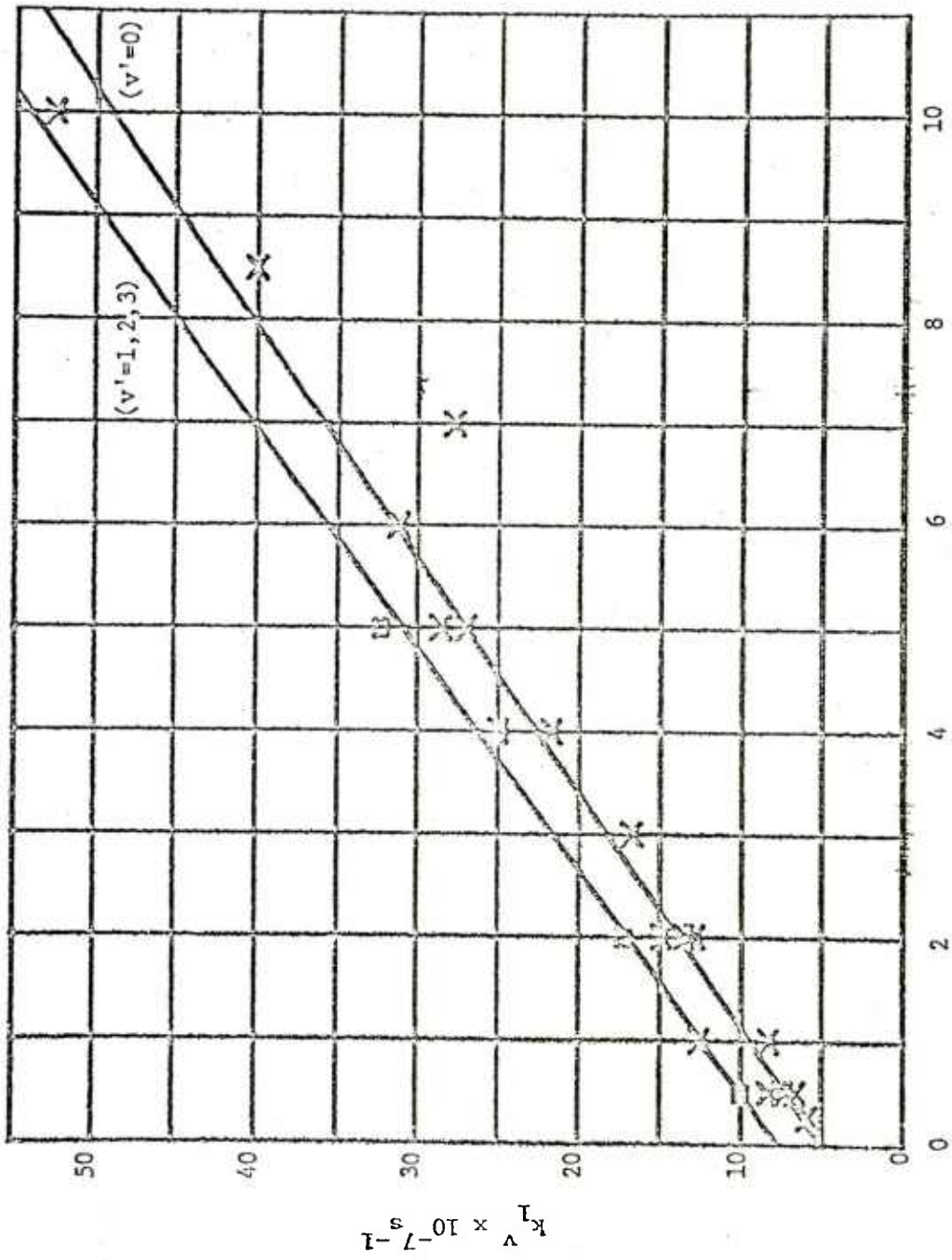


Figure 2

$\text{CH}_3\text{CN}$  pressure dependence of the  $\text{CN B}^2\Sigma^+$  formation rate constant,  $k_1^v$ , for  $v'=0$  and  $v' > 0$ .

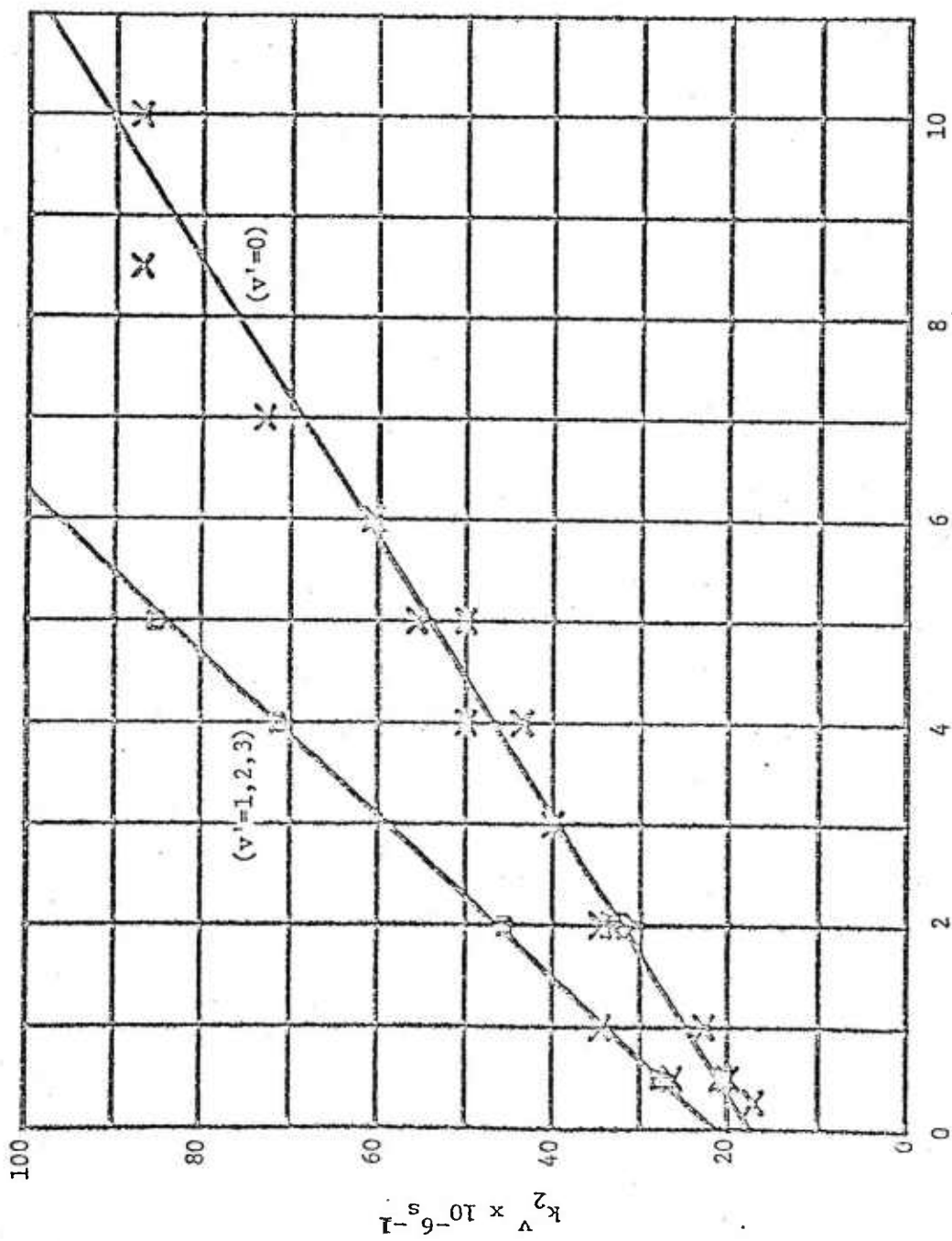


Figure 3

CH<sub>3</sub>CN pressure dependence of the CN B<sub>2</sub>Σ<sup>+</sup> destruction rate constant, k<sub>2</sub><sup>v</sup>, for v=0 and v' > 0.

Lawrence S. Goldberg  
Naval Research Laboratory  
Washington, D.C. 20375, USA

## 1. Introduction

Coherent anti-Stokes Raman scattering (CARS) provides a potentially useful diagnostic approach to the identification and study of transient molecular fragment species produced as the primary events in UV laser photolysis of molecules. GROSS, GUTHALS, and NIBLER [1] applied nanosecond dye laser techniques to obtain scanned as well as broadband single-shot CARS spectra of transient species from 266-nm photolysis of benzene vapor and derivatives. This work was extended to the picosecond time scale by HETHERINGTON III, KORENOWSKI, and EISENTHAL [2] who used optical parametric generation to provide tunable frequency Stokes pulses for a point-by-point probe of the photolysis spectrum. Earlier, GREEN, WEISMAN, and HOCHSTRASSER [3] had demonstrated single frequency picosecond CARS measurements in molecular nitrogen. In the present paper, development of a broadband picosecond CARS probe technique is reported. The method uses the picosecond white-light continuum [4] as Stokes light and enables an extensive anti-Stokes spectrum to be obtained in a single 5-ps laser pulse.

## 2. Experimental

Figure 1 shows a schematic of the experimental arrangement. A recently developed modelocked Nd:phosphate glass laser system produces energetic pulses (25 mJ, 5 ps) of high beam quality at 1054 nm and harmonics, at a pulse repetition rate of 0.2 Hz [5]. The laser second harmonic at 527 nm serves as the pump frequency,  $\omega_1$ , for the four-wave nonlinear CARS interaction. Its near transform-limited spectral width of  $\sim 4 \text{ cm}^{-1}$  defines the spectral resolution of the measurements. A picosecond pulse continuum, extending throughout the visible and near IR spectrum, was produced by focusing the 1054-nm fundamental into a 5-cm liquid D<sub>2</sub>O cell (Fig. 2, upper trace). A 50% mixture of D<sub>3</sub>PO<sub>4</sub>/D<sub>2</sub>O also has been used and produces a lower intensity, but spectrally more-uniform continuum (Fig. 2, lower trace). The continuum beam is collimated and filtered to pass wavelengths  $> 530 \text{ nm}$ , thus providing a broad band of light at Stokes frequencies,  $\omega_2$ . The  $\omega_1$  and  $\omega_2$  pulses are then combined spatially and temporally, and focused collinearly into a 22-cm gas sample cell. Relatively strong coherent anti-Stokes signals are generated over the spectrum of frequencies,  $\omega_3 = 2\omega_1 - \omega_2$ , corresponding to Raman-active vibrational resonances,  $\omega_1 - \omega_2$ , in the third-order susceptibility  $\chi^{(3)}$  of the system under study. The  $\omega_3$  beam is spectrally filtered using short-pass dielectric filters and focused into a 0.3-m grating spectrograph. The dispersed CARS spectrum is then recorded by an OMA II intensified vidicon

system. For photolysis experiments, the fourth-harmonic beam at 264 nm is sent through an independent delay path, recombined collinearly with the probe pulse pair and focused into the sample cell.

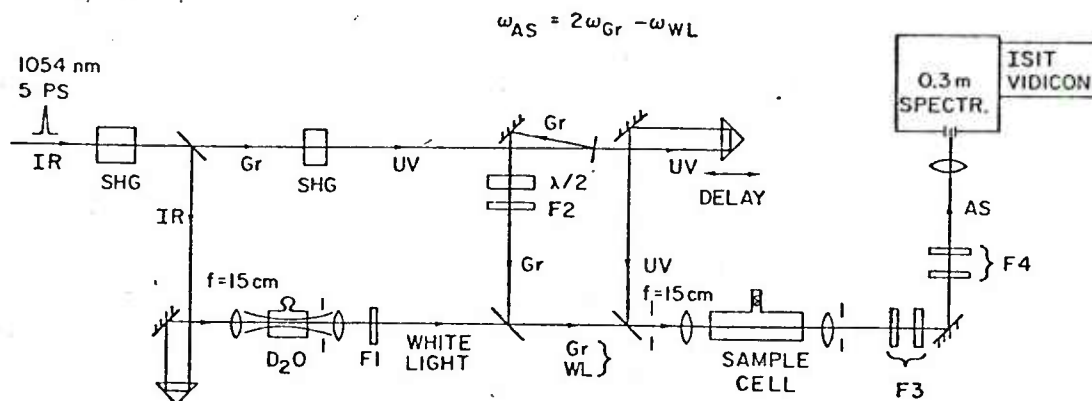


Fig.1 Schematic of the broadband CARS probe and photolysis experiment.

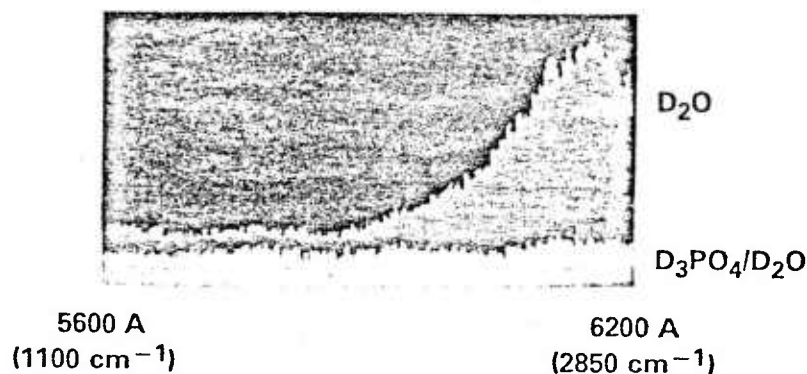


Fig.2 Single-shot spectrum of white-light continuum in  $D_2O$  and in 50%  $D_3PO_4/D_2O$  mixture. The equivalent range of antistokes wavelengths are given in parentheses.

### 3. Results

Figure 3 (lower trace) presents a CARS spectrum obtained at low resolution with a single 5-ps laser pulse from ground-state benzene vapor at 60 torr. The prominent narrow spectral features are identified as the fully symmetric  $3070\text{ cm}^{-1}$  C-H stretch and  $992\text{ cm}^{-1}$  C-C stretch modes of benzene. The vibrational frequency range encompassed in this measurement extends well over  $2000\text{ cm}^{-1}$ . In direct estimates of signal strengths using the vidicon system, the CARS signal at  $3070\text{ cm}^{-1}$  was determined to be  $\sim 10^{-4}$  of the corresponding white-light signal. A joulemeter measurement of the white-light pulse energy gave  $\sim 10\text{ }\mu\text{J}$  from  $550 < \lambda < 620\text{ nm}$ , yielding an average of  $\sim 5\text{ nJ/cm}^{-1}$ . This corresponds to approximately  $10^6$ - $10^7$  photons in the antistokes signal over a linewidth of  $4\text{ cm}^{-1}$ .

Upon photolysis of benzene (Fig.3, upper trace), dramatic new spectral features appear in the region from 2300-2600  $\text{cm}^{-1}$ . The sample was probed  $\sim 200$  ps after arrival of the UV pulse. Figure 4 shows CARS spectra for ground-state and photolyzed toluene vapor at 20 torr. The new spectral lines appear the same for both molecules, although there are differences in line intensities that may be traceable to shot-to-shot variations in white-light intensity. There is also some correlation in the occurrence of intense green pulses with production of particularly strong fragment signals.

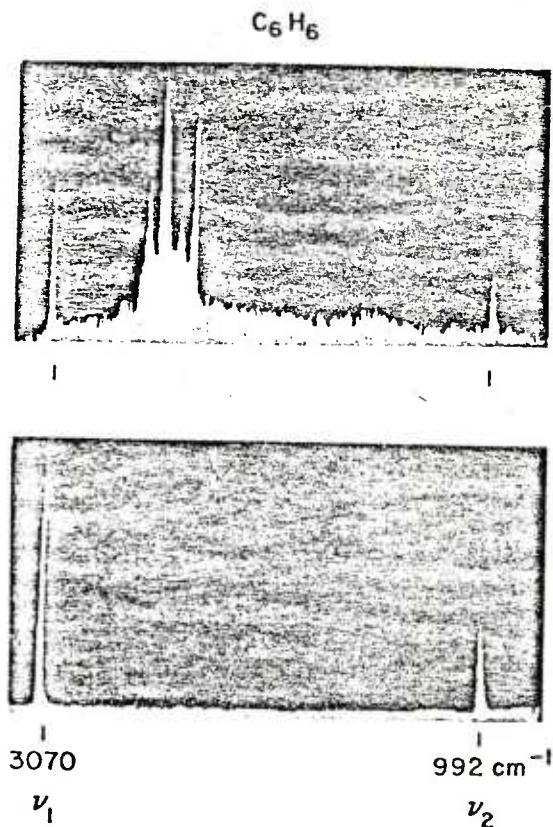


Fig.3 Single-shot CARS spectrum of benzene at 60 torr (bottom), after photolysis (top).

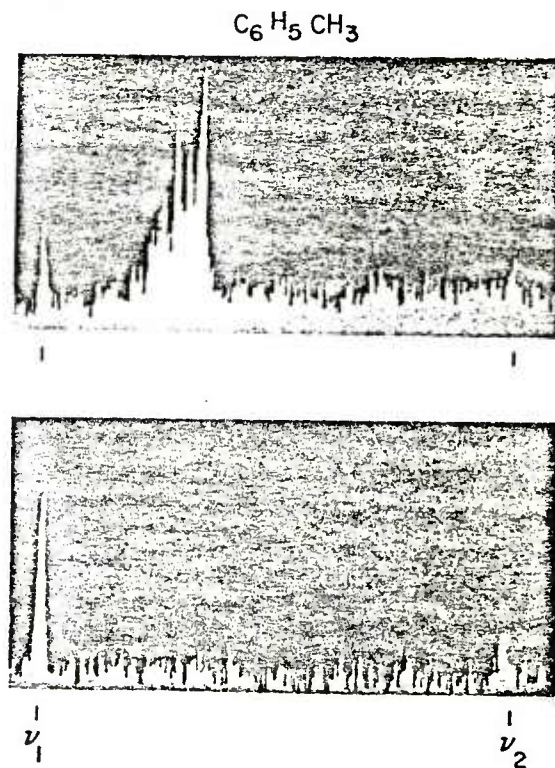


Fig.4 CARS spectrum of toluene at 20 torr (bottom), after photolysis (top).

#### 4. Discussion

These measurements have shown an intense CARS product spectrum strikingly similar, albeit appearing in a distinctly different spectral region, to the complex spectrum attributed by GROSS *et al.* [1] to the  $\text{C}_2$  diradical. Their spectrum in the 2800-3000  $\text{cm}^{-1}$  region was shown to have no hydrocarbon component and was interpreted as arising from multiply resonantly-enhanced CARS signals of  $\text{C}_2$ . HETHERINGTON III *et al.* [2] observed the same spectral lines to be present within the 25 ps duration of their overlapping photolysis and probe pulses. BOESL *et al.* [6] and later HERING *et al.* [7], using mass spectrometry detection, have demonstrated that 2-photon UV ionization is the primary step in fragmentation of benzene yielding  $\text{C}_6\text{H}_6^+$ , and that subsequent

photons, most effectively in the visible spectrum, lead to efficient further fragmentation of the parent ion species.

The strength of the new bands observed in the current experiments relative to the dominant  $\nu_1$  and  $\nu_2$  modes of benzene suggests that they also arise from strong multiple resonant enhancements [8] in the susceptibility of the product species. On the assumption that  $C_2$  is the origin of these CARS signals, the difference in spectrum compared with that of [1] and [2] may result from the different laser wavelengths (527 nm vs. 532 nm) that define  $\omega_1$ . The antistokes frequencies  $\omega_3$  then fall among the vibrational-rotational transitions in the  $\Delta v = +1$  Swan series of  $C_2$  ( $d^3\Pi_g \rightarrow a^3\Pi_u$ ), while  $\omega_2$  lies in the region of  $\Delta v = -2$ , giving opportunity for several multiple resonances to occur.

### References

1. K. P. Gross, D. M. Guthals, and J. W. Nibler, *J. Chem. Phys.* 70, 4673 (1979).
2. W. M. Hetherington III, G. M. Korenowski, and K. B. Eisenthal, *Chem. Phys. Lett.* 77, 275 (1981).
3. B. I. Greene, R. B. Weisman, and R. M. Hochstrasser, *Chem. Phys. Lett.* 59, 5 (1978).
4. The continuum has previously been applied to inverse Raman scattering; R. R. Alfano and S. L. Shapiro, *Chem. Phys. Lett.* 8, 631 (1971).
5. L. S. Goldberg, P. E. Schoen, and M. J. Marrone, *Appl. Optics* 21, 1474 (1982).
6. U. Boesl, H. J. Neusser, and E. W. Schlag, *J. Chem. Phys.* 72, 4327 (1980).
7. P. Hering, A. G. M. Maaswinkel, and K. L. Kompa, *Chem. Phys. Lett.* 83, 222 (1981).
8. S. A. J. Druet, B. Attal, T. K. Gustafson, and J. P. E. Taran, *Phys. Rev.* A18, 1529 (1978).

APPLICATION OF TIME-RESOLVED LASER SPECTROSCOPIES  
TO THE STUDY OF ENERGETIC MATERIALS

B. Craig, P. Schoen, A. Campillo, W. Faust,  
L. Goldberg, M. Marrone, J. Schnur, and R. Weiss  
Naval Research Laboratory  
Washington, D.C. 20375

This report describes recent progress in NRL's research involving the application of advanced spectroscopies to the study of energetic materials.

The goal of these spectroscopic studies is to provide the appropriate species identification protocols suitable for the study of fast energetic reactions stimulated by light, heat, and/or shock.

One of the major objectives of this study is to identify and characterize the important initial stages of energetic reactions as a function of initiation mode. In order to do this, techniques must be developed to observe the critical chemical fragments in the required time scales (e.g.  $10^{-11}$  sec) and to elucidate their kinetics. Using these data attempts will be made to modify and control the course of the observed energetic reactions.

The initial species identification experiments have been performed in the Short Pulse Section of the Optical Probes Branch (Code 6510) at NRL. Collaboration with the Chemistry Departments of Georgetown University, Johns Hopkins University and Washington State University, have been quite useful to the program during the past year.

The time definition inherent in picosecond pulse excitation enables the near-instantaneous deposition of energy into the molecular system before secondary reactions or collisions can occur. As a consequence of the high optical flux densities obtainable from our short pulse lasers, we can readily excite molecular systems through either single or multiphoton absorption processes.

Unimolecular processes are of interest in regard to the determination of primary photo-induced events. There are many questions about unimolecular photodissociation which are likely to be answered through the application of recently developed short pulse techniques. For isolation of specifically unimolecular and early collisional processes, we have been performing experiments on a variety of simple gas-phase organic molecules. (Table I)

Table I

Gases and Fragments Investigated

<u>GASES</u>		<u>EMISSIVE SPECIES/STATES</u>
CH <sub>3</sub> NO <sub>2</sub>	C <sub>2</sub>	d <sup>3</sup> π <sub>g</sub> a <sup>3</sup> π <sub>u</sub> ; C <sup>1</sup> π <sub>g</sub> A <sup>1</sup> π <sub>u</sub>
C <sub>2</sub> H <sub>2</sub>	CN	B <sup>2</sup> Σ <sup>+</sup> + X <sup>2</sup> Σ <sup>+</sup>
CH <sub>3</sub> CN	CH	A <sup>2</sup> Δ + X <sup>2</sup> π
CH <sub>2</sub> CO	H <sub>α</sub> , H <sub>β</sub>	Balmer Series
CO	C	3 <sup>1</sup> p <sup>o</sup> + 2 <sup>1</sup> s
CH <sub>4</sub>	C <sup>+</sup>	3 <sup>2</sup> p <sup>o</sup> + 2 <sup>2</sup> s
HCN	O	3 <sup>5</sup> p + 3 <sup>5</sup> s ; 3 <sup>3</sup> p 3 <sup>3</sup> s

Approved for public release; distribution unlimited.

## Acetylene

Extensive data have been collected for short pulse uv photolysis (25 ps, 266 nm, 10 mJ) of  $C_2H_2$ . The dominant emissive fragment product is the carbon diradical,  $C_2 d^3\pi_g$ , and its consequent Swan emission ( $d^3\pi_g + a^3\pi_u$ ). The characteristic approaches which we have developed fix upon individual species isolated spectroscopically and detected in emission. Our results have given conclusive evidence that the lowest order process yielding emissive  $C_2^*$  is unimolecular and occurs in less than a nanosecond. Streak camera data indicate a grow-in time for this fragment of about 200 picoseconds. The unimolecular nature of the process was confirmed by performing isotopic labeling experiments utilizing mixtures of  $^{12}C_2H_2$  and  $^{13}C_2H_2$ . Emission characteristic of the collisionally produced fragment ( $^{12}C^{13}C$ ) $^*$  was sought, but very little signal attributable to this species was observed at early times of less than a few nanoseconds. After several nanoseconds, a grow in of the ( $^{12}C^{13}C$ ) $^*$  fragment was detected.

Thus  $C_2^*$  also is produced intermolecularly from fragments of acetylene in secondary processes that are exhausted within several nanoseconds ( $\sim 7$  ns at 5 torr). This development must be regarded as fast on the scale of collision rates, although it is readily observed by our instrumentation. The collision partners in this  $C_2^*$  formation process appear to be pairs of excited  $CH^*$  radicals. Emission spectra from  $CH A^2\pi$  have been observed. These spectra exhibit parent quenching with  $k_Q \sim 3 \times 10^{-10} \text{ sec}^{-1}$ , which is typical for radicals and/or excited electronic states. (Normal molecules give substantially lower rates.) Employing the hypothesis of a collisional formation rate proportional to  $(CH^*)^2$  and considering known  $C_2^*$  decay rates, the  $CH^*$  emission time profiles indicate that these are pertinent rates of precursor exhaustion.

## Carbon Monoxide

$C_2 d^3\pi_g$  is also formed upon the irradiation of CO with intense picosecond pulses at 266 nm. The processes involved in the formation of  $C_2$  from CO are clearly different from those for other molecules studies, e.g. acetylene, acetonitrile, ketene, methane, etc. There is in fact an extensive literature on related observations of  $C_2$  Swan emission from CO parents. The anomalous features in the emission spectrum, first reported by Fowler some 70 years ago, have attracted repeated spectroscopic and kinetic studies. There has, however, been a deficiency in temporal studies, probably due to lack of instrumental capability.

The most striking feature that is observed is a strong relative enhancement of  $V' = 6$  in the Swan spectrum. This is not quite unique to CO, having been also observed in  $CH_4$  and flames. Our time resolved studies reveal that Swan excitation occurs through distinct early and late processes. However, even the early process produces emission protracted far beyond the radiation lifetime of 120 ns. The late process endures for over 20  $\mu$ s and is not affected by pressure. In addition, we have demonstrated that it is the late process which is exclusively responsible for the  $V' = 6$  enhancement; the early process yields a vibrational distribution typical of the other parent species listed above.

Our results are consistent with a hypothesis that resonant curve crossing within  $C_2^*$  is responsible for  $V' = 6$  enhancement; indeed a single-triplet transfer  $I^1A_g + d^3\pi_g$  may even account for 20  $\mu$ s delays. Protracted chemiluminescence from such a simple parent as CO is quite unusual and was not expected.

## Acetonitrile

The temporal profiles of fragment emission from  $CH_3CN$  have been obtained. The dominant emissive components are the CN  $B^2\Sigma^+$  violet and  $C_2 d^3\pi_g$  Swan systems. The populations develop with simple formation rates, which are linear in pressure, with non-zero intercepts. The formation rates of the emissive fragments must correspond to the decay rates of unobserved precursors; and the zero-pressure intercepts reflect unimolecular processes depleting the precursor. The precursors are removed in collisions with the parent  $CH_3CN$  with very large  $k_Q$ 's (for CN B  $k_Q = 1.3 \times 10^{-10} \text{ cm}^3\text{s}^{-1}$  and for  $C_2$   $k_Q = 1.9 \times 10^{-10} \text{ cm}^3\text{s}^{-1}$ ).

With isotopically labeled acetonitrile we have characterised several distinct source channels of fragmentation. Two unimolecular channels of CN B have been recognised: one in which the C-N bond is preserved, consistent with C-C cleavage, and another channel in which the methyl carbon is associated with the nitrogen atom, necessitating a rearrangement or isomerisation process. The

rise of emission at the  $^{12}\text{C}^{14}\text{N}$  (0,1) band head for  $^{13}\text{CH}_3^{12}\text{C}^{14}\text{N}$  and for  $^{12}\text{CH}_3^{13}\text{C}^{14}\text{N}$  parents is indistinguishable (over the range of pressures studied, 0.5-5 Torr). We infer a common precursor for the two intramolecular CN B channels. Remarkably, our results also support intramolecular  $\text{C}_2$  d formation. Such a process involves considerable reorganization of the parent  $\pi$  electron system, and elimination of four atoms.

It is our understanding that successive absorption of UV quanta favours formation of quasi-stable superexcited or highly excited (dependent upon the extent of H elimination) states. These may be represented by a general molecular formula  $\text{C}_2\text{H}_n\text{N}^{**}$  (where  $0 < n < 3$ ), possibly of a cyclic structure. To account for the two channels of unimolecular CN B production and intramolecular  $\text{C}_2$  d formation, we believe that such species undergo rearrangement on a timescale which competes with that of fragmentation. The modest unimolecular decay rates of the precursors and their large collisional decay rates may both be associated with the great spatial extent of the Rydberg orbitals in superexcited states.

#### Photolysis of Gas-Phase Nitromethane

While the single beam experiments described previously have proven to be quite fruitful in elucidating processes involving excited-state products, they provide no information about the non emissive ground-state fragments. These fragments might well be the major products of the fast energetic reaction under study. As a consequence, a two-beam excite and probe experiment has been undertaken during the past year. The experiment utilizes an Nd:phosphate glass laser system in which the 4th harmonic at 264 nm dissociates the molecule under investigation and a second beam at 527 nm probes for the absorption of the fragments utilizing the technique of laser-induced fluorescence. The laser system was perfected during the past year and has been applied to study the gas-phase photolysis of nitromethane.

The fluorescence signature of the expected  $\text{NO}_2$  fragment was first determined in  $\text{NO}_2$  vapor before attempting the nitromethane photolysis experiments. The observed fluorescence decay curves could be constructed from single-exponential fits and were consistent with previously published work on  $\text{NO}_2$ . It was found that pressures of  $> 5$  torr nitromethane strongly quenched  $\text{NO}_2$  fluorescence. Therefore, the two beam photolysis experiment was conducted at pressures between 0.1 and 2 torr.

Nitromethane was then photolyzed and probed for ground-state fragments with the 527 nm pulse. Induced fluorescence was observed which was identical in spectral and temporal behavior to that observed in  $\text{NO}_2$ /nitromethane mixture studies. The formation kinetics of the attributed  $\text{NO}_2$  fragment were investigated by varying the delay time between the 264 nm and 527 nm pulses. A sharp step in the intensity of the induced fluorescence vs. delay was observed. The position of the onset and rapid rise in signal appear to indicate extremely rapid ( $< 5$  ps) formation of the fragment. The fluorescent signal was found to be linear in UV excitation and probe laser energy indicating dissociation from the lowest energy  $n \rightarrow \pi^*$  transition of nitromethane.

In the coming year work will proceed on the development of the species identification techniques. One technique that looks particularly promising is the recent development in our laboratory of a picosecond-white light CARS (coherent-antistokes Raman scattering) technique in which for the first time an entire Raman spectra can be observed with one picosecond laser pulse. We are now investigating the applicability of this technique to the study of energetic reactions.